Summer 8-17-2018

Properties of Synaptic Transmission from Rods and Cones in The Outer Plexiform Layer of The Vertebrate Retina

Xiangyi Wen
University of Nebraska Medical Center

PROPERTIES OF SYNAPTIC TRANSMISSION FROM RODS AND CONES IN THE OUTER PLEXIFORM LAYER OF THE VERTEBRATE RETINA

by

Xiangyi Wen

A DISSERTATION

Presented to the Faculty of
the University of Nebraska Graduate College
in Partial Fulfillment of the Requirements
for the Degree of Doctor of Philosophy

Pharmacology & Experimental Neuroscience
Graduate Program

Under the Supervision of Professor Wallace B. Thoreson

University of Nebraska Medical Center
Omaha, NE

August, 2018

Supervisory Committee:
Wallace B. Thoreson, Ph.D.
Woo-Yang Kim, Ph.D. Anna Dunaevsky, Ph.D.
George Rozanski, Ph.D. Huangui Xiong, M.D. Ph.D.

This work is dedicated to my family.

Acknowledgements

I would like to thank my mentor Dr. Wallace (Wally) B. Thoreson for his careful instruction and support throughout my graduate study. Wally patiently answered any questions about science and non-science, discussed and designed detailed steps with me. His precise attitude to science guided me into the world of science and my future career. I would also like to thank my dissertation committee: Dr. Woo-Yang Kim, Ph.D., Dr. Anna Dunaevsky, Ph.D., Dr. George Rozanski, Ph.D., and Dr. Huangui Xiong, M.D. Ph.D. for their advice and support with my thesis project.

I would like to thank all the laboratory members who directly or indirectly helped me to finish my work. In particular, I would like to thank Dr. Matthew (Matt) J. Van Hook for his great help in experiments and especially in learning new techniques. He is a great teacher for electrophysiological techniques and helped me to be familiar with the environment when I joined our lab. He also contributed to some of the data shown in Figure 8. I would like to thank Dr. Minghui Chen and Grant Saltzgaber for their kind help with TIRFM experiments. I would also like to thank Dr. Karlene Cork, Dr. Ted Warren, Justin Grassmeyer, Cody Barta, Asia Cahill, and Cassandra Hays for discussion and support in helping to obtain my degree.

I would like to thank Dr. Scott Nawy from the Department of Ophthalmology & Visual Sciences for discussion and suggestions for my projects. I would like to thank Tom Bargar from the Electron Microscopy Core Facility (EMCF) for his help with electron microscopy imaging in Figures 2 and 17. I am grateful to the late Dr. Richard Hallworth from Creighton University for assistance with the FRAP experiments in Figure 3.

I would also like to thank staff members within the Departments of Ophthalmology & Visual Sciences and Pharmacology & Experimental Neuroscience for their kind help with ordering and other paperwork.

Finally, I want to thank my family for their support for my years of education.

Table of Contents

PROPERTIES OF SYNAPTIC TRANSMISSION FROM RODS AND CONES IN THE OUTER PLEXIFORM LAYER OF THE VERTEBRATE RETINA

Xiangyi Wen, Ph.D.

University of Nebraska, 2018

Supervisor: Wallace B. Thoreson Ph.D.

Abstract

Photoreceptors are the first neurons in the visual system. They transduce changes in light intensity into graded changes in membrane potential that are then transformed into chemical signals by regulating the release of glutamate-filled synaptic vesicles. Rod and cone photoreceptors release glutamate continuously in darkness and release slows in light. To help track rapid changes in light intensity, photoreceptors are capable of both rapid exocytosis and rapid endocytosis of synaptic vesicles.

Endocytosis is needed for recycling synaptic vesicles but also appears to be important for removing proteins and lipids from active zones to restore release site function after prior vesicle fusion. Synaptic exocytosis from vertebrate photoreceptors involves synaptic ribbons that cluster vesicles near the presynaptic membrane. We hypothesized that such clustering increases the likelihood that exocytosis at one ribbon release site may disrupt release at an adjacent site. Consistent with this, studies described in Chapter 2 showed that endocytosis is needed to rapidly restore release site competence at photoreceptor ribbon synapses. We combined optical and electrophysiological techniques to show that endocytosis is important for restoring late steps in the vesicle fusion process but does not appear to be needed for vesicles to dock

successfully at the membrane. Release site clearance by endocytosis is thus essential for continuous release in photoreceptors.

We explore mechanisms that contribute to efficient synaptic vesicle exocytosis and endocytosis in Chapter 3. Exocytosis and endocytosis of synaptic vesicles can be coupled in two general ways. In the full-collapse model, the vesicle membrane merges completely with the plasma membrane and so vesicles must be fully reconstructed before they can be retrieved by endocytosis. In the kiss-and-run model, a vesicle briefly contacts the plasma membrane through a small fusion pore that permits release of small molecules but the vesicle does not flatten into the plasma membrane. The vesicle with its complement of proteins is quickly recycled to the cytoplasm after closure of the fusion pore during kiss-and-run. Using a combination of techniques including total internal reflectance fluorescence microscopy (TIRFM), confocal microscopy, electron microscopy, and membrane capacitance measurements, we found that kiss-and-run exocytosis and endocytosis contributes to more than 50% of the release events in photoreceptors. In addition to speeding endocytosis, kiss-and-run fusion may limit disruption of release site structure during fusion, providing an efficient mechanism to facilitate sustained release.

HCs not only receive excitatory feedforward signals from photoreceptors, but also send inhibitory feedback signals back to photoreceptors. At normal physiological membrane potentials in cones, inhibitory feedback from HCs to cones increases the activity of L-type voltage-gated Ca^{2+} channels producing inward feedback currents that increase the synaptic release of glutamate. In the final chapter of this thesis, we describe studies using paired whole cell recordings to determine if, in addition to Ca^{2+} currents, other currents also contribute to these inward feedback currents in cones. We found that feedback currents in cones involve a smaller than expected contribution from Ca^{2+}-

activated Cl^- currents and a larger than expected contribution from Cl^- currents associated with glutamate transporter activity in cones.

Chapter 1 Introduction

I. Retinal Anatomy

Eyes have evolved specialized structures to serve their role in vision. The eye is surrounded by a tough outer layer formed by the cornea and sclera anteriorly and posteriorly, respectively (Fig. 1A). Within the eye, the iris and lens separate the anterior and posterior chambers of the eye. After passing through the cornea and lens, light passes through the transparent vitreous body that occupies most of the posterior chamber, ultimately falling on the light-sensitive retina. Beneath the retina is a pigmented cell layer called the retinal pigment epithelium (RPE). In addition to other functions, the RPE serves as part of the blood-retinal barrier, separating the retina from the choroid, a rich vascular plexus that rests beneath the inner surface of the sclera.

Because it derives from embryonic diencephalon and is an outgrowth of the developing brain, the retina is considered part of central neural system (CNS). It shows a well-organized laminar structure that is shared by all vertebrates (Fig. 1B). From the outer surface adjoining the RPE to the inner surface contacting the vitreous body are the outer nuclear layer (ONL), outer plexiform layer (OPL), inner nuclear layer (INL), inner plexiform layer (IPL) and retinal ganglion cell (RGC) layer. Somata of photoreceptors form the ONL while somata of HCs and bipolar cells form the INL. Synaptic terminals of photoreceptors contact dendrites of HCs and bipolar cells in the OPL. Bipolar cell terminals contact dendrites of amacrine cells and RGCs in the IPL. Because photoreceptors lie at the back of the retina, light passes through RGCs and bipolar cells before it is absorbed by photoreceptors. However, after being absorbed, light signals are transmitted forward from photoreceptors, to retinal bipolar cells and then to RGCs. The dendrites of HCs and amacrine cells extend laterally in the OPL and IPL, respectively, to provide feedback signals that modify responses of photoreceptors, bipolar cells, and

ganglion cells. The axons of RGCs form the optic nerve and exit the eye through the optic nerve to make synapses in higher visual centers of the brain. Müller cells are the principal glial cells in retina and span the retina from the inner limiting membrane at the vitreal surface to the outer limiting membrane that separates the somata and inner segments of photoreceptors. Müller cells have a number of functions, including cleaning up the waste products from metabolic reactions, protecting neural cells through recycling neural transmitters, and structural support.

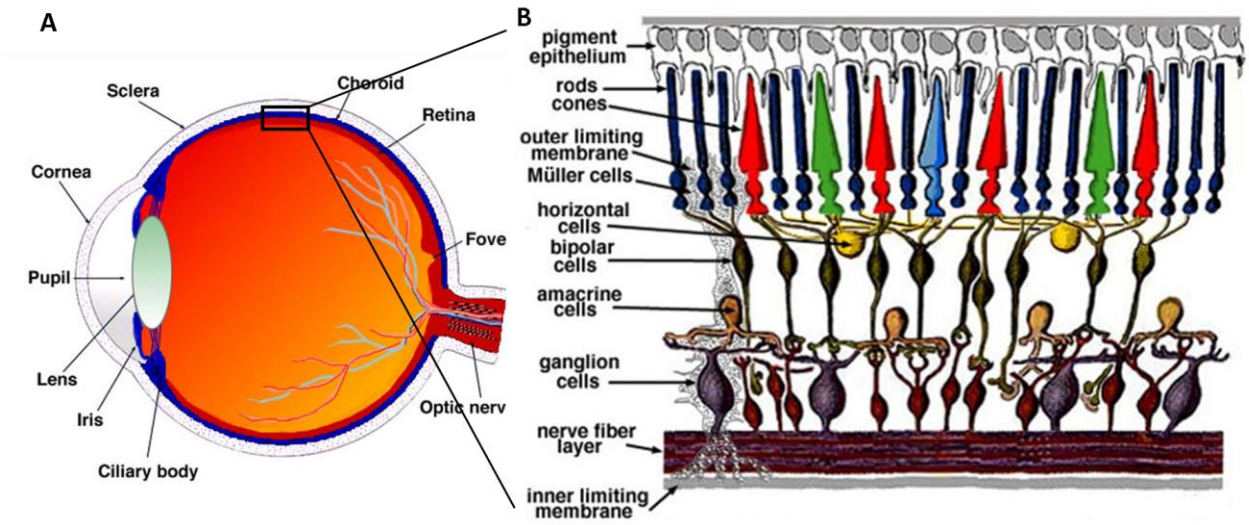

Figure 1. Retinal anatomy

(A) Gross anatomy of the eye. (B) The retina consists of five major cell types: photoreceptors, retinal bipolar cells, HCs, amacrine cells, retinal ganglion cells (RGCs). From the outer surface adjoining the RPE to the inner surface contacting the vitreous, these layers are the outer nuclear layer (ONL), outer plexiform layer (OPL), inner nuclear layer (INL), inner plexiform layer (IPL) and RGC layer. Somata of photoreceptors form the ONL and somata of HCs and bipolar cells form the INL. Synaptic terminals of photoreceptors contact dendrites of HCs and bipolar cells in the OPL. Bipolar cell terminals contact dendrites of amacrine cells and retinal ganglion cells in the IPL. Photoreceptors are categorized into cones and rods by the shapes of the outer segment (OS). Reproduced under a Creative Commons license from: “Simple anatomy of the retina” by Helga Kolb, webvision.med.utah.edu.

II. Photoreceptor anatomy

a. Photoreceptors

Photoreceptors are the primary light-sensing neurons and transduce light into a graded membrane voltage change. The light-sensitive machinery of photoreceptors is contained within a large modified cilium known as the outer segment (OS). Photoreceptors are generally categorized into two general types, cones and rods, based on the shapes of the OS (Fig. 1B). Rods with more cylindrical outer segments are more sensitive to light than cones and can even detect a single photon. Cones have conical outer segments and are less sensitive to light but exhibit faster responses. Rods thus contribute more to scotopic vision in dim light, while cones contribute to photopic vision in brighter light, providing higher acuity and color vison. The OS is separated from the inner segment (IS) and neighboring cell soma by a thin connecting cilium. In most photoreceptors, the synaptic terminal is separated from the soma by a thin axon. The IS contains mitochondria, endoplasmic reticulum (ER) and the Golgi apparatus that are essential for metabolism and protein production. After transcription and expression, phototransduction proteins are assembled in the IS, then passed to the OS and finally embedded in disc membranes in the OS. The disc membrane is generated from out-pouchings of the cell plasma membrane. In rods, this folded double membrane ultimately detaches from the cell membrane to form individual flat, membrane-bound discs in rods. In the case of cones, the disc membranes remain attached to the cell membrane and form stacks of invaginations (Arikawa et al., 1992). The soma contains the photoreceptor nucleus. Photoreceptors typically exhibit a triad synapse in which two dendrites of postsynaptic HCs and a single bipolar cell dendrite enters an invagination in the base of the synaptic terminal, terminating just beneath the photoreceptor active zone (Fig. 2).

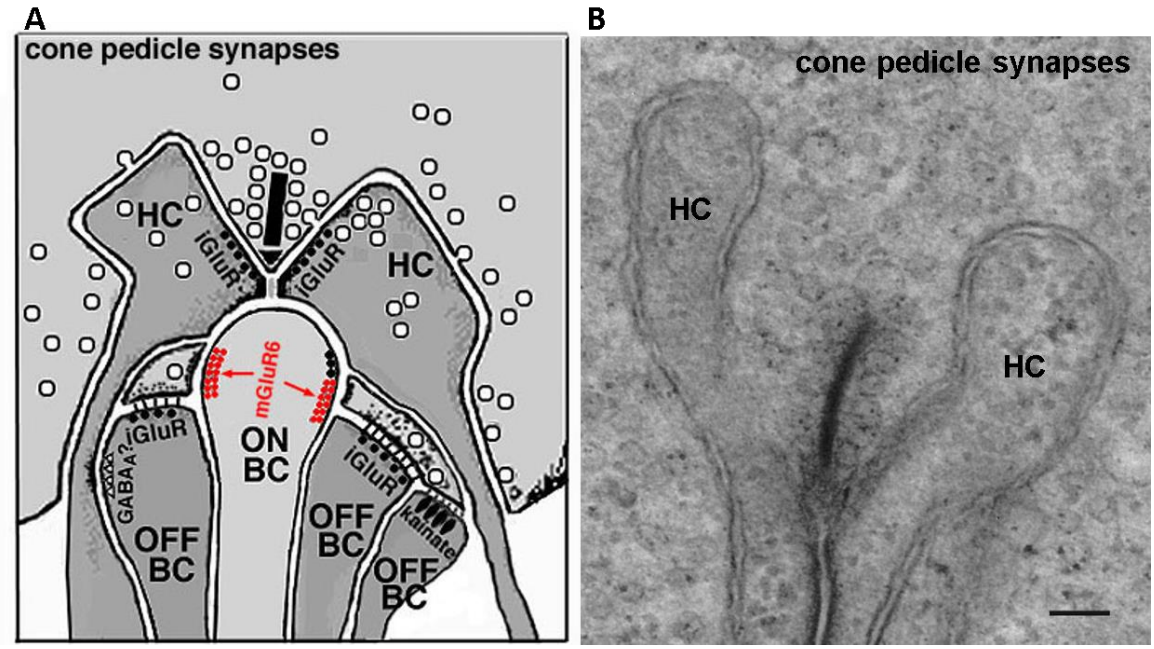

Figure 2. Photoreceptor ribbon terminal and the triad synapses.

(A) Schematic diagram of the invaginating triad synapse. The synaptic ribbon is represented as a black, vertical bar with white circles representing synaptic vesicles. HCs and bipolar cells (BC) both enter the cone terminal. Typically, an ON BC enters the invagination at the center with two flanking HC dendrites. OFF BCs are located outside of the invagination at the base of the synaptic terminal. Ionotropic glutamate receptors (iGluR) are expressed on HCs and OFF BCs whereas type 6 metabotropic glutamate receptors (mGluR6) are expressed on ON BCs. (B) An electron microscope (EM) image showing two HC dendrites entering an invagination within the terminal of a salamander cone. The bar-like dense structure in the middle of the image is the synaptic ribbon. Scale bar: 100 nm. (A) is reproduced under a Creative Commons license from: “Cone pathways through the retina” by Helga Kolb, webvision.med.utah.edu.

b. Ultrastructure of photoreceptor ribbon synapses

A number of sensory neurons including photoreceptors, retinal bipolar cells, cochlear hair cells, vestibular hair cells, lateral line organ hair cells, and electroreceptors were found to possess special electron-dense structures at the active zones of their synaptic terminals called synaptic ribbons (Heidelberger et al., 2005; LoGiudice and

Matthews, 2009; Matthews and Fuchs, 2010; Vaithianathan et al., 2013). While hair cell ribbons are often more spherical, photoreceptor ribbons are usually flat plate-like structures with a thickness of ~35 nm. In rods, the base can extend along the plasma membrane by as much 1 micron and the ribbon can extend up to 1 micron into the cytoplasm (Sterling and Matthews, 2005). Cone ribbons are typically smaller than rod ribbons, with a base of less than 0.5 microns and extending only a few hundred nanometers into the cytoplasm (Dowling and Boycott, 1966; Kolb, 1970; Sterling and Matthews, 2005). In salamander retina, there are ~7 ribbons/rod (Townes-Anderson et al., 1985; Van Hook and Thoreson, 2015) and ~13 ribbons/cone (Bartoletti et al., 2010; Pang et al., 2008). In mammals, rods typically possess only a single ribbon while cones can have as many as 45 ribbons (Haverkamp et al., 2001). The diameter of synaptic vesicles averages 45 nm in salamander photoreceptors (Lasansky, 1973; Thoreson et al., 2004). It is estimated that each ribbon has ~700 synaptic vesicles tethered on it in mammalian and amphibian rods (Rao-Mirotznik et al., 1995; Thoreson et al., 2004). Each vesicle is tethered to the ribbon by 3-5 thin filaments (Usukura and Yamada, 1987). The whole terminal contains approximately 250,000 vesicles in lizard cones, 27,000 vesicles in salamander rods, and up to 7500 vesicles in mouse rods (Rea et al., 2004; Zampighi et al., 2011). Ultrastructurally, one can distinguish three vesicle pools: cytoplasmic vesicles, ribbon-associated vesicles, and membrane-docked vesicles. Elecrophysiologically, one can also distinguish three vesicle pools. With strong stimulation, a pool of vesicles can be released very readily and so this pool is termed the readily releasable pool (RRP). In cones, maintained stimulation then depletes a second reserve pool. In salamander cones, the number of vesicles in the RRP averages 15-20 vesicles per ribbon, matching the number of vesicles that lie along the bottom two rows of the ribbon in contact with the adjacent plasma membrane (Bartoletti et al., 2010; Thoreson et al., 2016). The reserve pool consists of about 90 more vesicles, matching

the number of vesicles that are tethered to the rest of the ribbon (Bartoletti et al., 2010). After depletion of these two pools, release from cones can be maintained at a roughly linear rate, presumably reflecting replenishment of ribbons from the large cytoplasmic reserve pool.

Unlike conventional synapses where most cytoplasmic vesicles are tethered to the cytoskeleton through the interactions involving the protein synapsin, vesicles in the reserve pool at ribbon synapses which lack synapsin (Mandell et al., 1990) are thought to be quite mobile (Holt et al., 2004; Mandell et al., 1990; Von Kriegstein et al., 1999). With the assistance of the late Dr. Richard Hallworth (Creighton University), we tested the mobility of synaptic vesicles in salamander by performing fluorescence recovery after photobleaching (FRAP) experiments with fluorescently-labeled vesicles. We loaded vesicles of rods and cones by incubating retinas with 3-kDa or 10-kDa dextran-conjugated Texas Red dyes. After enzymatic isolation, we plated photoreceptors onto glass coverslips. We bleached dye-loaded vesicles within a small rectangular region in the terminals of isolated, dye-loaded rods or cones. We then measured the recovery of fluorescence in this region which should reflect the movement of vesicles from unbleached regions of the photoreceptor terminal. The time constants for fluorescent recovery reflect the time constants of vesicle mobility. The fraction of fluorescence that did not totally recover provides a measure of the immobile fraction of vesicles. The time constants for recovery did not differ between 3-kDa and 10-kDa Texas Red, in both cones (3-kDa, 7.5 ± 1.33 s, N=40 cells; 10-kDa, 7.7 ± 1.05 s, N=34; P = 0.93) and rods (3-kDa, 9.92 ± 3.27 s, N=20; 10-kDa, 9.86 ± 1.27 s, N=24; P=0.99) (Fig. 3A). These data suggest that both dyes were loaded into similarly mobile structures, presumably synaptic vesicles. The immobile fraction also did not differ significantly for the two dyes in rods (3-kDa, 0.82 ± 0.028, N=20; 10-kDa, 0.86 ± 0.017, N=24; P=0.24). In cones, a

slightly greater fraction of 10-kDa Texas Red fluorescence was immobile compared to 3-kDa Texas Red (3-kDa, 0.84 ± 0.014, N=40; 10-kDa, 0.88 ± 0.011, N=34; P=0.039) (Fig. 3B), perhaps reflecting capture of some of these larger dye molecules in endosomes or other intracellular structures. The immobile fraction observed in our experiments was larger than previously reported for synaptic vesicles loaded with FM1-43 in lizard cone terminals (Rea et al., 2004). To test whether this difference might be a consequence of the use of dextran-conjugated dyes, we performed FRAP experiments after loading photoreceptors with FM1-43 (15 μM, Synaptogreen, Biotium, Fremont, CA, USA, 3 min incubation), as used in the earlier study. We found a similar immobile fraction (0.84, N=9 cones; 0.88, N=3 rods) as we found with the dextran-conjugated dyes, suggesting that the low mobility observed in our experiments is not a consequence of the selection of dyes but is due to other differences between preparations. Unlike the retinal slice preparation used previously by Rea et al. (2004), the terminals of isolated rods flatten out when they are plated onto coverslips and this may limit vesicle mobility. Alternatively, this could be a cell- or species-dependent difference between lizard cones studied by Rea et al. (2004) and salamander photoreceptors used in our studies.

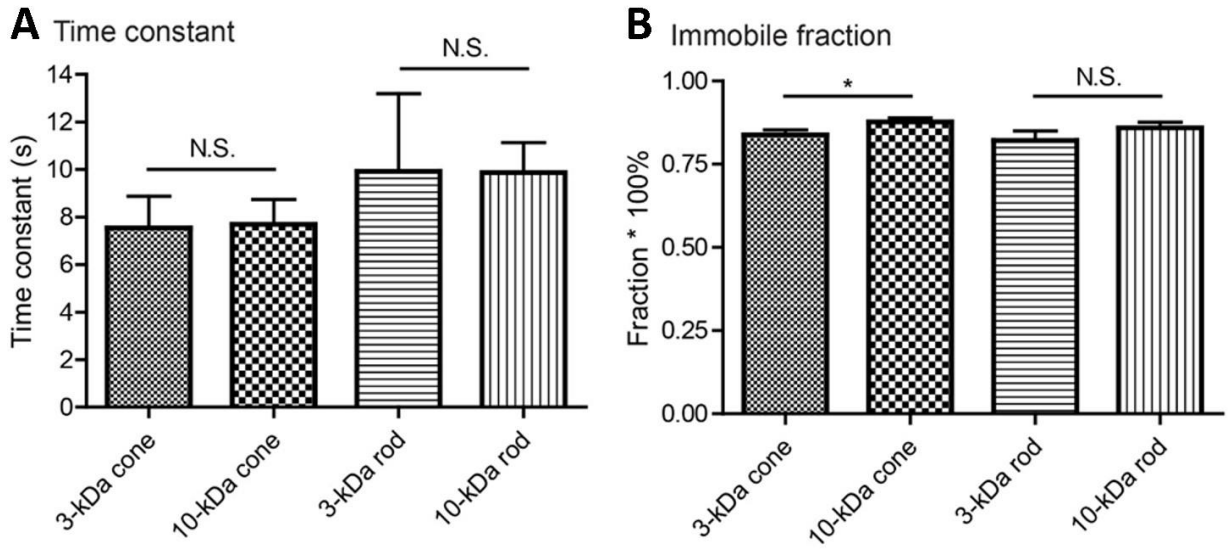

Figure 3. FRAP of dye-loaded synaptic vesicles in photoreceptors.

Bar graphs showing recovery time constants (A) (cones: 3-kDa, N=40 cells; 10-kDa, N=34; P = 0.93; rods: 3-kDa, N=20; 10-kDa, N=24; P=0.99) and immobile fractions (B) (cones: 3-kDa, N=40; 10-kDa, N=34; P=0.039; rods: 3-kDa, N=20; 10-kDa, N=24; P=0.24) observed during fluorescence recovery after photobleaching (FRAP) experiments performed with a rectangular region of laser illumination targeted to terminals of isolated rods and cones loaded with 3-kDa or 10-kDa Texas Red. Data show mean ± SEM. * P<0.05, N.S. P>0.05 (Student's t-test).

c. Proteins at the ribbon synapse

Release at photoreceptor ribbon synapses involves a number of specialized synaptic proteins. RIBEYE is the major structural protein of the ribbon. RIBEYE is an alternative splice variant of the transcriptional repressor C-terminal binding peptide 2 (CtBP2) and is composed of both A and B domains. The B domain is identical in both forms of CtBP2 whereas the ribbon-specific A domain is only found in RIBEYE. There are also a number of other ribbon-associated proteins. KIF3A co-localizes with RIBEYE and is a component of the kinesin II motor protein holoenzyme (Hirokawa and

Takemura, 2004; Kondo et al., 1994; Muresan et al., 1999). However, ATP does not appear to be required for release of vesicles from the ribbon suggesting that motor proteins are not required to deliver vesicles to the ribbon base. Instead, this enzyme may function in transporting active zone proteins to the terminal (Heidelberger et al., 2005). Piccolo and bassoon are another two ribbon-associated proteins. Piccolo is located at the distal portion of the ribbon whereas bassoon is located at the base of ribbon. Bassoon appears to be important for anchoring the ribbon and assuring its proper orientation (Dick et al., 2001).

Synaptic vesicles are membrane-confined organelles with many membrane proteins attached to or inserted in the membrane. Vesicle fusion is mediated by soluble NSF attachment protein receptors (SNARE) complexes. Synaptobrevin is a vesicle-anchored SNARE protein (v-SNARE). Synaptosomal associated protein-25 (SNAP-25) and syntaxin are anchored in the target plasma membrane, and are thus called t-SNAREs. During release, v-SNARE and t-SNAREs bind together to form a four-helix bundle in which SNAP-25 contributes two helices, syntaxin provides one, and synaptobrevin provides one. Ca^{2+} sensor protein, synaptotagmin (syt), is the engine for vesicle fusion. Syt has a short transmembrane domain inserted into the vesicle membrane and a large cytoplasmic Ca^{2+}-binding C2 domain (C2A and C2B). After binding with Ca^{2+}, syt binds to the C-terminal H3 region of syntaxin which results in a SNARE-syt- Ca^{2+}-phospholipid complex (Rizo and Rosenmund, 2008) and the C2 domains of syt insert into the phospholipid membrane. The twisting of SNARE proteins then triggers fusion of the vesicle membrane with the cell membrane. The isoforms syt1, syt2, syt7, syt9, and syt10 are considered to be Ca^{2+} sensors for exocytosis (Craxton, 2010; Pang and Sudhof, 2010; Sudhof, 2013; Walter et al., 2011). While syt1 and syt2 are the most common Ca^{2+} sensors in traditional synapses of neurons, they are missing

in photoreceptor ribbon synapses in non-mammalian vertebrates (Berntson and Morgans, 2003; Fox and Sanes, 2007; Heidelberger et al., 2003). Compared with the high Ca^{2+} cooperativity (N=5 Ca^{2+} ions) and low Ca^{2+} affinity in traditional neurons (Sun et al., 2007), synaptic release from photoreceptors shows a lower cooperativity (N=2 Ca^{2+} ions) and higher Ca^{2+} affinity (Duncan et al., 2010; Thoreson et al., 2004). Although the identity of Ca^{2+} sensors in photoreceptors is still unknown, this suggests that there may be special Ca^{2+} sensors working at photoreceptor ribbon synapses. Other specialized proteins are also expressed in photoreceptors include syntaxin 3 rather than 1 (Morgans et al., 1996) and complexins 3 and 4 rather than 1 and 2 (Reim et al., 2005). Syntaxin, complexin, and synaptotagmin have all been implicated in regulating fusion pore size and duration (Archer et al., 2002; Dhara et al., 2014; Han et al., 2004; Rao et al., 2017; Wang et al., 2003; Zhang et al., 2011) and thus may contribute to the high frequency of kiss-and-run events found in experiments described in Chapter 3 of this thesis.

The influx of Ca^{2+} through L-type voltage-gated Ca^{2+} channels (VGCCs) is the main regulator of synaptic release from photoreceptors. While there are four types of L-type VGCCs, only voltage-gated Ca^{2+} channel 1.4 ($Ca_v1.4$) and $Ca_v1.3$ are expressed in photoreceptors (Berntson et al., 2003; Xiao et al., 2007) and only $Ca_v1.4$ locates beneath the ribbons at synapses (Liu et al., 2013b). $Ca_v1.4$ is the predominant Ca^{2+} channel in mammalian rods (Firth et al., 2001; Morgans, 2001; Morgans et al., 2001), whereas in tree shrew retina, $Ca_v1.3$ was found in long wavelength-sensitive cones but not short wavelength-sensitive cones (Morgans, 1999; Taylor and Morgans, 1998). However, in mouse retina, $Ca_v1.4$ was also found to be expressed in all cones and knockout of $Ca_v1.4$ causes a loss of cone-based vision (Regus-Leidig et al., 2014; Waldner et al., 2018; Zabouri and Haverkamp, 2013). It is thus not clear what subtype of

Ca^{2+} channel mediates release from cones. One possibility is that release from cones may involve a splice variant of $Ca_v1.4$ (Haeseleer et al., 2016).

III. Phototransduction

a. Rhodopsin cascade

As introduced above, phototransduction occurs in the specialized OS of photoreceptors. In rods, the chromophore 11-cis-retinal is covalently bound to a G-protein coupled receptor (GPCR), rhodopsin. 11-cis-retinal absorbs the energy from photons and is transformed to all-trans-retinal through photoisomerization (Fig. 4). This conformational change in retinal activates rhodopsin so that it assumes its active configuration, metarhodopsin (Arshavsky et al., 2002; Pugh, E.N., Jr. and T.D. Lamb, 2000). Metarhodopsin is intrinsically unstable and the chemical energy is transferred to its coupled G-protein, transducin. Bound GDP on transducin is replaced with GTP and then the alpha subunit of transducin with GTP dissociates from the beta/gamma subunit. The GTP-bound active alpha subunit activates phosphodiesterase (PDE) which breaks cytoplasmic cGMP into 5'-GMP. The decreased concentration of cGMP leads to closure of cGMP-gated cation channels, and hyperpolarization of the photoreceptor membrane potential. Increasing the number of absorbed photons increases the amplitude of this membrane hyperpolarization in photoreceptors allowing changes in light intensity to be encoded by changes in photoreceptor membrane potential.

A single rhodopsin molecule activates 10-25 transducin molecules in mouse (Krispel et al., 2006) and hundreds of transducin molecules in frog rods (Vuong et al., 1984). While each transducin molecule activates only a single PDE, each PDE can hydrolyze thousands of cGMP molecules (Baehr et al., 1979; Leskov et al., 2000). This

tremendous amplification in the phototransduction cascade provides rods with the sensitivity to detect single photons (Pugh, E.N., Jr. and T.D. Lamb, 2000; Pugh and Lamb, 1993).

After photoactivation, the rhodopsin phototransduction cascade must be rapidly shut off so that the photoreceptor can detect another photon. In darkness, intracellular free Ca^{2+} is high and Ca^{2+} binds to a regulatory protein, recoverin (Rec). Rec-Ca^{2+} binds to rhodopsin kinase GRK1 to inhibit its activity. In light, decreased Ca^{2+} relieves inhibition of GRK1 which phosphorylates metarhodopsin to allow binding to arrestin (Arr1) which in turn caps the catalytic activity of metarhodopsin. The active alpha subunit of transducin is shut down by hydrolyzing GTP to GDP. Although transducin has intrinsic GTPase activity, this hydrolysis is accelerated by a GTPase activating protein (GAP) complex which is formed by regulator-of-G-protein-signaling proteins (RGS9-1), the long form of Gβ5 subunit (Gβ5-L), and a membrane anchor protein (R9AP). After the PDE-mediated hydrolysis of cGMP is shut down, the concentration of cGMP is restored, opening cGMP-gated cation channels and returning the photoreceptor to a more depolarized membrane potential (Pugh, E.N., Jr. and T.D. Lamb, 2000; Pugh and Lamb, 1993). Together, shutoff of rhodopsin and transducing activity terminates phototransduction, preparing rhodopsin to be activated by another incoming photon.

After photoisomerization, all-trans-retinal must also be converted back to its light-sensitive form, 11-cis-retinal. There is no isomerase in the OS of the rods; instead, all-trans-retinal is transported out of the rod OS and delivered to adjacent RPE cells where it is reduced back to 11-cis-retinal. 11-cis-retinal is then transferred back to the rods. While the all-trans-retinal in rods is recycled only via RPE, all-trans-retinal can also be recycled via Müller cells in cones.

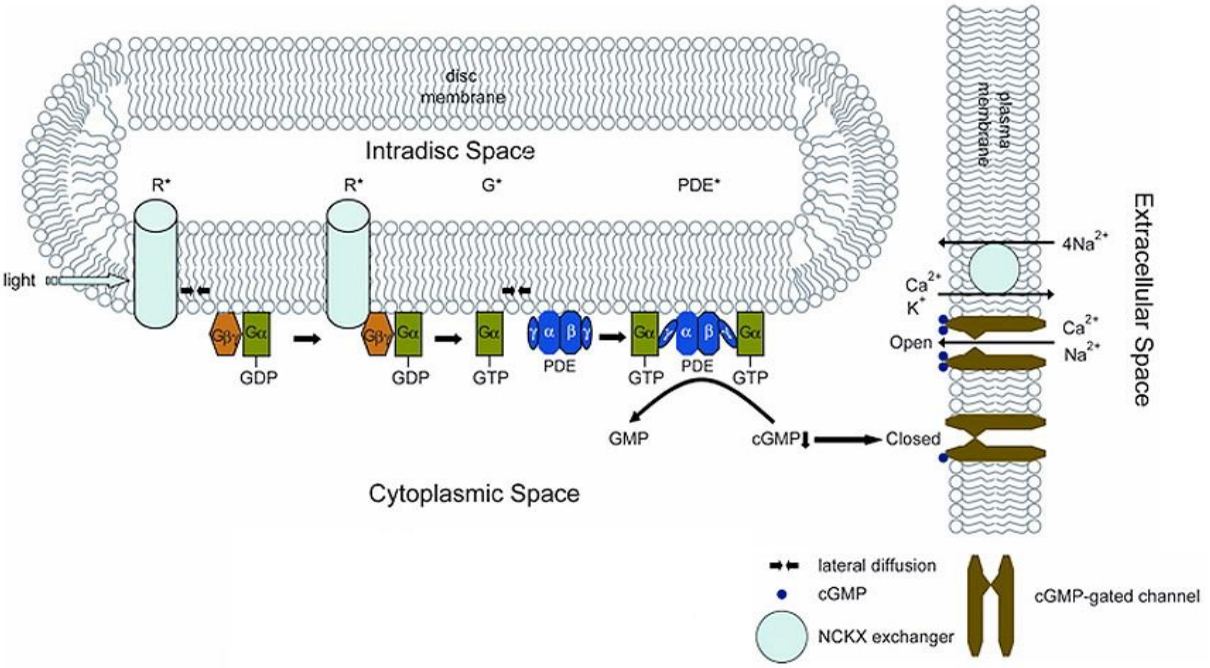

Figure 4. Phototransduction of rod photoreceptors.

Schematic diagram of phototransduction. (R^*) active configuration of rhodopsin, metarhodopsin; (G^*) active form of alpha subunit of transducin with GTP; (PDE^*) active form of phosphodiesterase (PDE). Reproduced under a Creative Commons license from: “Phototransduction in rods and cones” by Yingbin Fu, webvision.med.utah.edu.

b. Cone opsins and their spectral sensitivity

Like rods, the photopigment molecules of cones, opsins, are contained in the membranous discs in the OS. As described previously, unlike the membranous discs in rods that are detached from the plasma membrane, the membranous discs in cones are formed by stacked invaginations from cell membrane. Cones are less sensitive to light than rods but exhibit faster responses. Cones are classified as different types based on differences in their opsin expression. Different types of opsins have different sensitivities to different wavelengths of light, allowing the capability for color vision. The differing spectral sensitivities of different cone subtypes is determined by the spectral absorbance of the photopigments that each possess. Humans and other Old World primates have a

trichromatic system using three different types of cones: L (long wavelength or red-sensitive), M (middle wavelength or green-sensitive), and S (short wavelength or blue-sensitive) cones (Bowmaker et al., 1991; Jacobs, 1996; Schnapf et al., 1988). Most other mammals possess only S and M cones and are dichromatic. Most birds and lizards possess four spectrally distinct opsins and are tetrachromatic (Jacobs, 2018).

IV. Synaptic release from photoreceptors

a. Ribbon release

As described in phototransduction, cones are tonically depolarized and release neurotransmitter-filled vesicles in darkness. When hyperpolarized by light, cones slow the rate at which they release vesicles. The graded changes in membrane potential are converted into graded changes in release rate with differing intensities of light. Abrupt depolarization when light is abruptly turned off causes a fast, phasic release of vesicles in the RRP, followed by slower, tonic release in both cones and rods (Jackman et al., 2009; Van Hook and Thoreson, 2015). Cones release vesicles exclusively at ribbons (Snellman et al., 2011; Van Hook and Thoreson, 2015) but as discussed further below, rods are also capable of significant slow release involving non-ribbon release sites. The initial transient part of exocytosis is considered to represent release from the RRP of vesicles that are tethered to the base of ribbons (Graydon et al., 2011), triggered by Ca^{2+} influx through VGCCs., The kinetics of synaptic release is therefore affected by the diffusion and buffering of Ca^{2+} from the Ca^{2+} channels. Fast release from rods and cones involves vesicles that lie within Ca^{2+} nano-domains < 100 nm from individual Ca^{2+} channels (Mercer et al., 2011a). Release of a single vesicle from a cone can be triggered by opening of only 2-3 Ca^{2+} channels (Bartoletti et al., 2011) and release from

rods requires opening of only 3-4 channels (Van Hook and Thoreson, 2015). $Ca_v1.4$ Ca^{2+} channels in photoreceptors show little or no voltage- or Ca^{2+}-dependent inactivation (Corey et al., 1984; Koschak et al., 2003; Lee et al., 2015; Rabl and Thoreson, 2002) allowing illumination-dependent voltage changes in photoreceptor to be steadily transmitted as changes in release.

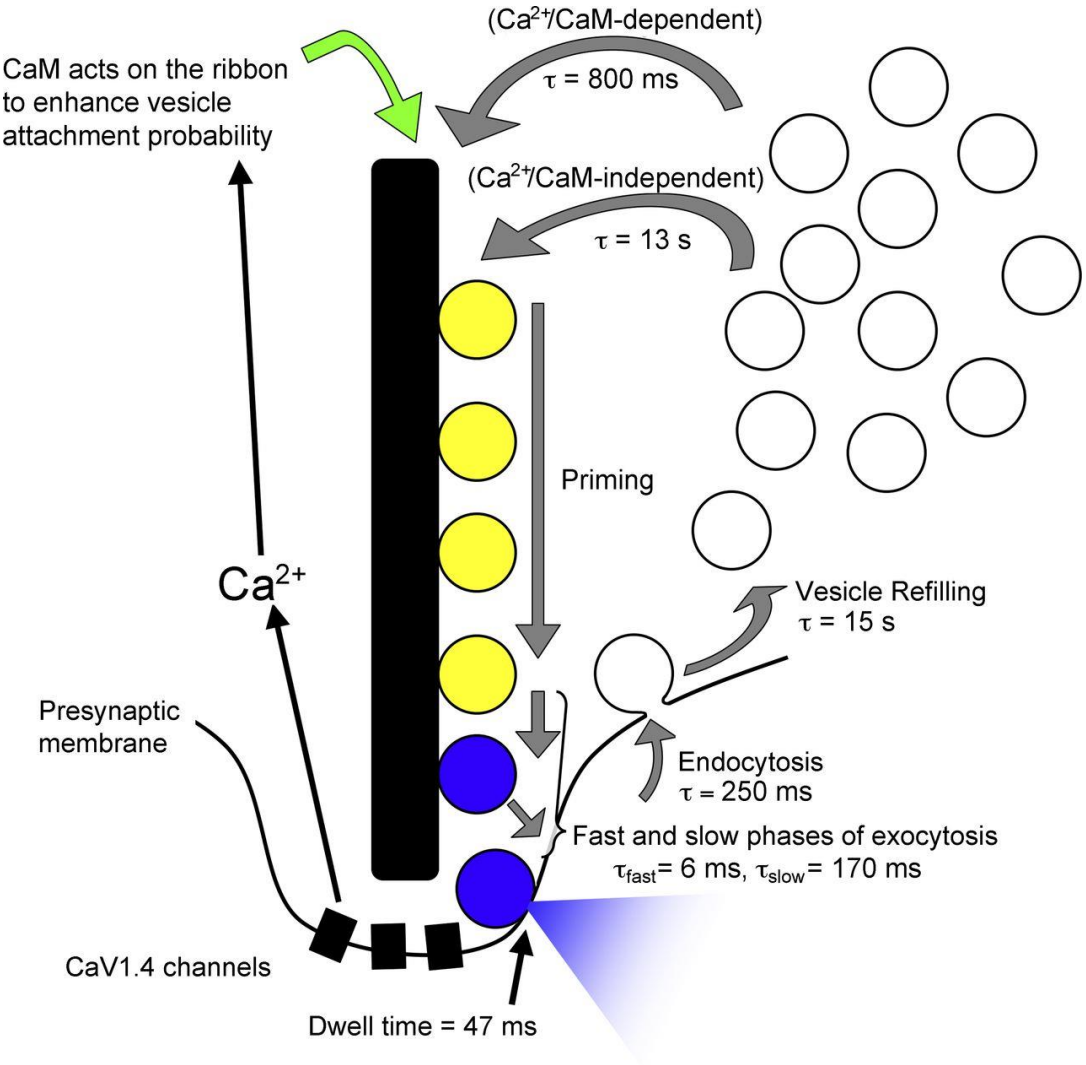

Figure 5. The synaptic vesicle cycle at the cone synapse.

The black vertical bar represents the ribbon. The time constants (τ) of each step are shown. Image is taken under a Creative Commons license from Van Hook, M. J., Parmelee, C. M., Chen, M., Cork, K. M., Curto, C., and Thoreson, W. B. (2014).

Calmodulin enhances ribbon replenishment and shapes filtering of synaptic transmission by cone photoreceptors. J. Gen. Physiol. 144, 357–378.

To continuously transmit visual signals, the terminals of cones contain large synaptic vesicle pools. However, even the large pool of 194,000 mobile vesicles (out of 215,600 total vesicles) in a salamander cone synapse would be emptied in <15 min by sustained release in darkness if not replenished by endocytosis (Sheng et al., 2007). Moreover, release from cones is regulated purely by release probability (P) but not pool size (N) (Thoreson et al., 2016). Therefore, the recycling of synaptic vesicles is essential for continued release. It was proposed that the ribbon works much like a capacitor, rapidly discharging vesicles when cones depolarize in darkness and slowly recharging with vesicles when cones hyperpolarize in light (Jackman et al., 2009). After exocytosis, synaptic vesicles are regenerated through endocytosis. The empty vesicles are then refilled with glutamate molecules by glutamate transporters on vesicles. The filled vesicles join the large reservoir pool from which they can be delivered to the ribbon for later release. What is the rate-limiting step in this process? Figure 5 shows different time constants (τ) at each step of the vesicle cycle in cone synapses. The τ of release consists of a ~6 ms fast phase which represents the fast fusion of vesicles in the RRP and a ~170 ms slow phase which represents the movement of vesicles in the ribbon-associated pool down the ribbon to replenish the RRP, thereby contributing to slower tonic release (Bartoletti et al., 2010; Rabl et al., 2005; Thoreson et al., 2004). After reaching the base of the ribbon, vesicles appear to dwell at the membrane surface for ~47 ms before fusion (Chen et al., 2013; Van Hook et al., 2014). Retrieval of vesicles in photoreceptors involves ultrafast endocytosis with τ ~250 ms (Van Hook and Thoreson, 2012). The τ for glutamate refilling is about 15 s (Hori and Takahashi, 2012). Finally, vesicle replenishment to the ribbon involves a bi-exponential process with τ ~800 ms and τ ~ 13 s. Contributions from the faster component of replenishment can be

increased by the actions of Ca^{2+} acting on CaM (calmodulin) while the slower component is a Ca^{2+}/CaM-independent process (Van Hook et al., 2014). Usually, the rate-limiting step is determined by the slowest step which, in this case, is glutamate refilling with τ ~15 s. However, glutamate refilling is not normally the rate-limiting step because the large number of vesicles in the reservoir pool provides an extensive buffer of loaded vesicles (Van Hook et al., 2014). Thus, although it takes a long time for glutamate refilling, there are plenty of previously filled vesicles to replenish release sites even if glutamate refilling is temporarily interrupted. Thus, the rate-limiting step in both cones (Van Hook et al., 2014) and rods (Van Hook and Thoreson, 2015) is instead the fast delivery of vesicles to the ribbon that can be enhanced by Ca^{2+}/CaM (Babai et al., 2010a; Van Hook et al., 2014). Analytical modeling of the replenishment process suggests that CaM acts not on vesicles but on ribbon attachment sites (Van Hook et al., 2014).

Although Ca^{2+}/CaM replenishment is normally the rate-limiting step in replenishment, continued release also requires that there are a sufficient number of functional release sites available for replenishment (Babai et al., 2010a; Singer and Diamond, 2006). As at other synapses, the number of release sites at photoreceptor ribbon synapses is limited (Clements and Silver, 2000). Some synapses have many release sites with low release probability, like calyx of Held (Borst and Soria van Hoeve, 2012; Neher and Sakaba, 2008), whereas other neurons signal through a smaller number of release sites with high release probability, like cerebellar mossy fiber boutons (cMFB) (Delvendahl and Hallermann, 2016). Photoreceptors have a limited number of release sites on each ribbon and exhibit high release probability (Bartoletti et al., 2010). Synapses with a limited number of release sites need to keep receiving new vesicles for continuous release and quickly restore release sites to functionality so that they can be

reused. Many different proteins on the vesicle and plasma membrane participate in vesicle fusion. After a successful fusion, “used” proteins appear to stay in or near the release site, limiting the release of subsequent vesicles at that site (Hosoi et al., 2009; Kim and von Gersdorff, 2009). Thus, even though there may be sufficient space on the membrane for another vesicle, the release site may not be functionally capable of docking or releasing another vesicle and thus remain refractory until the release site is cleared of previously released proteins and lipids (Neher, 2010). How does synapse clear release sites? Several studies showed that inhibition of endocytic processes rapidly leads to inhibition of vesicle exocytosis (Chen et al., 2003; Ferguson et al., 2007; Hosoi et al., 2009; Kawasaki et al., 2000; Shupliakov et al., 1997); this effect was too fast to be caused by the depletion of vesicles. Thus, endocytosis seems to be needed to clear used release proteins and lipids which is in turn necessary to restore release sites to functionality. In ribbon synapses, neighboring vesicle release sites along the ribbon base may be separated as little as 10 nm (Lasansky, 1978; Thoreson et al., 2004). Because of the dense packing of vesicles and tight spatial coupling of vesicles and Ca^{2+} channels, we hypothesized that the efficient clearance of release may be of particular importance at ribbon synapses. In Chapter 2, we used a number of complementary measurements of synaptic function after inhibiting dynamin-dependent endocytosis to explore the function of endocytosis in the clearance of release sites in rod photoreceptors.

b. Exocytosis and endocytosis

After the release of neurotransmitters by vesicle exocytosis, homeostatic maintenance of the cell plasma membrane requires that synaptic vesicles be regenerated via endocytosis. Classical, clathrin-mediated endocytosis was suggested by

ultrastructural observations of membrane invagination (Heuser and Reese, 1973; Saheki and De Camilli, 2012; Wu et al., 2014). In addition to clathrin-mediated endocytosis, bulk endocytosis (Clayton et al., 2008; Gaffield et al., 2011; Holt et al., 2003; Matthews and Sterling, 2008; Teng et al., 2007; Wenzel et al., 2012) and kiss-and-run endocytosis (Albillos et al., 1997; Fulop and Smith, 2006; He et al., 2006; Holroyd et al., 2002; Vardjan et al., 2007; Wang et al., 2003) have been shown to contribute to vesicle regeneration.

In most forms of endocytosis, it appears that the GTPase dynamin functions during the scission step to pinch off the newly formed vesicle from the cell membrane after hydrolyzing GTP (Marks et al., 2001; Roux et al., 2006; Sweitzer and Hinshaw, 1998). However, dynamin-independent endocytosis has also been found in the calyx of Held (Xu et al., 2008), hippocampal neurons (Chung et al., 2010), and cones (Van Hook and Thoreson, 2012) after disruption of dynamin. Dynamin was shown to be in the terminals of both rods and cones by immunohistochemistry (Sherry and Heidelberger, 2005; Ullrich and Sudhof, 1994). Endocytosis in rods depends more strongly on dynamin than in cones (Van Hook and Thoreson, 2012). The different dynamin dependence found in rods and cones suggests different modes or mechanisms of exocytosis and endocytosis in rods and cones. We examine this possibility further in experiments where we compared effects of a dynamin inhibitor on endocytosis in rods and cones in Chapter 3.

After intense or long stimulation, large endocytic structure were observed using EM and termed “bulk” endocytosis (Clayton et al., 2008; Gaffield et al., 2011; Holt et al., 2003; Matthews and Sterling, 2008; Teng et al., 2007; Wenzel et al., 2012). Along with the large membrane invagination, bulk endocytosis was also found to produce a rapid decline in membrane capacitance (Wu and Wu, 2007). Recently, an extremely rapid form of bulk endocytosis was found in mouse hippocampal neurons using “flash-and-

freeze" electron microscopy (Watanabe et al., 2013). In addition, endosome-like structures were found after the bulk endocytosis from which synaptic vesicles were newly generated (Watanabe et al., 2014). Clathrin was not found on membrane-associated vesicles but only on coated vesicles that were generated from large endosomes. This suggests that rapid endocytosis was not clathrin-dependent but that after bulk retrieval into large endosome-like structures, clathrin was required for vesicle generation from the endosome (Watanabe et al., 2014).

The third mode of endocytosis is kiss-and-run. Exocytosis and endocytosis of synaptic vesicles can be coupled in two general ways in neurons and non-neural cells (Alabi and Tsien, 2013; Wu et al., 2014). With full-collapse fusion, the vesicle membrane merges completely with the plasma membrane and vesicles must be fully reconstructed and retrieved by clathrin-mediated or bulk endocytosis. With kiss-and-run fusion, a vesicle briefly contacts the plasma membrane through a small fusion pore that permits release of small molecules but the vesicle does not flatten into the plasma membrane (Ceccarelli et al., 1973). The vesicle with its complement of proteins is quickly recycled to the cytoplasm after closure of the fusion pore. This mechanism avoids the problem of having to re-assemble the various proteins that were scattered about the presynaptic membrane during full-collapse fusion, providing a simple mechanism for rapid vesicle retrieval.

Full-collapse fusion and kiss-and-run fusion events appear to co-exist in neurons and neuroendocrine cells (Albillos et al., 1997; Fulop and Smith, 2006; He et al., 2006; Holroyd et al., 2002; Vardjan et al., 2007; Wang et al., 2003). Besides rapid and efficient retrieval, another advantage of using kiss-and-run is that it allows differential release of small vs. large molecules (Fulop et al., 2005; Fulop and Smith, 2006). Thus, in neuroendocrine cells (e.g. chromaffin cells), the small fusion pore formed during kiss-and-run only allows release of small molecules (e.g., catecholamines), whereas full-

collapse fusion can release everything in the vesicles, including both catecholamines and large neuropeptide molecules. Neuropeptides are synthesized in the soma and must be transported to the axon whereas small neurotransmitters can be synthesized locally in the terminal and are thus more readily available. By varying the mode of exocytosis, vesicles can selectively release different contents under different conditions: catecholamines are more readily released under basal stimulation while both catecholamines and neuropeptides are released less often under acute stress (Fulop et al., 2005; Liang et al., 2017).

Experiments described in Chapter 2 of this dissertation showed that mechanisms for rapid and robust endocytic retrieval are essential for sustaining continuous release at photoreceptor ribbon synapses. Ultrafast endocytosis has been found in photoreceptors using capacitance measurements (Cork and Thoreson, 2014; Van Hook and Thoreson, 2012) but the mechanisms are still elusive. Both bulk endocytosis and kiss-an-run endocytosis have sufficiently fast kinetics to contribute to ultrafast endocytosis in photoreceptors. In Chapter 3, we combined electrophysiological and optical techniques to show that significant amounts of release from rods and cones involve kiss-and-run.

c. CICR and non-ribbon release from rods

Like cones, rods are capable of fast initial release due release of the RRP from ribbons (Chen et al., 2013) and employ similar ribbon replenishment mechanisms (Van Hook and Thoreson, 2015). However, in addition to these ribbon-related mechanisms, rods also show a large slow component of release at non-ribbon sites (Thoreson, 2007). Evidence for this includes the finding that selectively damaging ribbons inhibited fast release but not slower release from rods (Chen et al., 2013; Chen et al., 2014).

This additional slow glutamate release involves release of Ca^{2+} from intracellular stores in the ER. In addition to Ca^{2+} influx through VGCCs, intracellular Ca^{2+} can be released from intracellular stores by calcium-induced calcium release (CICR) or by the second messenger IP3. While there is no evidence for IP3-mediated release in photoreceptors, CICR has been shown to contribute to synaptic release from rods (Babai et al., 2010b; Cadetti et al., 2006; Chen et al., 2013; Chen et al., 2014; Chen et al., 2015; Krizaj et al., 1999; Krizaj et al., 2003; Suryanarayanan and Slaughter, 2006). Furthermore, CICR can directly trigger release of vesicles at non-ribbon release sites in rods (Chen et al., 2013; Chen et al., 2014). In CICR, Ca^{2+} ions are released from ER which is further from release sites than VGCCs (Babai et al., 2010b). Consequently, in addition to promoting Ca^{2+}-dependent replenishment as in cones, the diffusion of Ca^{2+} from CICR maintains the Ca^{2+} concentration at a high level and contributes to sustained release from rods in darkness (Chen et al., 2015). Blocking CICR with high concentrations of ryanodine in mouse or salamander retina greatly reduces light responses of second order neurons, suggesting that CICR-driven non-ribbon release is a major mechanism for sustaining release from rods in darkness (Babai et al., 2010b; Cadetti et al., 2006; Chen et al., 2014; Krizaj et al., 2003; Suryanarayanan and Slaughter, 2006). Furthermore, deletion of Bassoon which causes ribbons to detach from the membrane did not abolish visual cortical responses or bipolar cell responses assessed with the electroretinogram b-wave in mouse (Dick et al., 2003; Goetze et al., 2010). These data suggest that non-ribbon release plays an important role in visual signal transmission.

In darkness, rods are continually depolarized and continually release glutamate. Thus, if CICR is an important mechanism for sustained release, it must work continually in darkness. How is CICR maintained during maintained depolarization and why doesn't

the ER simply run out of calcium during maintained darkness? FRAP experiments using a dye that labeled proteins in the ER membrane (ER-tracker green) showed that the ER lumen forms a continuous network that spans from the soma to the terminal of rods (Chen et al., 2014). Measurements with Ca^{2+}-sensitive dyes inside the ER showed that Ca^{2+} can diffuse within the ER from soma to terminal (Chen et al., 2015). In darkness, Ca^{2+} released into the cytoplasm by CICR maintains release and a soma-to-terminal Ca^{2+} gradient within the ER continuously resupplies intraterminal ER with Ca^{2+} delivered from soma ER. This allows for a nearly inexhaustible Ca^{2+} source to maintain slow release in rods (Chen et al., 2014; Chen et al., 2015).

V. Retinal circuits

The retinal network initiates the first steps in visual processing through a multitude of feedforward and feedback pathways. Generally, light signals are transmitted radially from photoreceptors to retinal bipolar cells, and then to RGCs. HCs and amacrine cells, whose processes extend laterally, provide feedback signals in the OPL and IPL, respectively. Due to their different light sensitivities and functions, rod and cone signals utilize different circuits in the mammalian retina.

In darkness, cGMP-gated cation channels in the OS are continuously active and so both cone and rod photoreceptors are tonically depolarized to a membrane potential of -35 to -45 mV in darkness. Thus, photoreceptors release the neurotransmitter, L-glutamate, continuously in darkness and release slows when photoreceptors hyperpolarize in response to light. There are two general classes of bipolar cells that differ in their expression of postsynaptic glutamate receptors: ON bipolar cells possess type 6 metabotropic glutamate receptors (mGluR6) and OFF bipolar cells possess

ionotropic glutamate receptors (iGluR of the AMPA or KA subtype). In mammals, cones connect to both types of bipolar cells whereas rods contact only ON-type bipolar cells through a specialized rod bipolar cell. The iGluRs are glutamate-gated ion channels that allow inward cation flow upon binding of glutamate and thereby depolarize bipolar cells in darkness when glutamate release is maximal. Conversely, when light is on, the reduced release of glutamate from photoreceptors causes OFF bipolar cells to hyperpolarize in response to light so that the response polarity matches that of the photoreceptors. On the other hand, mGluR6 GPCRs in ON bipolar cells link to their associated channels through a second messenger G_o pathway. In darkness, the sustained released glutamates keep activating mGluR6 which closes the transient receptor potential 1 (TRPM1) cation channel through regulation of the G_o pathway. With the reduced release of glutamate in light, this inhibition of TRPM1 cation channels is dismissed causing ON bipolar cells to depolarize, thus producing a response that is inverted in polarity relative to the hyperpolarizing photoreceptor light response (Morgans et al., 2009).

In the visual system, each neuron has a receptive field that is defined as the particular region of retina in which changes in illumination can stimulate changes in that neuron. Based on whether a neuron is depolarized by a centered spot of light at onset or offset, the neurons can be classified as either ON-center or OFF-center cells. As described previously, photoreceptors hyperpolarize to light and bipolar cells can either hyperpolarize or depolarize to light depending on whether they express iGluRs or mGluR6s. RGCs can also be classified as ON-type cells that depolarize and increase action potential frequency in response to light onset, OFF-type cells that diminish action potential firing to light, or ON-OFF RGCs that increase firing at both the onset and offset of light.

Retinal neurons, even as early as cones, exhibit antagonistic receptive field surrounds (Allman et al., 1985). Center-surround receptive fields were first discovered in cat RGCs by Stephen Kuffler (1953) (KUFFLER, 1953) that exhibit a central region and a concentric ring, called the surround, in which light generates responses of opposite polarity (Fig. 6). Thus, shining a spot of light into the receptive field center will increase firing in an ON cell, but illuminating the surround with an annulus will inhibit firing. Conversely, shining a spot of light into the center of an OFF cell will diminish firing whereas illumination of the receptive field surround will increase firing. The center-surround receptive fields that are created in the retina are retained by lateral geniculate neurons downstream from RGCs (Wiesel and Hubel, 1966).

Center-surround receptive fields enhance comparisons between global and local changes in light intensity. Although negative feedback from the surround dampens feedforward transmission of visual signals, it plays an important role in subtracting the global background intensity. The large receptive field surround collects light from a wide area of retina, providing a measure of the global intensity. Thus, light changes that fall equally on both the center and surround will tend to cancel one another out whereas changes that occur only in the center will become more salient. By promoting detection of local changes relative to global changes, center-surround receptive fields enhance the ability to detect spots and edges. How does the retina achieve center-surround receptive fields? As first discovered by Hartline and colleagues in Limulus retina (HARTLINE et al., 1956), center-surround receptive fields can be achieved by mechanisms known as lateral inhibition or center-surround antagonism in which surrounding neurons make inhibitory contacts onto neurons in the center of a given receptive field. In vertebrate retina, these lateral inhibitory connections involve both horizontal cell contacts onto photoreceptors and bipolar cells in the outer retina (Thoreson and Mangel, 2012) and

amacrine cell contacts onto bipolar and ganglion cells in the inner retina (Lukasiewicz, 2005; Zhang and Wu, 2009). In the next section, we discuss the mechanisms of lateral inhibition from horizontal cells to cones.

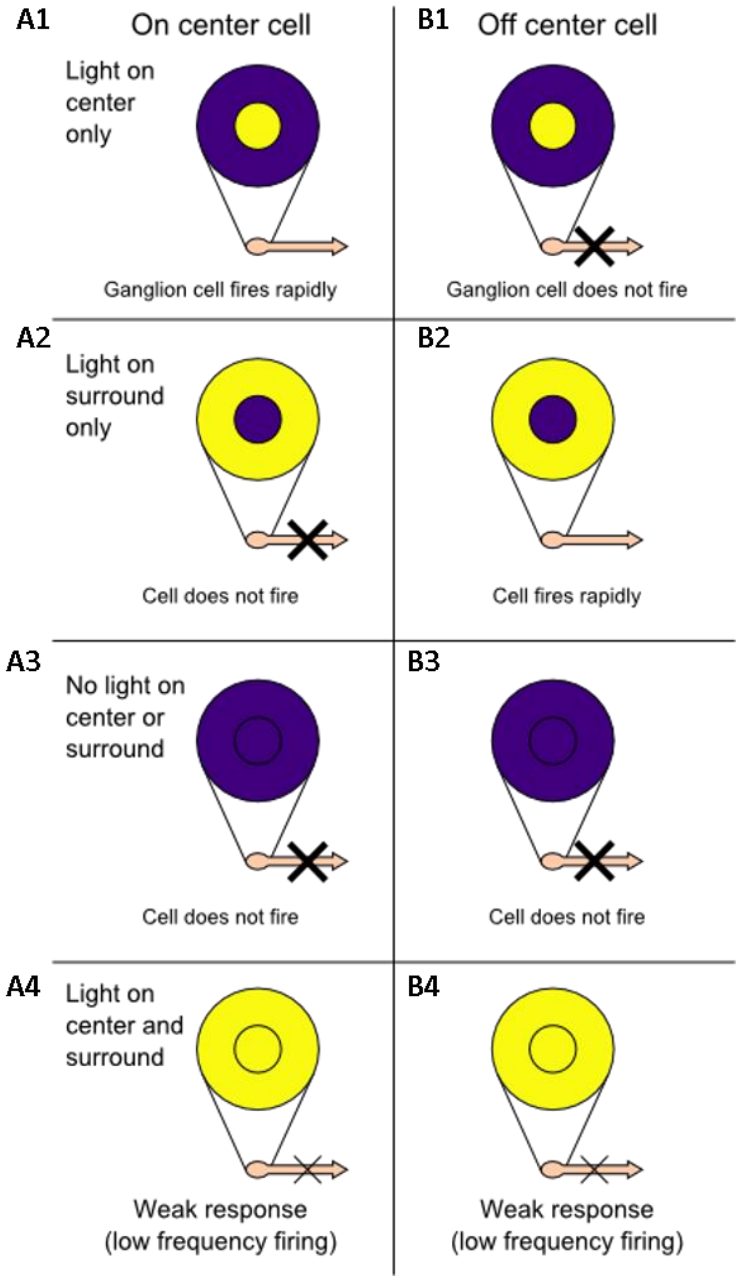

Figure 6. Schematic diagrams of center-surround receptive fields of ON-center and OFF-center RGCs.

(A1-4) Responses evoked by different combinations of center and surround illumination of ON-center RGCs. (B1-4) Responses evoked by different combinations of center and surround illumination of ON-center RGCs. (A1) A centered spot of light strongly activates ON-center RGCs. (A2) An annulus of light does not activate ON-center RGCs. (A3) Full field darkness does not activate ON-center RGCs. (A4) Full field illumination activates ON-center RGCs more weakly than a centered spot of light. (B1) A centered spot of light does not activate OFF-center RGCs. (B2) Annular illumination stimulates OFF-center RGCs. (B3) Full field darkness does not activate OFF-center RGCs. (B4) Full field illumination weakly activates OFF-center RGCs. Reproduced under a Creative Commons license from: “Receptive field”, en.wikipedia.org

VI. Lateral feedback signals in the OPL

If the retina simply transferred signals from photoreceptors to higher centers without processing, the visual images reaching our brain would remain coarse and blurry. Inhibitory feedback onto cones, bipolar cells and RGCs in the OPL and IPL helps to sharpen and enhance images by creating the center-surround receptive field arrangements described above. Of particular importance to this process is the inhibitory feedback from HCs to cones (Jackman et al., 2011; Mangel, 1991; Stroh et al., 2018; Wu, 1991).

Inhibitory feedback from HCs to cones was discovered decades ago. When researchers flashed annular light onto retina, depolarizing responses were found in cones sitting at the center of the annular region (Baylor et al., 1971; Gerschenfeld and Piccolino, 1980; Kleinschmidt and Dowling, 1975; Piccolino and Gerschenfeld, 1977; Thoreson and Burkhardt, 1990). HCs spread their dendrites far from their somas and

also communicate with neighboring HCs via gap junctions (Malchow et al., 1993). HCs thus exhibit a large receptive field. The properties of this receptive field closely matched those of the inhibitory surround in cones suggesting that the depolarizing responses in cones originated from inhibitory feedback from HCs (Baylor et al., 1971). Further evidence for hypothesis included the ability to eliminate receptive field surrounds in cones by blocking HC light responses (Gerschenfeld and Piccolino, 1980; Kleinschmidt and Dowling, 1975; Piccolino and Gerschenfeld, 1977; Thoreson and Burkhardt, 1991) and the ability to alter surround responses in RGCs by directly polarizing HCs in paired recordings (Mangel and Miller, 1987). The scenario that has emerged is that light-evoked reduction in glutamate release from cones in the receptive field surround causes HCs to hyperpolarize. This hyperpolarization reduces tonic inhibition from HCs to cones, producing a sign-inverted depolarizing signal in the central cones (Fig. 7). Lateral inhibitory feedback from HCs has also been found in rods and appears to operate by similar mechanisms to feedback from HCs to cones (Babai and Thoreson, 2009; Thoreson et al., 2008). In addition to negative feedback, HC to cone positive feedback has also been found (Jackman et al., 2011).

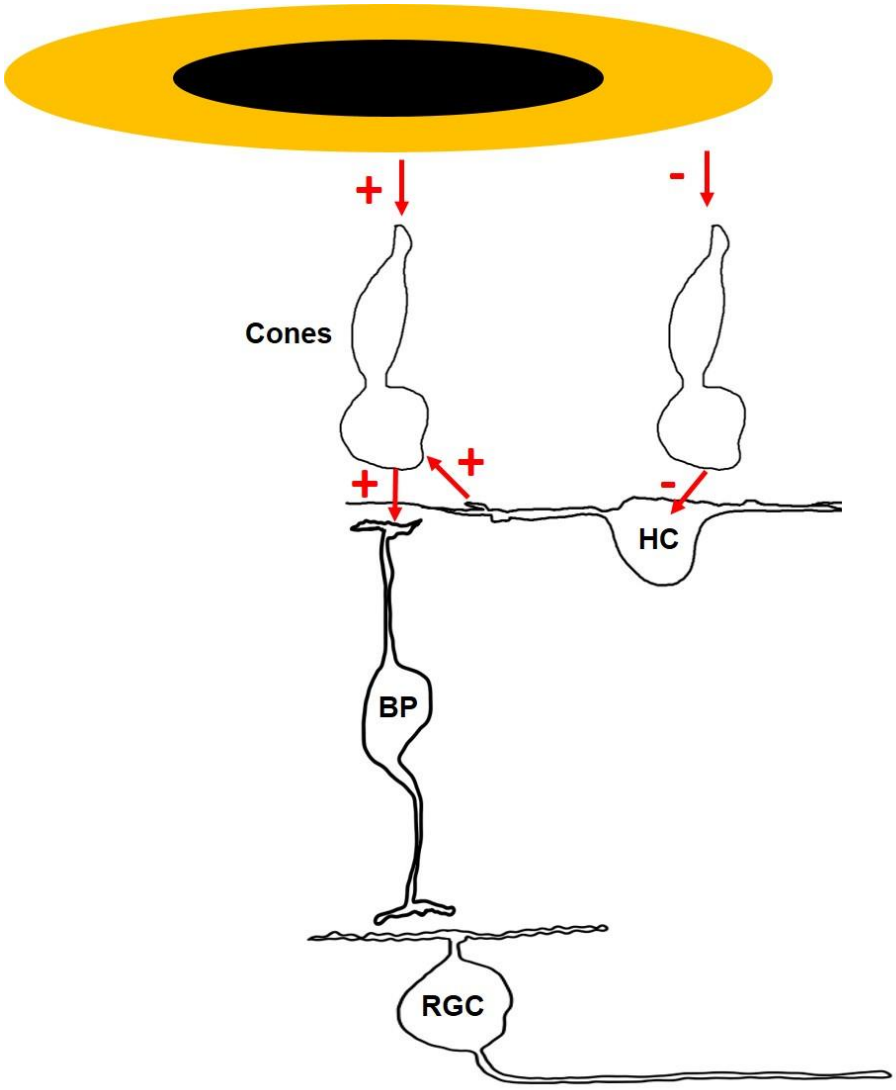

Figure 7. Schematic diagram of Lateral inhibition in center-surround receptive.

When shining an annulus light on retina, surrounding cones and HCs are hyperpolarized whereas a cone in the center of the annulus is depolarized.

The local lateral inhibitory feedback from HCs to cones creates sign-inverted center-surround receptive fields. Because of their large receptive fields, HCs integrate light intensities over a broad area of the retina. By feeding an inhibitory signal back to the cones, the response to the average, global background light intensity is subtracted.

For example, if an annular light is flashed onto the retina with a dark center, the center cones would be even more depolarized than in the condition without the annulus light. This is thought to contribute to the visual phenomenon known as Mach bands (von Bekesy, 1967), in which dark edges at a border between light and dark appear darker than dark regions further away from the border. The border between light and darkness is thus more easily detected and the object more easily identified.

In addition to edge detection and image sharpening, lateral inhibition also contributes to color detection by creating what is known as color opponency (HURVICH and JAMESON, 1957). The theory of color opponency was formally proposed by Ewald Hering in 1892 (Hering, 1964). He noted that there are several pairs of colors that cannot be perceived together, like greenish red and yellowish blue, and instead appear to be opponent to each other. Hurvich and Jameson (1957) formalized and provided quantitative evidence in support of this theory. Although different types of cones are sensitive to different regions of the spectrum, individual cones are “color blind” and respond only to the number of photons caught by their photopigments regardless of their spectral sensitivity (Baylor et al., 1987). For example, consider a cone that is particularly sensitive to red light. After absorbing a certain number of photons with moderate red light, these cones respond with a modest hyperpolarization. However, shining a strong green light onto the same red-sensitive cone, even though it is less sensitive to green light, can stimulate absorption of the same amount number of photons and thus generate the same response as the weaker red light. Therefore, cones produce a univariant response reflecting only the amount of energy they absorb. To detect differences in color, the nervous system must compare responses of different cones with differing spectral sensitivities. One way in which this is achieved is by lateral inhibition from horizontal cells (Burkhardt, 1993; SVAETICHIN and MACNICHOL, 1959). For

example, in primates, H2 type horizontal cells contact both L and S cones, but can only feedback to S cones (Packer et al., 2010). Thus, L cones which show a peak sensitivity to yellowish light send an antagonistic signal to S cones which are more sensitive to blue light, promoting the ability to distinguish blue and yellow lights. Besides the lateral inhibition between HCs and cones, the arrangement of synapses between bipolar cells ad RGCs also contributes to color opponency. For example, S cones connect only to a particular subtype of ON bipolar cells while L cones connect to both ON and OFF bipolar cells. The S cone ON bipolar cell makes synapses with a bistratified RGC at dendrites in the inner part of the IPL while L cone OFF bipolar cells connect to the same bistratified RGC at its outer arbor (Dacey and Lee, 1994). Thus, blue light can activate the S cone ON bipolar cell pathway to depolarize bistratified S-cone RGCs and yellow light can inhibit these same RGCs by stimulating the L cone OFF pathway.

Despite years of study, the mechanisms of lateral inhibition remain unsettled. Three main hypotheses have been proposed to account for HC to cone feedback. Originally, as a GABAergic neuron, HCs were thought to release GABA which opened GABA-gated chloride channels in the cone membrane. Although the expression of GABA-gated chloride channels was found in the cones of turtle and pig (Kaneko and Tachibana, 1986; Picaud et al., 1998), GABA antagonists have little (Murakami et al., 1982; Wu, 1991) or no (Piccolino, 1995; Thoreson and Burkhardt, 1990; Verweij et al., 1996; Verweij et al., 2003) effect on feedback antagonism. While GABA may play a role in modulating feedback (Kaneko and Tachibana, 1986), the inability of GABA antagonists to block feedback indicates this is not the main mechanism.

Due to the deeply invaginating structure of the triad synapses between photoreceptors and HCs (Fig. 2), ephaptic effects have been hypothesized as mechanism for generating feedback at the cone synapse (Byzov and Shura-Bura, 1986).

“Ephapse” is coined from a Greek word which means “to closely touch” (Arvanitaki, 1942). Ephapses or ephaptic synapses refer to synapses in which the voltage change is communicated across the synapse by changes in the extracellular voltage, rather than by directly altering the intracellular voltage. This differs from conventional chemical synapses as well from electrical synapses where the interiors of two neurons are connected through gap junctions. Because HCs terminate within a deep invagination in the cone terminal, the synaptic cleft may be capable of offering high electrical resistance to current flow (Dmitriev and Mangel, 2006). In the original hypothesis of Byzov et al. (1986), it was suggested that currents flowing through open glutamate receptors into HC dendrites during darkness will pass through this extracellular resistance, thereby causing the voltage within the invaginating synaptic cleft to be slightly more negative than the surrounding extracellular voltage. This extracellular negative voltage balances some of the intracellular negative membrane voltage, yield a small net trans-membrane depolarization that is sensed only in the cone terminal. Kamermans and colleagues (Kamermans et al., 2001) modified this hypothesis by proposing that instead of flowing through glutamate receptors, currents flowed through the synaptic invagination into connexin hemichannels at the tips of HC dendrites. The voltage drop, which equals a slight depolarization on photoreceptors’ membrane, activates L-type VGCCs and causes more glutamate release. Blocking hemigap junctions pharmacologically (Kamermans et al., 2001) or eliminating them from zebrafish cones appears to reduce HC to cone feedback (Klaassen et al., 2011). However, the effects of hemigap junction blockers appear to be non-specific effects of these agents (Cadetti and Thoreson, 2006; Davenport et al., 2008; Verweij et al., 1996). In mouse retina, eliminating gap junctions from HCs just reduces the receptive field of HC (Shelley et al., 2006), but does not appear to eliminate HC feedback (Kranz et al., 2013; Shelley et al., 2006). Effects of eliminating gap junctions from zebrafish HCs may due to effects on HC receptive field

organization caused by the loss of HC to HC coupling. One specific prediction of the hypothesis that tonically open gap junctions are responsible for ephaptic signal transmission is that ephaptic signals should be almost instantaneous (Blot and Barbour, 2014). However, direct measurements of the kinetics of HC to cone feedback using paired recordings showed that the kinetics of inhibitory feedback is far too slow to be due to such an ephaptic effect (Warren et al., 2016b).

The third proposed mechanism involves extracellular pH changes (Hirasawa and Kaneko, 2003; Warren et al., 2016a). Extracellular protons can block Ca^{2+} channels and alter the voltage-dependence of Ca^{2+} channels to make them less sensitive to depolarizing voltages and thus elevate their activation threshold (Zhou and Jones, 1996). In this scenario, hyperpolarization of HCs causes a negative shift of the voltage dependence of Ca^{2+} channels and increases the amplitude I_{Ca} in cones by causing the extracellular pH in the cleft to become more alkaline (Cadetti and Thoreson, 2006; Hirasawa and Kaneko, 2003). In support of this idea, HEPES and other pH buffers reversibly block inhibitory feedback, which suggests that the change in protons is required for feedback (Cadetti and Thoreson, 2006; Vessey et al., 2005). Wang et al. (2014) linked a fluorescent pH sensor to the extracellular domain of photoreceptor Ca^{2+} channels to show directly that changes in HC membrane potential caused changes in extracellular pH predicted for lateral inhibition (Wang et al., 2014). Na^+ /H^+ exchangers (NHEs) were found to be the major source of synaptic cleft protons for feedback (Warren et al., 2016a) although the pH changes during feedback are thought to be due to changes in extracellular buffering produced by the flux of bicarbonate (Liu et al., 2013a) or phosphate (Vroman et al., 2014) across the HC membrane.

A key aspect of lateral inhibitory feedback is that it alters the voltage-dependence of L-type VGCCs in photoreceptors to alter the release of glutamate (Hirasawa and

Kaneko, 2003; Verweij et al., 1996). When HCs are hyperpolarized by annular illumination, the I-V curve of cone I_{Ca} is shifted slightly to the left (in a more negative direction), increasing I_{Ca} in the cone and producing an inward feedback current (Verweij et al., 1996). Thus, there can be an increase in I_{Ca} activation even without a detectable change in the cone membrane potential. The increase in I_{Ca} triggers more glutamate release from cones. Additional Ca^{2+}-dependent changes can result from changes in Ca^{2+}-influx. Cones have both Ca^{2+}-activated chloride (Barnes and Deschenes, 1992; Kraaij et al., 2000; Packer et al., 2010; Thoreson and Burkhardt, 1991; Verweij et al., 2003) and Ca^{2+}-activated K^+ currents (Barnes and Hille, 1989). Furthermore, increases in cone I_{Ca} can stimulate glutamate release which can in turn activate glutamate transporters that are coupled to chloride channels (Arriza et al., 1997; Szmajda and Devries, 2011), providing another way for Ca^{2+} to alter membrane potential indirectly.

An outward K^+ current was found in salamander cone photoreceptors that is sensitive to TEA and Ca^{2+} (Barnes and Hille, 1989). Activation of these Ca^{2+}-activated K^+ currents would be predicted to hyperpolarize cones and thus oppose the depolarizing influence of Ca^{2+} channel activation during HC feedback. The K^+ efflux accompanying activation of Ca^{2+}-activated K^+ currents in salamander rods can also facilitate glutamate release by direct actions on I_{Ca} (Xu and Slaughter, 2005). However, depolarizing responses evoked by surround illumination were not affected by the K^+ channel blocker TEA (Thoreson and Burkhardt, 1991) suggesting that Ca^{2+}-activated K^+ currents are not likely contributed to negative feedback from HCs to cones.

Early studies showed that Ca^{2+}-activated chloride currents ($I_{Cl(Ca)}$) could be detected in the inner segments of isolated cones and rods (Bader et al., 1982; Barnes and Hille, 1989). However, a later study of isolated salamander rods found that $I_{Cl(Ca)}$ could only be detected in intact rods but not terminal-ablated rods, indicating that $I_{Cl(Ca)}$

are localized to rod terminals (MacLeish and Nurse, 2007). There is evidence for both anoctamin-1 (Ano1/ TMEM16a) (Jeon et al., 2013; Mercer et al., 2011b) and anoctamin-2 (Ano2/ TMEM16b) proteins (Dauner et al., 2013; Stohr et al., 2009) Ca^{2+}-activated chloride channels in the terminals of cones and rods. Chloride equilibrium potential (E_{Cl}) of cones appears to be close to the dark resting membrane potential (Thoreson and Bryson, 2004). When cones are hyperpolarized by light, E_{Cl} is more positive than the resting membrane potential and so $I_{Cl(Ca)}$ will tend to depolarize the cone membrane. The use of $I_{Cl(Ca)}$ antagonists reduced the feedback-induced depolarization in cones (Barnes and Deschenes, 1992; Endeman et al., 2012; Kraaij et al., 2000; Packer et al., 2010; Thoreson and Burkhardt, 1991; Verweij et al., 2003). Some of these changes may result from effects of Cl^- channel activity on feedback-induced changes in I_{Ca} that can alter the strength of feedback (Endeman et al., 2012). However, they may also suggest that Cl^- flux through $I_{Cl(Ca)}$ may contribute to feedback-induced changes in cone membrane potential.

Another chloride conductance in rods and cones are the chloride channels associated with plasma membrane glutamate transporters. Glutamate released from cones is taken back up into cones by EAAT (excitatory amino acid transporter) glutamate transporters (Arriza et al., 1997). These transporters are associated a chloride conductance so that when glutamate is retrieved, anion channels will open (Arriza et al., 1997; Szmajda and Devries, 2011). Diffusion of glutamate to neighboring cones can activate the glutamate-associated Cl^- current ($I_{Cl(Glut)}$) which depolarizes the cone to counter the reduction in I_{Ca} that occurs when cones are hyperpolarized by strong light (Vroman and Kamermans, 2015). Glutamate can also act locally on the cone from which it was released . Thus, the $I_{Cl(Glut)}$ may also contribute to Cl^- conductance in feedback.

In Chapter 4, we explore the contributions of these two chloride currents to negative feedback from HCs to cones. Our results suggest that activation of $I_{Cl(Glut)}$ by local release of glutamate makes a much larger contribution to feedback currents than has been previously recognized.

Chapter 2 Endocytosis sustains release at photoreceptor ribbon synapses by restoring fusion competence

I. Abstract:

Endocytosis is an essential process at sites of synaptic release. Not only are synaptic vesicles recycled by endocytosis, but the removal of proteins and lipids by endocytosis is needed to restore release site function at active zones following vesicle fusion. Synaptic exocytosis from vertebrate photoreceptors involves synaptic ribbons that serve to cluster vesicles near the presynaptic membrane. Here we hypothesize that this clustering increases the likelihood that exocytosis at one ribbon release site may disrupt release at an adjacent site, and therefore that endocytosis may be particularly important for restoring release site competence at photoreceptor ribbon synapses. To test this, we combine optical and electrophysiological techniques in salamander rods. Pharmacological inhibition of dynamin-dependent endocytosis rapidly inhibits release from synaptic ribbons and slows recovery of ribbon-mediated release from paired pulse synaptic depression. Visualization of single synaptic vesicles by TIRFM reveals that inhibition of endocytosis reduces the likelihood of fusion among vesicles docked near ribbons and increases the likelihood that they will retreat from the membrane without fusion. Vesicle advance towards the membrane is also reduced but the number of membrane-associated vesicles is not. Endocytosis therefore appears to be more important for restoring later steps in vesicle fusion than for restoring docking.

II. Introduction:

At presynaptic active zones, the organization of key synaptic proteins influences the efficiency of synaptic vesicle exocytosis. For example, the coupling distance between voltage-gated Ca^{2+} channels and exocytotic Ca^{2+} sensors can give rise to either

micro- or nano-domain control of exocytosis (Eggermann et al, 2011), permitting fine adjustments in release kinetics within and between cells (Johnson et al., 2017). Exocytotic fusion of synaptic vesicles results in the addition of lipids and vesicle-associated synaptic proteins to the presynaptic membrane. Compensatory synaptic vesicle endocytosis is needed to retrieve these constituents and replenish vesicle pools for ongoing synaptic transmission. Several studies have also shown that inhibition of endocytosis causes rapid changes in synaptic transmission on timescales several orders of magnitude too fast to be attributable simply to depletion of the synaptic vesicle pool (Kawasaki et al, 2000; Hosoi et al., 2009; Neher, 2010; Hua et al., 2013; Lipstein et al., 2013; Mahapatra et al., 2016). This implies that endocytosis also plays a key role in homeostasis of the presynaptic active zone by regulating the availability and arrangement of key presynaptic proteins and clearing the active zone of used vesicle fusion machinery (Neher 2010, 2017). When studied at conventional synapses, this role for endocytosis is evident at high stimulation frequencies of 100 Hz or greater (Lipstein et al., 2013) and may set an upper limit to release rates (Neher, 2017).

Rapid synaptic transmission by rods and cones involves synaptic ribbons, protein structures that tether multiple vesicles near the presynaptic membrane and prepare them for exocytosis (LoGiudice and Matthews, 2009; Schmitz, 2009). Rapid, ribbon-mediated exocytosis in photoreceptors is exquisitely sensitive to Ca^{2+} - a result of low cooperativity and high affinity for Ca^{2+} in the exocytotic sensor together with nanodomain coupling between Ca^{2+} channels and the synaptic vesicle release machinery (Thoreson et al., 2004; Mercer et al., 2011b; Van Hook and Thoreson, 2015). This leads to highly efficient coupling between presynaptic Ca^{2+} influx and vesicle exocytosis so that the opening of only a handful of Ca^{2+} channels - <3 in cones and <5 in rods - are needed to release a single synaptic vesicle (Bartoletti et al., 2011; Van Hook and Thoreson, 2015).

Hexagonal arrays of vesicles are tethered to photoreceptor ribbons, with the bottom two rows contacting the plasma membrane (Lasansky, 1978; Thoreson et al., 2004; Jackman et al., 2009). The number of vesicles in these bottom two rows corresponds to the size of the physiologically-defined readily releasable pool of vesicles that is released in a synchronous burst by strong depolarizing stimulation (Bartoletti et al., 2010). Neighboring vesicles on the ribbon are separated by as little as 10 nm (Lasansky, 1978; Thoreson et al., 2004). We reasoned that because of the dense packing of vesicles and tight spatial coupling of vesicles and Ca^{2+} channels, addition of lipids and proteins to the presynaptic membrane from the fusion of a synaptic vesicle might impair the release of a neighboring vesicle, making ribbon-mediated synaptic vesicle exocytosis particularly sensitive to disruption of release site function when endocytosis is inhibited.

In this study, we tested the hypothesis that efficient synaptic transmission by rod photoreceptor requires endocytosis to restore the structural and functional integrity of the presynaptic active zone. This was accomplished by using multiple complementary measures of synaptic function after inhibiting dynamin-dependent endocytosis in rod photoreceptors from tiger salamander retina. Use of large salamander rods allowed us to combine a number of optical and electrophysiological techniques including internal reflection fluorescence microscopy (TIRFM) of vesicle behavior and whole-cell patch-clamp electrophysiology. We focused on rods because ultrafast endocytosis is more effectively inhibited by use of dynamin inhibitors in rods than cones (Van Hook and Thoreson, 2012). Synaptic transmission from rods involves fast release from ribbons, amplified by slower release at ectopic sites away from synaptic ribbons driven by Ca^{2+}-induced Ca^{2+} release from intracellular stores (Krizaj et al., 1999; Suryanarayanan and Slaughter, 2006; Cadetti et al., 2006; Babai et al., 2010; Chen et al., 2013; Chen et al., 2014). We found that inhibition of dynamin-dependent endocytosis slowed recovery of

ribbon-mediated release from synaptic depression. TIRFM techniques provided insights into the behavior of individual synaptic vesicles. In control rods, newly arriving vesicles typically fused soon after descending the ribbon and membrane-associated vesicles at the ribbon base rarely retreated without fusion. After inhibiting endocytosis, vesicles approaching a ribbon were less likely to fuse and membrane-associated vesicles were more likely to retreat. Inhibiting endocytosis also impaired advance of vesicles towards the membrane, but did not impair membrane attachment. These results suggest that endocytosis is more important for restoring functionality of proteins that participate in late stages of vesicle release than in early docking steps. By maintaining the functional organization of the presynaptic active zone, endocytosis is critical for allowing rods to maintain release from ribbon synapses.

III. Materials and Methods

a. Animal care and use

Aquatic tiger salamanders (Ambystoma tigrinum, 18 to 25 cm; Sullivan Company, Nashville, TN, USA) were maintained on a 12-h light/dark cycle and sacrificed after $\geq$1 h of dark adaptation. Salamanders were anaesthetized by immersion in 0.25 g/L Tricaine-S (tricaine methanesulfonate, Western Chemical, WA, USA) for >15 min, decapitated with heavy shears, and then pithed. Procedures were approved by the University of Nebraska Medical Center Institutional Animal Care and Use Committee.

b. Retinal slices

A detailed description of retinal slice preparation and whole cell recording

techniques has been published previously (Van Hook and Thoreson, 2013). Briefly, after enucleation, the front of the eye was removed and the resulting eyecup was cut into 2-4 pieces. A piece of retina was placed vitreal side down on a piece of nitrocellulose membrane (5 x 10 mm; type AAWP, 0.8 μm pores; EMD Millipore). The filter paper was then submerged in cold amphibian saline and the sclera peeled away, leaving the retina attached to the membrane. The retina was cut into 125-μm slices using a razor blade tissue slicer (Stoelting Co, Wood Dale, IL, USA). Slices were rotated 90 degrees to view retinal layers and anchored in the recording chamber by embedding the ends of the nitrocellulose membrane in vacuum grease. For light response experiments, slice preparation was performed in darkness using GenIII image intensifiers (Nitemate NAV3, Litton Industries, Tempe, AZ, USA) mounted on a dissecting microscope. For recording, the recording chamber was mounted on an upright fixed-stage microscope (Olympus BH2-WI, Shinjuku, Tokyo, Japan) and slices were superfused at ~1 ml min^{-1} at room temperature with oxygenated normal amphibian saline solution containing (in mM): 116 NaCl, 2.5 KCl, 1.8 $CaCl_2$, 0.5 $MgCl_2$, 5 glucose, and 10 HEPES (pH 7.8).

c. Patch-clamp electrophysiology

Patch pipettes were fabricated with borosilicate glass (1.2 mm OD, 0.9 mm ID, with an internal filament; World Precision Instruments, Sarasota, FL, USA) using a PC-10 or PP-830 vertical puller (Narishige, Tokyo, Japan). Patch pipettes had tip diameters of ~1 μm and resistances of 10-15 MΩ.

The pipette solution for rods contained (in mM) 50 Cs-gluconate, 40 Cs-glutamate, 10 TEA-Cl, 3.5 NaCl, 1 $CaCl_2$, 1 $MgCl_2$, 10 ATP-Mg, 0.5 GTP-Na, 10 HEPES, and 5 EGTA. The addition of glutamate to the presynaptic pipette solution enhances

post-synaptic currents in HCs during paired whole-cell recording (Bartoletti and Thoreson, 2011). The pipette solution for HC pipettes was identical except that the 40 mM Cs-glutamate was replaced with 40 mM Cs-gluconate. Reported voltage values were not corrected for a liquid junction potential of 13 mV.

Synaptic transmission was monitored using paired whole-cell recordings from rods and HCs using a Multiclamp 700A amplifier, pClamp 10.5 software, and Digidata 1550 digitizer (Molecular Devices, Sunnyvale, CA, USA). Rods were identified by their morphology. HCs were identified by their morphology, position in the slice, and electrophysiological characteristics (Van Hook and Thoreson 2013). HCs were voltage-clamped at -60 mV and rods at -70 mV. Synaptic vesicle exocytosis from rods was evoked by steps to -10 mV. For measurements of the presynaptic rod Ca^{2+} current (I_{Ca}), leak and capacitative currents were subtracted using a P/8 leak subtraction protocol. We waited at least 1 min between trials to allow recovery.

Rod-driven excitatory post-synaptic currents (EPSCs) involve both fast and slow components. The fastest component involves release from ribbons while the slower component involves non-ribbon release triggered by calcium-induced calcium release (CICR) as well as release from neighboring rods that can be stimulated by spread of depolarizing current through gap junctions (Chen et al., 2014). To minimize release from neighboring rods, trials were performed in the presence of bright white light to hyperpolarize the rod network (Van Hook and Thoreson, 2015).

d. Reagents

3- and 10-kDa dextran-conjugated AlexaFluor488 were obtained from Molecular Probes (Invitrogen, Carlsbad, CA, USA). Unless otherwise noted, other reagents were

from Sigma-Aldrich Chemicals (St. Louis, MO, USA).

e. Photoreceptor isolation

For studies on isolated cells, after cutting the eyecup into 4 pieces, the retina was isolated in Ca^{2+}-free, high-Mg^{2+} amphibian saline consisting of (in mM): 116 NaCl, 2.5 KCl, 5 $MgCl_2$, 5 glucose, and 10 HEPES (pH 7.4). Retinal pieces were incubated with 30 units/ml papain (Worthington, Lakewood, NJ, USA) in this Ca^{2+}-free high-Mg^{2+} saline solution for 35 min at room temperature after activating papain with 0.2 mg/ml cysteine. To terminate digestion, retinal pieces were transferred to ice-cold Ca^{2+}-free high-Mg^{2+} saline supplemented with 1% bovine serum albumin for 3 min. Retinal pieces were washed an additional 3 min in ice-cold Ca^{2+}-free high-Mg^{2+} saline and then incubated in ice-cold Ca^{2+}-free high-Mg^{2+} saline containing DNase (4000 u/ml; Worthington, Lakewood, NJ, USA) for another 5 min. Photoreceptors were isolated by gently triturating retinal pieces ~10 times through the tip of a fire-polished, bent Pasteur pipette. The resulting cell suspension was transferred onto glass coverslips that had previously been coated with 3.5 μg/cm^2 Cell-Tak (BD Biosciences, San Jose, CA, USA) and allowed to settle for 20 min. For QD experiments, we used standard #1 glass coverslips (Warner Instruments, Hamden, CT, USA). For TIRFM experiments, we used sapphire coverslips with a refractive index of 1.78 (Olympus, Shinjuku, Tokyo, Japan).

f. TIRFM experiments

TIRFM experiments were performed as described previously (Chen et al., 2013; Wen et al., 2017). A solid-state laser (561 nm; Melles Griot, Rochester, NY, USA) was focused off-axis through the objective (100X, 1.65 N.A., oil immersion, Olympus) so that

the beam underwent total internal reflection at the interface between the coverslip and the overlying cell membrane or aqueous solution. We used an incident angle of ~60 deg that generates an evanescent wave with length constants of ~65 nm and ~57 nm for 561 and 488 nm lasers, respectively (Chen et al., 2013; Wen et al., 2017). Fluorescence emission was collected through 609 nm bandpass filters (54 nm wide, Semrock, Rochester, NY, USA) and 525 nm bandpass filters (45 nm wide, Semrock) using an EMCCD camera (Hamamatsu) at 40 ms/frame with a pixel size of 80 nm/pixel.

To load synaptic vesicles of rods with fluorescent dye, tissue was dissected and retinas were isolated in darkness using GenIII image intensifiers (Nitemate NAV3, Litton Industries, Tempe, AZ, USA) mounted on a dissecting microscope. Maintaining retinae in a dark-adapted state keeps photoreceptors at a depolarized resting membrane potential of ca. -40 mV and thus promotes vesicle cycling. Retinal pieces were incubated with either 3-kDa AlexaFluor488 (400 µg/ml) for 1.5 min or 10-kDa AlexaFluor488 (500 µg/ml) for 3 min. We have found that the lower background membrane staining observed with fluid phase indicators compared to lipophilic dyes such as FM1-43 yields a better signal-to-noise ratio (Chen et al., 2013). Use of short incubation times loads only a small percentage of vesicles (Chen et al., 2013; Wen et al., 2017).

For some TIRFM experiments, synaptic vesicle release was stimulated by depolarizing rod terminals with a 2-s puff of 50 mM KCl. For puff application, a glass patch pipette was filled with 50 mM KCl amphibian saline (in mM: 68.6 NaCl, 50 KCl, 1.8 $CaCl_2$, 0.5 $MgCl_2$, 5 glucose, 10 HEPES, pH 7.8) and connected to a pressure valve system (Toohey Company, Fairfield, NJ, USA; 8 psi). The tip of the puffer pipette was positioned 10-20 µm away from rod terminals. For other experiments, we stimulated release by applying depolarizing voltage steps (-70 to -10 mV, 100 ms) to voltage-clamped, isolated rods. In some, we also introduced a Ribeye-binding peptide

(tetramethylrhodamine -EQTVPLDLSKRDR; Biomatik, Wilmington, DE, USA) conjugated to tetramethylrhodamine (50 μM) through the pipette (Zenisek et al., 2004; Francis et al, 2011). We measured the distance from the center of each vesicle to the edge of the nearest ribbon. We constructed the relative frequency histogram of events using a bin size of 350 nm, matching the optical point spread function measured with this objective (Chen et al., 2013). We calculated the radial density distribution using the following formula:

Equation 3: $$d(r) = N(r)/\pi[\left(r + \frac{n}{2}\right)^2 - \left(r - \frac{n}{2}\right)^2]$$

where r is the radial distance to the center of each bin, n is the bin size (350 nm), and N(r) is the number of events in each bin.

Data were acquired and analyzed using MetaMorph software. Only vesicles showing a signal-to-noise ratio 4 times more than the peak-to-peak baseline noise within a 7x7 pixel region of interest were selected for analysis. As described in detail elsewhere (Chen et al., 2013; Wen et al., 2017), kinetic differences between vesicle appearance during advance and vesicle disappearance were used to distinguish release events from non-release events where vesicles depart the membrane without fusion. If a vesicle departs without fusion, then its fluorescence should decline at a rate similar to the increase in fluorescence that accompanies advance of the vesicle towards the membrane as it moves through the exponentially increasing evanescent field. If a vesicle fuses and releases its contents, then its fluorescence will decline almost instantaneously. To be defined as a release event, we required that vesicle fluorescence fall to <40% of the original peak fluorescence in the first 40 ms frame during the decline phase and to baseline levels by the second frame (Chen et al., 2013). Fusion events that fulfill these criteria showed release kinetics matching those measured by capacitance

techniques and were blocked by Co^{2+} or Cd^{2+}, confirming that a majority of these events were due to Ca^{2+}-dependent release (Chen et al., 2013; Wen et al., 2017; present results).

g. Statistical Analysis

Most statistical analyses were performed using GraphPad Prism 4.0 (GraphPad Software, La Jolla, CA, USA) and results are presented as mean ± standard error of the mean (SEM). Z-tests were performed using an on-line calculator (http://www.socscistatistics.com/tests/ztest_sample_mean).

IV. Results

a. Paired pulse depression is extended by inhibiting endocytosis

Ultrafast endocytosis can be blocked by dynasore in cones (Van Hook and Thoreson, 2012). If inhibition of endocytosis impairs clearance of ribbon release sites and thereby disrupts active zone function, then this should impair replenishment of the releasable vesicle pool. Impaired replenishment should in turn result in slower recovery from paired pulse depression of fast, ribbon-mediated EPSCs at rod synapses (Rabl et al., 2006; Innocenti and Heidelberger, 2008). We tested this prediction by applying pairs of depolarizing pulses (100 ms) separated by varying interpulse intervals to rods while recording EPSCs from a simultaneously voltage-clamped HC. The paired pulse protocol is illustrated for a control rod/HC pair in Figure 8A. We focused primarily on the fast, ribbon-mediated component of release (arrows, Fig. 8). At the beginning of the trial, the readily releasable pool of vesicles at the ribbon base was emptied by applying a brief

depolarizing pulse (100 ms to -10 mV) to the rod. In this control cell pair, after waiting 0.5 s, the same test pulse evoked a fast, ribbon-mediated component that was ~40% of the original response, indicating that ~40% of the readily releasable pool had recovered within that 0.5 s interval. We tested effects of three different dynamin inhibitors on recovery from paired pulse depression: dynasore (80 μM; Fig. 8B); a more potent dynasore analog, dyngo-4A (30 μM, Abcam; Fig. 8C; McCluskey et al., 2013); and a peptide that inhibits dynamin-dependent endocytosis by binding to a proline rich region of dynamin (1 mM, QVPSRPNRAP, Tocris; Fig. 8D; Grabs et al., 1997; Jockusch et al., 2005). To avoid the potential for post-synaptic effects, we introduced these inhibitors into individual rods through the presynaptic patch pipette. To allow sufficient time for compounds to diffuse from the patch pipette to the synapse, we waited at least 7 minutes after rupturing before beginning measurements (Van Hook and Thoreson, 2014). With all three dynamin inhibitors, there was significantly less recovery of the fast, ribbon-mediated component of release compared to control after an interpulse interval of 0.5 s (vehicle control [0.1% DMSO], N=10; dynasore, N=15, P=0.0082, unpaired t-test; dyngo-4A, N=10, P = 0.0025; dynamin inhibitory peptide, N=7, P=0.0029). Dynamin inhibitory peptide also significantly reduced recovery after 1 s interpulse intervals (P=0.0195) but effects of dyngo-4A (P=0.0565) and dynasore (P=0.1454) did not attain statistical significance.

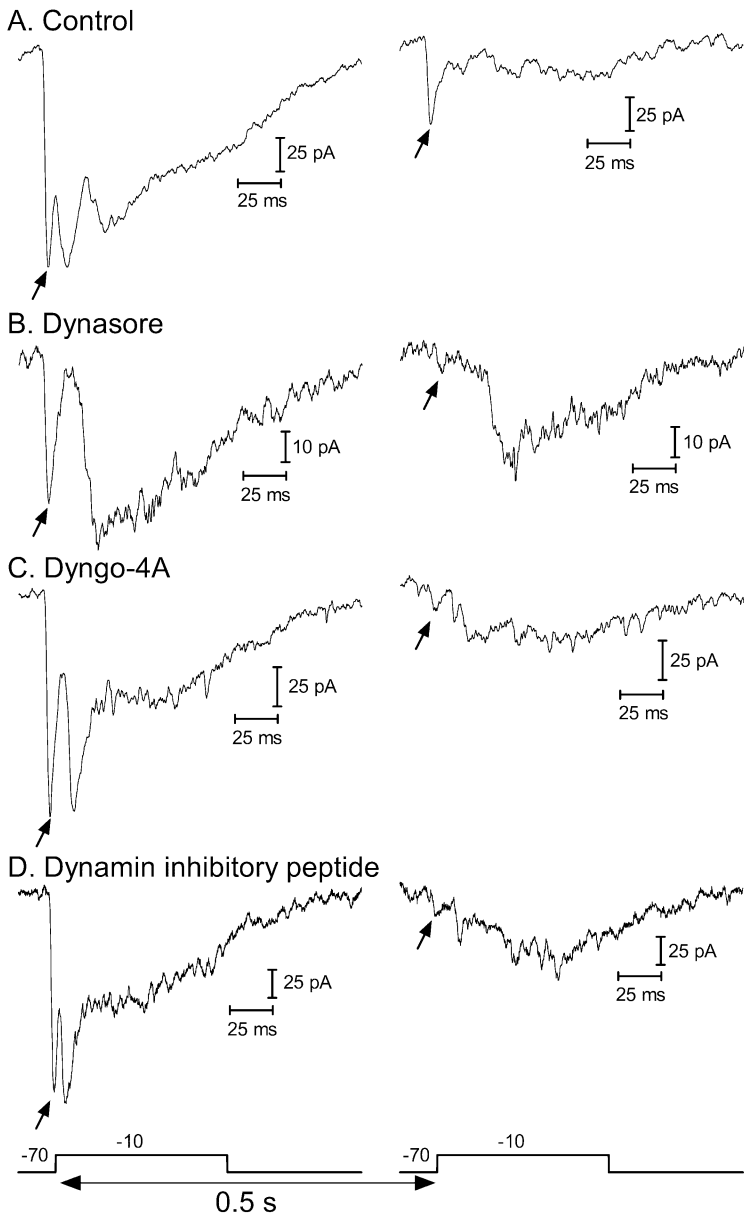

Figure 8. Examples of recovery from paired pulse depression of EPSCs evoked in HCs by depolarizing steps (-70 to -10 mV, 50 ms) applied to simultaneously voltage-clamped rods.

In the left column are initial control EPSCs and in the right column are the EPSCs evoked after an interpulse interval of 500 ms. The stimulus protocol is illustrated at the bottom of the figure. (A) The fast, ribbon-related component (arrows) of the EPSC in this vehicle control (0.1% DMSO) rod/HC pair recovered by ~40% after a 500 ms interval.

(B) HC EPSCs from a different rod/horizontal cell pair after introducing dynasore (80 μM) into the presynaptic rod through a patch pipette. After introducing dynasore into the rod, the fast EPSC component (arrow) showed less recovery after 0.5 s than in the control response illustrated in A. (C) The fast EPSC component recorded from a voltage-clamped HC also showed little recovery with an interpulse interval of 0.5 s after dyngo-4A (30 μM) was introduced into a rod through a patch pipette. (D) Similar to the other inhibitors, the fast HC EPSC showed little recovery with an interpulse interval of 0.5 s after dynamin inhibitory peptide (1 mM) was introduced into a rod through a patch pipette.

We varied the interpulse interval to measure the rate at which EPSCs recovered. This recovery is largely due to vesicle replenishment (Rabl et al., 2005). Recovery of fast, ribbon-mediated EPSCs was fit with a double exponential function (Fig. 9A). For clarity, data obtained with shorter interpulse intervals are replotted in Fig. 9B at higher magnification; data points for dyngo-4A were also nudged by +0.1 s in Fig. 9B to avoid overlap. Under control conditions, the fast time constant for recovery from paired pulse depression averaged 618 ms (Fig. 9A-B), similar to fast time constants for recovery from paired pulse depression of ribbon-mediated release at salamander cone ribbon synapses (663-815 ms; Van Hook et al., 2014; Thoreson et al., 2016). The fast time constant for recovery from paired pulse depression of ribbon-mediated EPSCs slowed from 618 ms to 2.5 s after introducing dynasore into presynaptic rods (Fig. 9A-B). Introducing the more potent inhibitor dyngo-4A or dynamin inhibitory peptide slowed recovery further to 3.2 s and 3.1 s, respectively (dyngo-4A, $P<0.001$, F-test; dynamin inhibitory peptide, $P=0.0003$). While dynasore and its analog dyngo-4A may have effects on other mechanisms (Douthitt et al., 2011; Park et al., 2013; Girard et al., 2011; Preta et al., 2015), these are not likely to be shared with the dynamin inhibitory peptide and so

the finding that all three inhibitors produced similar effects argues that the slowing of replenishment was due to inhibition of dynamin-mediated endocytosis.

We also examined recovery from paired pulse depression for slower EPSC components that are largely due to non-ribbon release. When there was not a distinct second peak in the EPSC, we measured the average amplitude of the EPSC at the end of the test step. Recovery from paired pulse depression of slow EPSC components was fit with a single exponential. Time constants for recovery did not differ significantly between rods treated with vehicle control, dynasore, dyngo-4A, or dynamin inhibitory peptide (Fig. 9C). Thus, unlike fast ribbon-mediated release, the recovery of slow release was not prolonged by inhibition of endocytosis.

Presynaptic I_{Ca} charge transfer (Q_{Ca}) showed a modest paired pulse facilitation and not paired pulse depression with short interpulse intervals. Changes in Q_{Ca} were similar in both control and test conditions (Fig. 9D). The absence of any significant effects of dynasore, dyngo-4A, or dynamin inhibitory peptide on paired pulse measurements of I_{Ca} indicates that effects on paired pulse recovery of EPSCs were not secondary to changes in Ca^{2+} influx (Babai et al., 2010; Van Hook et al., 2014).

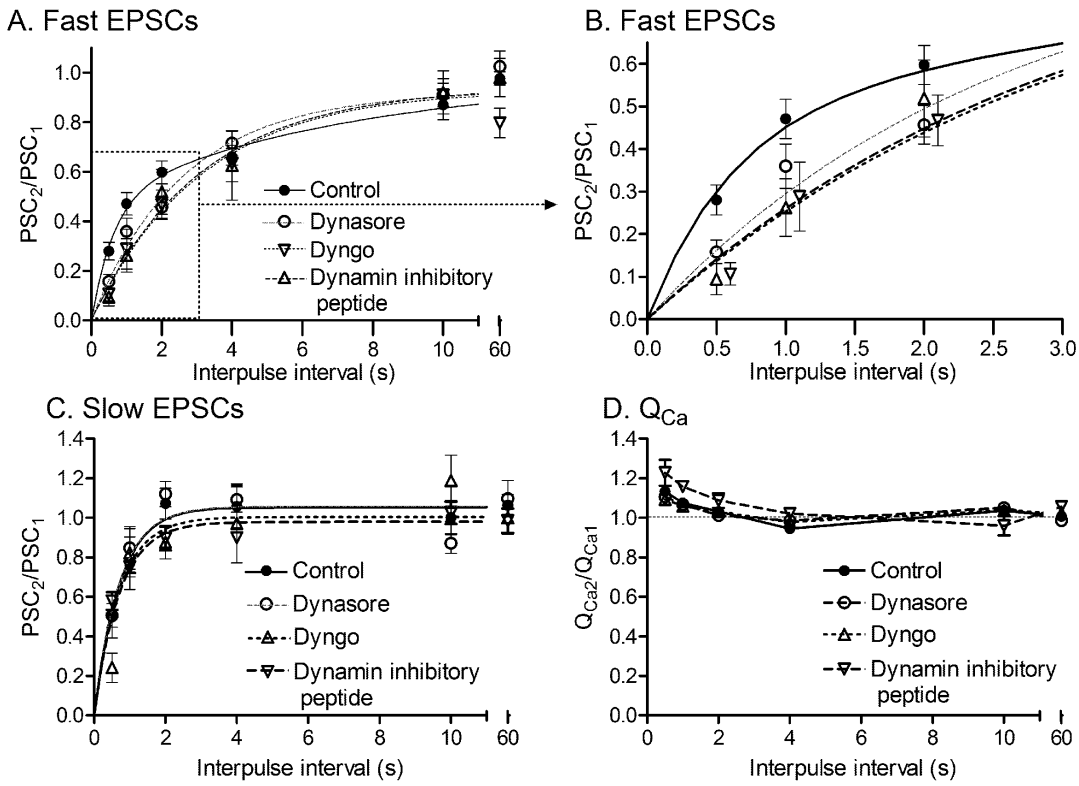

Figure 9. Recovery from paired pulse depression of fast HC EPSCs was slowed by inhibiting endocytosis with dynasore, dyngo-4A, or dynamin inhibitory peptide.

(A) Recovery from paired pulse depression of the fast EPSC component plotted as a function of interpulse interval (control, filled circles, N=11 pairs; dynasore, open circles, 80 μM, N=15 pairs; dyngo-4A, downward-pointing triangles, 30 μM, N=10; dynamin inhibitory peptide, upward-pointing triangles, 1 mM, N=7). The amplitude of the second EPSC was normalized to the first EPSC in each pair. Recovery of the fast EPSC component was fit with a double exponential function. The recovery observed with shorter interpulse intervals is re-plotted in panel B with the data points for dyngo-4A offset by 0.1 s from the others for ease of comparison. In control conditions, the fast time constant for recovery from paired pulse depression averaged 618 ms (solid lines, filled circles), slowing to 2.52, 3.24, or 3.06 s, respectively, in recordings where dynasore (dashed lines, open circles), dyngo-4A (dotted lines, downward triangles), or dynamin inhibitory peptide (long dashes, upward triangles) were included in the rod patch pipette solution. The fast time constants obtained with dyngo-4A ($P<0.001$; F-test) and dynamin inhibitory peptide ($P=0.0003$, F-test) were significantly slower than control. (C) Recovery

from paired pulse depression of slow EPSC components was fit with a single exponential function. Time constants did not differ significantly among the four conditions (control: 732 ms; dynasore: 635 ms; dyngo-4A: 1056 ms; dynamin inhibitory peptide, 584 ms; P=0.25, F-test). (D) Paired pulse responses of I_{Ca} charge transfer (Q_{Ca}) showed a slight enhancement with short intervals and no paired pulse depression. Paired pulse responses of Q_{Ca} also did not differ among the four conditions.

b. TIRFM imaging of single vesicles

The finding that inhibition of endocytosis slowed recovery of fast, ribbon-mediated responses from paired pulse depression suggests that it slowed the rate of vesicle replenishment at ribbon release sites. Slowing of replenishment can be caused by deficits in the delivery of vesicles to the membrane, docking, priming, or fusion. To distinguish various steps in the vesicle cycle, we examined the behavior of individual fluorescently-labeled vesicles using TIRFM. We loaded synaptic vesicles in rod terminals with the fluid phase indicators AlexaFluor488 conjugated to either 3-kDa or 10-kDa dextran (Chen et al., 2013; Wen et al., 2017). We loaded retinas in darkness to maintain rods in a depolarized state and thereby promote vesicle turnover. We incubated retinas with dye for only a few minutes to limit dye loading to a small percentage of vesicles and thus ensure that fluorescent spots in synaptic terminals were likely to be individual vesicles rather than clusters of vesicles (Chen et al., 2013). Dye-loaded rods were dissociated and plated on coverslips for TIRFM imaging. Where the cell membrane contacts the glass, evanescent illumination creates a faint fluorescent footprint in which one can see individual dye-loaded vesicles at or near the membrane.

With TIRFM, fluorescence of a vesicle rises as it approaches the membrane, advancing through the exponentially-increasing evanescent field of illumination at the interface between the membrane and the coverslip (Fig. 10A-D). This is illustrated by the

examples in Figures 10A and B which show image sequences (40 ms/frame) for single vesicles. Fluorescence changes measured within 7x7 pixel regions of interest are plotted as a function of time in Figures 10C and D. After reaching the membrane and attaining maximal brightness, there are three possible fates for a vesicle: remain at the membrane surface, retreat from the membrane without fusion, or fuse with the plasma membrane. After fusion and release of intravesicular dye, vesicle fluorescence should decline abruptly, as illustrated by the image sequence of Figure 10A and associated graph in Figure 10C. On the other hand, if a vesicle retreats from the membrane without fusion, its fluorescence should decline at roughly the same rate as it increased during membrane approach. This is illustrated by the example images in Figure 10B and graph in Figure 10D. Finally, vesicles can also remain stably associated with the membrane for many seconds. Vesicles in salamander rods average 45 nm in diameter (Thoreson et al., 2004) and so the evanescent field with a length constant of 65 nm (Chen et al., 2013) extends only about two vesicle diameters into the cell. In some ultrastructural studies, vesicles lying within two diameters of the membrane are defined as being docked (Verhage and Sørensen, 2008). Many of the membrane-associated vesicles visible by TIRFM ultimately went on to fuse with the plasma membrane and therefore also met functional criteria for being docked. Figure 10E shows an example of a vesicle that was stably associated with the membrane at the beginning of a trial and then fused, causing its fluorescence to decline abruptly. Other membrane-associated vesicles retreated from the membrane without fusion, marked by a more gradual decline in fluorescence (Fig. 10F). These data suggest that not all membrane-associated vesicles complete the docking process, but for the sake of brevity, we sometimes refer to membrane-associated vesicles as being “docked” in the text below.

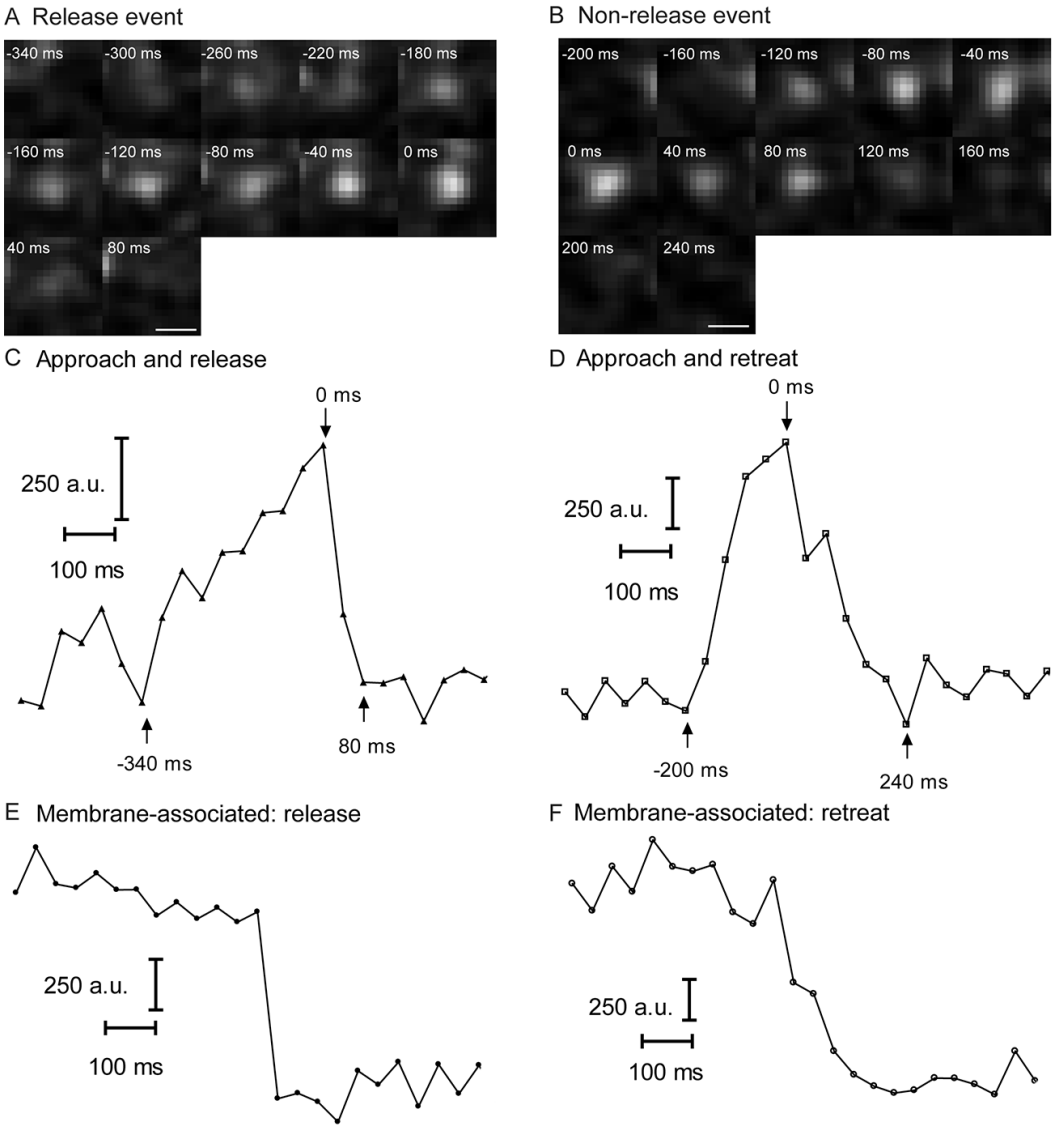

Figure 10. Behavior of individual vesicles visualized using TIRFM.

(A) Sequence of images (40 ms/frame) showing a single vesicle loaded with 10-kDa AlexaFluor488 as it approached the membrane and then fused. (B) Image sequence showing a vesicle that approached the membrane and then departed without fusion. Scale bars: 0.5 µm. (C) Changes in fluorescent brightness as a function of time plotted for a 7x7 pixel region of interest centered on the vesicle in A. Brightness increased as the vesicle approached the membrane and then declined abruptly after dye was released by fusion. Graph plots the fluorescence changes measured at -340 ms to +80 ms (arrows). (D) Changes in fluorescent brightness as a function of time for the vesicle in B. As the vesicle retreated from the membrane, its brightness declined at roughly the same rate as it

increased during membrane approach. Graph plots the fluorescence changes measured at -200 ms to +240 ms (arrows). (E) Fluorescence changes as a function of time from a vesicle that was stably associated with the membrane and then fused, causing its fluorescence to decline abruptly. (F) Fluorescence changes from a vesicle that was stably associated with the membrane but then departed without fusion, showing a gradual decline in fluorescence. These examples are all from rods loaded with 10-kDa AlexaFluor488.

To be defined as a release event, we required that vesicle fluorescence decline by at least 60% from peak fluorescence in the first frame of the decline phase and fall to baseline levels by the second frame (Chen et al., 2013; Wen et al., 2017). Figure 11A shows a sequence of images averaged from 16 fusion events. The fluorescence intensity measured in a 7x7 pixel region centered on the average vesicle is plotted in Figure 11C and shows a rapid decline in intensity following fusion. Consistent with earlier results from rods using this technique (Chen et al., 2013; Wen et al., 2017), average non-release, retreat events (N=20) showed a slower decline in fluorescence (Fig. 11B-C) than fusion events. If dye particles are free to diffuse, then they should exit the small measurement region within ~1 ms (Wen et al., 2017). However, faint fluorescence persisted in this central region for 160 ms after fusion (Fig. 11C). This may reflect persistence of sticky, dextran-conjugated dye molecules in the restricted sub-membrane space beneath the release site. Residual fluorescence might also involve contributions from vesicles docked further away from the membrane (e.g., up the ribbon) at the edge of the evanescent field. The average image of vesicles that retreated from the membrane without release showed a slightly more pronounced residual, central fluorescence suggesting the presence of a vesicle lingering at the edge of the evanescent field (Fig. 11B). This fluorescence might come from a vesicle that did not fully exit the evanescent field after retreating from the membrane or it might come from

an entirely different vesicle sitting further up the ribbon. Similar to results observed for vesicles loaded with 10-kDa pHrodo (Chen et al., 2013), fusion events defined by these criteria for vesicles loaded with 3-kDa AlexaFluor488 were increased by stimulation with depolarizing steps (-70 to -10 mV, 100 ms) applied to voltage-clamped, isolated rods (Fig. 11D). Vesicles that disappeared more slowly and did not fulfill these criteria were defined as non-release, retreat events. The frequency of non-release events did not appear to be increased by depolarizing stimulation (Fig. 11E).

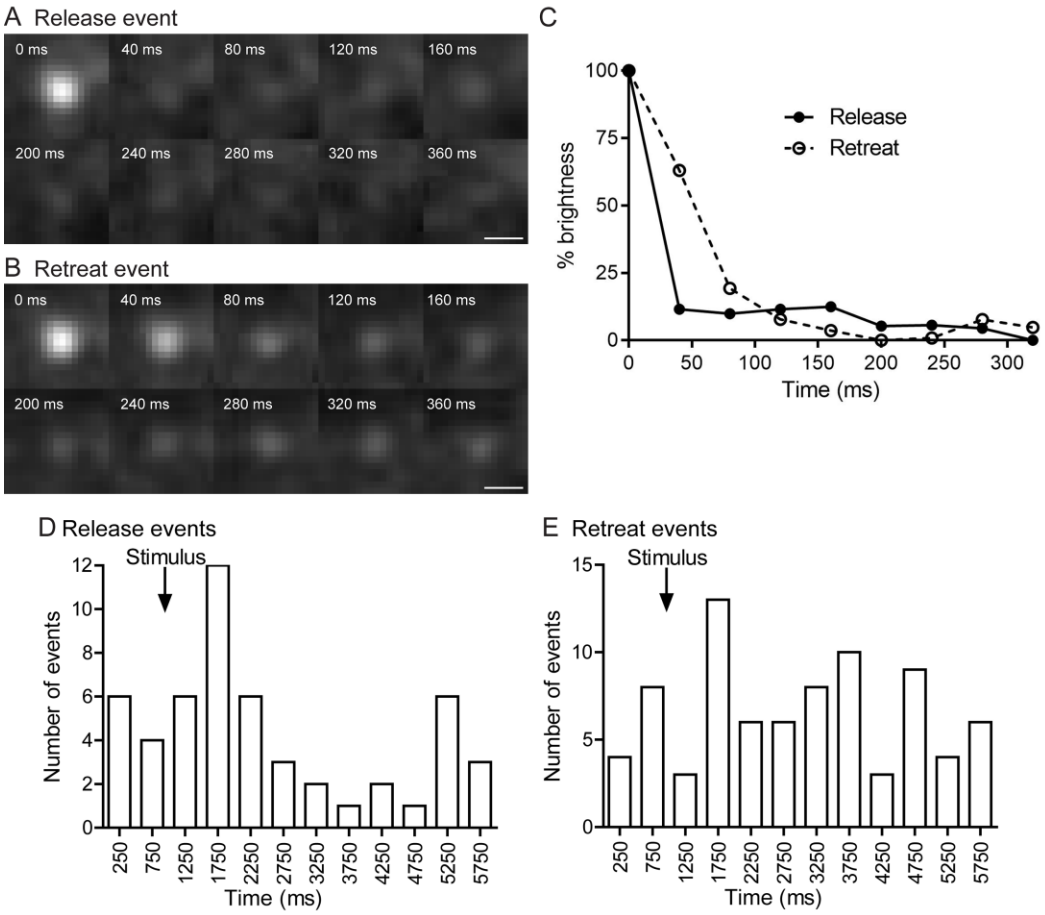

Figure 11. Average vesicle behavior visualized by TIRFM.

(A) Sequence of images (40 ms/frame) showing release events averaged from 16 vesicles. (B) Sequence of images (40 ms/frame) showing non-release, retreat events averaged from 20 vesicles. Scale bars: 0.5 µm. (C) Changes in fluorescent brightness as

a function of time measured within a 7x7 pixel region of interest centered on the vesicles in A and B. Brightness declined much more rapidly after fusion than when vesicles retreated from the membrane without fusion. (D) Histogram plotting the number of release events before and after application of a depolarizing step (-70 to -10 mV, 100 ms applied at 1 s) to voltage-clamped rods (52 events in 7 rods). (E) Histogram plotting the number of non-release, retreat events before and after application of a depolarizing step (-70 to -10 mV, 100 ms) to voltage-clamped rods (80 events in 7 rods). For experiments in this figure, rods were loaded with 3-kDa AlexaFluor488.

We compared vesicle behavior in rods during bath application of dynasore or vehicle control (0.1% DMSO) solution. We first examined the origins and fates of synaptic vesicles during 6 s trials with vesicles loaded with either 3-kDa AlexaFluor488 (Fig. 12A) or 10-kDa AlexFluor488 (Fig. 12B). In this experiment, synaptic release was stimulated by depolarizing rod terminals with a 2 s puff of 50 mM KCl. Because rods were loaded with dye prior to treatment with dynasore, we expected that slowing vesicle turnover by inhibiting endocytosis should promote the retention of dye-loaded vesicles. However, rather than seeing more vesicles, we saw fewer vesicles advance towards the membrane in rods treated with dynasore compared to control conditions (Fig. 12A-B), suggesting that vesicle delivery to the membrane was impaired by inhibiting endocytosis (3-kDa, $P<0.0001$; 10-kDa, $P<0.0001$; unpaired t-tests). The speed at which vesicles approached the membrane was unchanged by dynasore, suggesting this was not due to a general loss of vesicle mobility. We calculated vesicle velocity from the distance traveled by a vesicle between the final two frames (40 ms apart) as it approached the membrane. We converted the increase in fluorescence to distance using the length constant for TIRFM illumination measured with the 488 nm laser of ~57 nm (Chen et al., 2013; Wen et al., 2017). In control conditions, final approach velocity averaged 1004 $\pm$ 19 nm/s (N=25). We

obtained a similar average velocity in cells treated with dynasore (895 ± 14 nm/s, N=23, P =0.648).

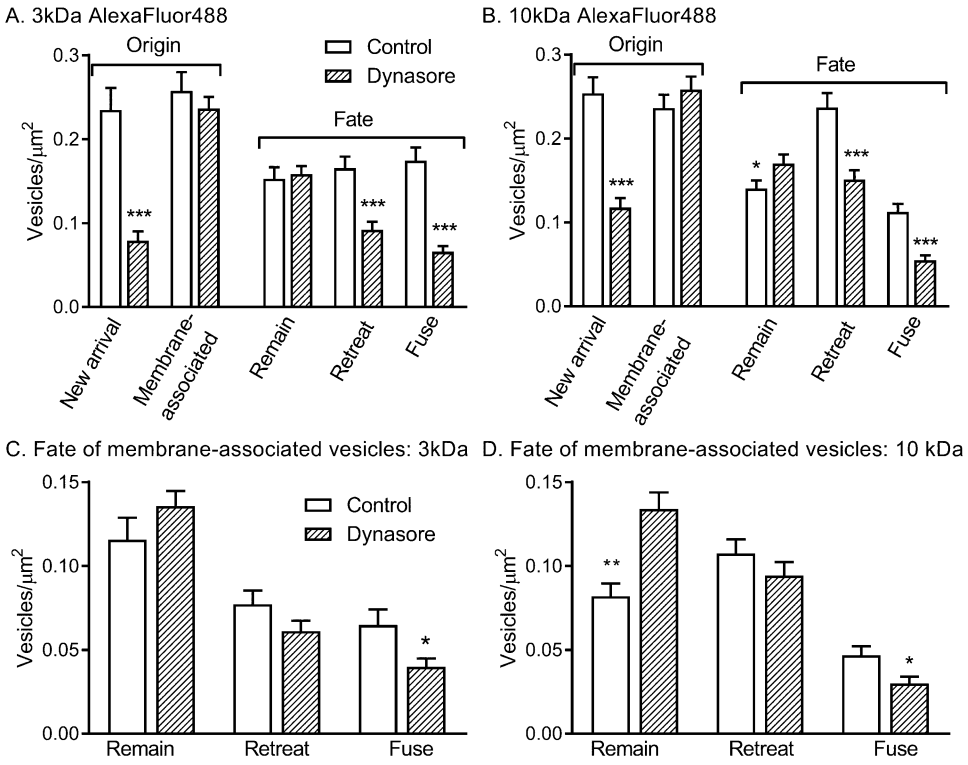

Figure 12. Comparing the origins and fates of vesicles in the presence and absence of dynasore.

(A-B) Vesicle behavior in vehicle control (0.1% DMSO) or dynasore (80 μM) during 6 s trials. Vesicles were loaded with either 3-kDa AlexaFluor488 (A) or 10-kDa AlexFluor488 (B). Synaptic release was stimulated by depolarizing rod terminals with a 2 s puff of 50 mM KCl. With both dyes, significantly more vesicles advanced towards the membrane in vehicle control solutions than in rods treated with dynasore (hatched bars; 3-kDa: P<0.0001; 10-kDa: P<0.0001; unpaired t-tests). The number of vesicles that began each trial stably associated with the membrane did not differ significantly between dynasore and control cells. The number of vesicles that remained at the membrane surface at the end of each trial was not altered significantly by dynasore treatment with 3-kDa-loaded vesicles but was increased slightly with 10-kDa vesicles (P=0.043). Dynasore treatment significantly reduced the frequency of vesicles that fused during depolarizing stimulation

with a puff of 50 mM KCl (3-kDa: P<0.0001; 10-kDa: P<0.0001). The number of vesicles that departed the membrane without fusion was also significantly reduced (3-kDa: P<0.0001; 10-kDa: P<0.0001). (C-D) In the subset of vesicles loaded with 3-kDa AlexaFluor488 (C) or 10-kDa AlexFluor488 (D) that began each trial as membrane-associated vesicles, we found no significant difference in the number of non-release retreat events (3-kDa, P=0.12; 10-kDa, P=0.25), but dynasore significantly decreased fusion (3-kDa, P=0.014; 10-kDa, P=0.012). The number of vesicles loaded with 10-kDa AlexaFluor488 that remained at the membrane throughout the entire trial was also increased significantly by dynasore (P<0.0001).

Although fewer vesicles advanced towards the membrane, the number of membrane-associated vesicles detected at the beginning of each trial did not differ significantly between dynasore and control cells (Fig. 12A-B). The number of vesicles that remained at the membrane surface at the end of each trial was also unchanged by dynasore treatment when we examined vesicles loaded with 3-kDa AlexaFluor488 and was increased slightly for vesicles loaded with 10-kDa AlexaFluor488 (P=0.043, unpaired t-test). These results show that although fewer vesicles approached the membrane in dynasore-treated rods, the ability of vesicles that reached the membrane to initiate early steps in the docking process was not significantly impaired by inhibition of endocytosis.

Dynasore treatment significantly reduced the frequency of vesicles that fused during depolarizing stimulation with a puff of 50 mM KCl (Fig. 12A-B). The frequency of vesicles that departed the membrane without fusion was also significantly reduced (Fig. 8A-B). Vesicles typically fused soon after reaching the membrane, akin to “crash fusion” observed in neuroendocrine cells (Verhage and Sorensen, 2008). One contributor to a reduction in the numbers of departure and fusion events was simply that fewer vesicles approached the membrane after dynasore treatment. To control for this, we examined

the fate of vesicles that began the trial as membrane-associated vesicles (Fig. 12C-D). In this subset, we found no significant difference in the number of non-release, retreat events with dynasore treatment (3-kDa, P=0.12; 10-kDa, P=0.25; unpaired t-tests) suggesting that the reduction in retreat events (Fig. 12A-B) was simply a consequence of a reduction in the number of vesicles approach events. On the other hand, dynasore significantly decreased fusion among membrane-associated vesicles (3-kDa, P=0.014; 10-kDa, P=0.012; unpaired t-tests), indicating that in addition to a reduction in the number of approaching vesicles, vesicle fusion was directly impaired by inhibition of endocytosis.

The number of vesicles loaded with 3-kDa AlexaFluor488 that began and ended trials as membrane-associated vesicles was not affected by dynasore (Fig. 12C). However, there was a significant increase in the number of vesicles loaded with the larger dye, 10-kDa AlexaFluor488, which remained at the membrane throughout each trial (Fig. 12D, P<0.001, unpaired t-test). Increased persistence of 10-kDa AlexaFluor488-loaded vesicles at the membrane with dynasore treatment was also evident from the analysis shown in Figure 12B. This increased persistence of membrane-associated vesicles loaded with 10-kDa dye is consistent with recent findings from our laboratory that 10-kDa dyes are retained more frequently in vesicles after fusion than 3-kDa dyes. These results were interpreted as being due to contributions from kiss-and-run fusion that releases small dyes more efficiently than larger dyes (Wen et al., 2017). The retention of more membrane-associated vesicles loaded with larger 10-kDa dyes may reflect vesicles that failed to release large dye molecules during kiss-and-run fusion and were subsequently trapped at the membrane when endocytic fission was blocked by dynasore (Logiudice et al., 2009).

c. Impact of dynasore on ribbon-mediated release visualized by TIRFM

Electrophysiological experiments suggested that ribbon-mediated release is more sensitive to inhibition of endocytosis than non-ribbon release. To compare the behavior of vesicles near and far from ribbons, we loaded retinas with 3-kDa dextran-conjugated AlexaFluor488 and then performed whole-cell patch clamp recordings in dissociated rods. We labeled the ribbons in these rods by introducing a tetramethylrhodamine-conjugated, Ribeye-binding peptide through the patch pipette. We examined the behavior of individual vesicles evoked by a depolarizing step (100 ms, -70 to -10 mV) in the presence or absence of 80 μM dynasore. Figure 13 shows fluorescent images of synaptic terminals from control and dynasore-treated rods visualized by TIRFM. The left panel shows the average fluorescence image of a rod terminal containing vesicles that were loaded with 3-kDa AlexaFluor488 (average of 150 frames, 40 ms apiece). Brightness differences among vesicles in this average image were largely due to differences in the amount of time that vesicles spent near the membrane during the acquisition period.

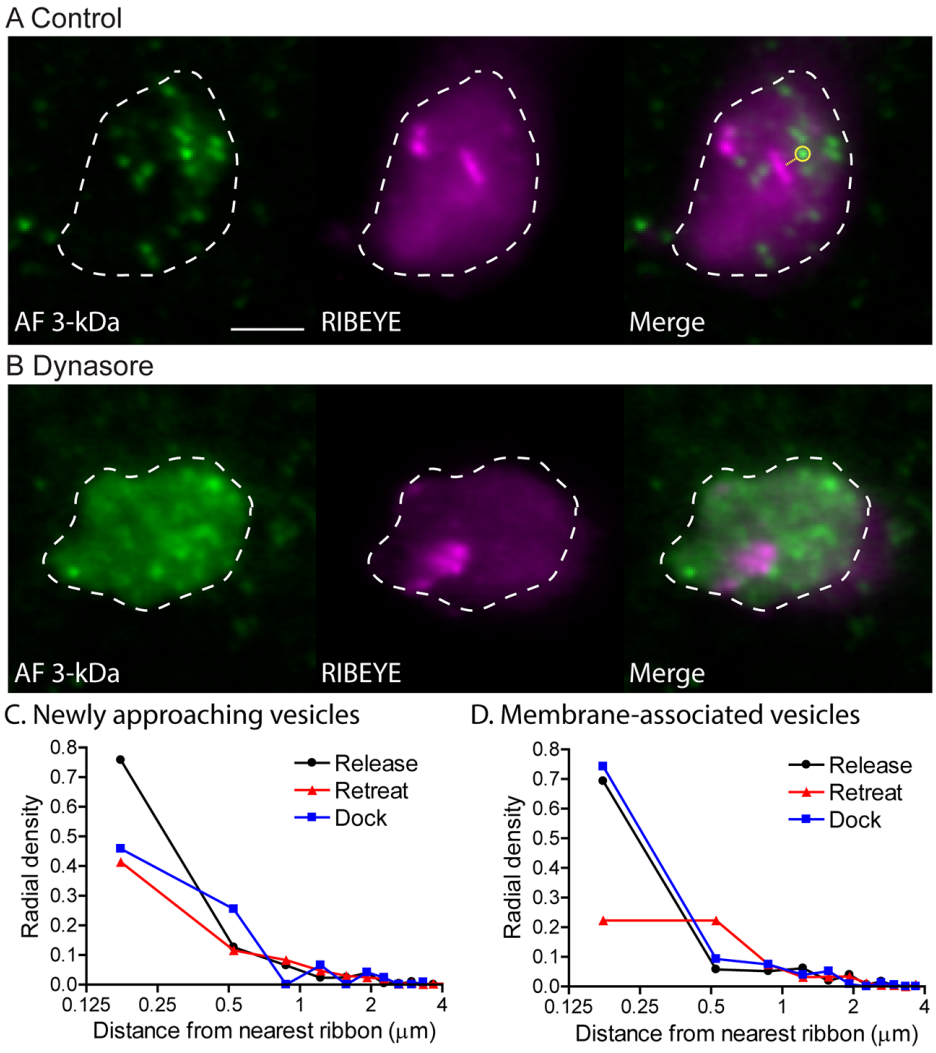

Figure 13. Visualization of vesicles and ribbons by TIRFM in rod terminals.

The figure shows the synaptic terminals of rods in which vesicles were loaded with 3-kDa AlexaFluor488 and ribbons were labeled by introducing a Ribeye-binding peptide conjugated to tetramethylrhodamine through the patch pipette. (A) Terminal of an isolated rod in control conditions (0.1% DMSO). (B) Rod terminal in the presence of dynasore (80 μM). The green fluorescence images at the left of A and B show vesicles loaded with 3-kDa AlexaFluor488 after averaging the entire trial (150 frames, 40 ms apiece). Differences in vesicle brightness in these average images were largely due to differences in the amount of time that a vesicle spent near the membrane during the acquisition period rather than intrinsic differences in vesicle brightness. The magenta images in the middle show the location of ribbons labeled by tetramethylrhodamine -

conjugated Ribeye-binding peptide. The 565 nm laser was tilted to deepen penetration of the evanescent field into the cell and illuminate tetramethylrhodamine -labeled ribbons more effectively. As illustrated in the merged image at the right of A, we measured the distance between the center of a vesicle to the edge of the nearest ribbon. Scale bar: 5 □m. (C) Fates of newly approaching vesicles in control conditions. The relative frequency histogram of vesicle events as a function of distance from the nearest ribbon was binned at 350 nm intervals and adjusted for radial density (see Methods). The likelihood of observing a newly approaching vesicle was consistently greater in the bin closest to the ribbon. However, the probability that fusion of a newly approaching vesicle (N=48 total events in 9 rods) would occur in the bin closest to the ribbon rather than further away was significantly greater than the probability that a newly approaching vesicle would dock at the membrane close to the ribbon (N=17; P = 0.023, z-test) or depart from ribbon-proximal membrane without fusion (N=157; P<0.0001, z-test). (D) Fates of vesicles that began a trial as membrane-associated or docked vesicles. Fusion of previously docked vesicles was significantly more likely to occur in the bin closest to the ribbon (N=30 total events; P=0.00014) than retreat from the membrane (N=35). The likelihood that a vesicle would remain docked throughout the trial was also significantly more likely in the bin closest to the ribbon (N=28; P<0.0001) than retreat.

Differences between control (0.1% DMSO) and dynasore-treated (80 μM) rods in the total number of events in voltage-clamp experiments were consistent with high K^+ stimulation experiments described above (Fig. 12). Half as many vesicles approached the membrane in dynasore-treated rods (106 vesicles, N=8 rods) than in control rods (222 vesicles, N=9 rods). And while vesicle advance was diminished in dynasore, the number of membrane-associated vesicles at the beginning (N=93, control vs. N=84, dynasore) and end (N=45, control vs. N=38, dynasore) of trials were similar in the two conditions. Finally, consistent with impaired fusion, the number of release events was reduced from 78 in control rods to 38 in dynasore-treated rods. Retreat events were also reduced from 192 in control to 106 in dynasore.

After acquiring 2-3 stimulation trials per cell, we imaged tetramethylrhodamine-labeled ribbons using 565 nm laser excitation. Rod ribbons sit above the plasma membrane atop an arciform density and can extend up to a micron into the cell. We angled the laser to deepen penetration of the evanescent field and illuminate the ribbons more effectively. The magenta images in the middle of Figure 13 show ribbons labeled by the tetramethylrhodamine-conjugated Ribeye-binding peptide. Merged vesicle and ribbon images are shown in the right panels of Figures 13A and B.

We measured the distance from the center of each vesicle to the edge of the nearest ribbon. We measured the relative frequency of events using a distance-from-ribbon bin size of 350 nm, matching the optical point spread function measured with this objective (Chen et al., 2013). We adjusted the frequency of events by the annular area occupied by each radial bin to calculate the radial density of events (see Methods).

In control conditions (0.1% DMSO), the likelihood that a newly arriving vesicle would be released was greatest in the bin closest to the ribbon and dropped off sharply with increasing distance from the ribbon (Fig. 13C). The likelihood that a newly arriving vesicle would retreat from the membrane or that it would remain as a membrane-associated vesicle were also both greater near ribbons. However, membrane retreat and stable association with the membrane were both less likely to occur near ribbons than fusion (Fig. 13C). For vesicles that began the trial as membrane-associated vesicles (Fig. 13D), most either fused before the end of the trial or remained as membrane-associated vesicles throughout the trial. Few of the membrane-associated vesicles located close to ribbons retreated from the membrane without fusion (Fig. 13D). This suggests that docked vesicles rarely retreat back up the ribbon and is consistent with studies from bipolar cells showing that vesicles almost always exit the ribbon at its base (Vaithianathan and Matthews, 2014). The clustering of vesicles near ribbons is

consistent with the central role of ribbons in release. However, there are also upper limits on the possible distance between a vesicle and its nearest ribbon due to limits in terminal size (up to 5 μm diameter) and the presence of multiple ribbons in the same salamander rod terminal (Townes-Anderson et al., 1985; Van Hook and Thoreson, 2015).

When endocytosis was inhibited by dynasore, various aspects of vesicle behavior were changed. As discussed above, the total number of vesicles that approached the membrane was reduced by dynasore treatment (Fig. 12). The radial distribution of vesicles that approached the membrane and then retreated without fusion did not differ in control vs. dynasore-treated cells indicating that the likelihood of membrane approach was impaired equally at both ribbon and non-ribbon sites (Fig. 14A). However, the frequency of vesicles that fused soon after reaching the membrane was diminished significantly in the bin closest to the ribbon by dynasore treatment (Fig. 14B). The frequency of vesicles that arrived near ribbons and then remained or docked at the membrane was increased in dynasore-treated rods (Fig. 14C). Thus, unlike control rods where fusion was more common than docking at ribbons, vesicles arriving at ribbons in dynasore-treated rods rarely fused and more often docked. This suggests that vesicles that failed to fuse soon after arriving at the membrane in dynasore-treated rods were capable of initiating the docking process. For vesicles that began trials as membrane-associated or docked vesicles, dynasore caused them to be less likely to remain docked and more likely to retreat from the membrane (Fig. 14D-E). Thus, while newly arriving vesicles can initiate docking at ribbons in dynasore-treated rods, inhibition of endocytosis appears to limit the ability of vesicles to progress to final stages of the release process. Although the overall likelihood of fusion was reduced by dynasore treatment, membrane-associated vesicles were still more likely to fuse at ribbons than at

non-ribbon locations (Fig. 14F), consistent with a key role for the ribbon in facilitating release even after endocytosis was inhibited.

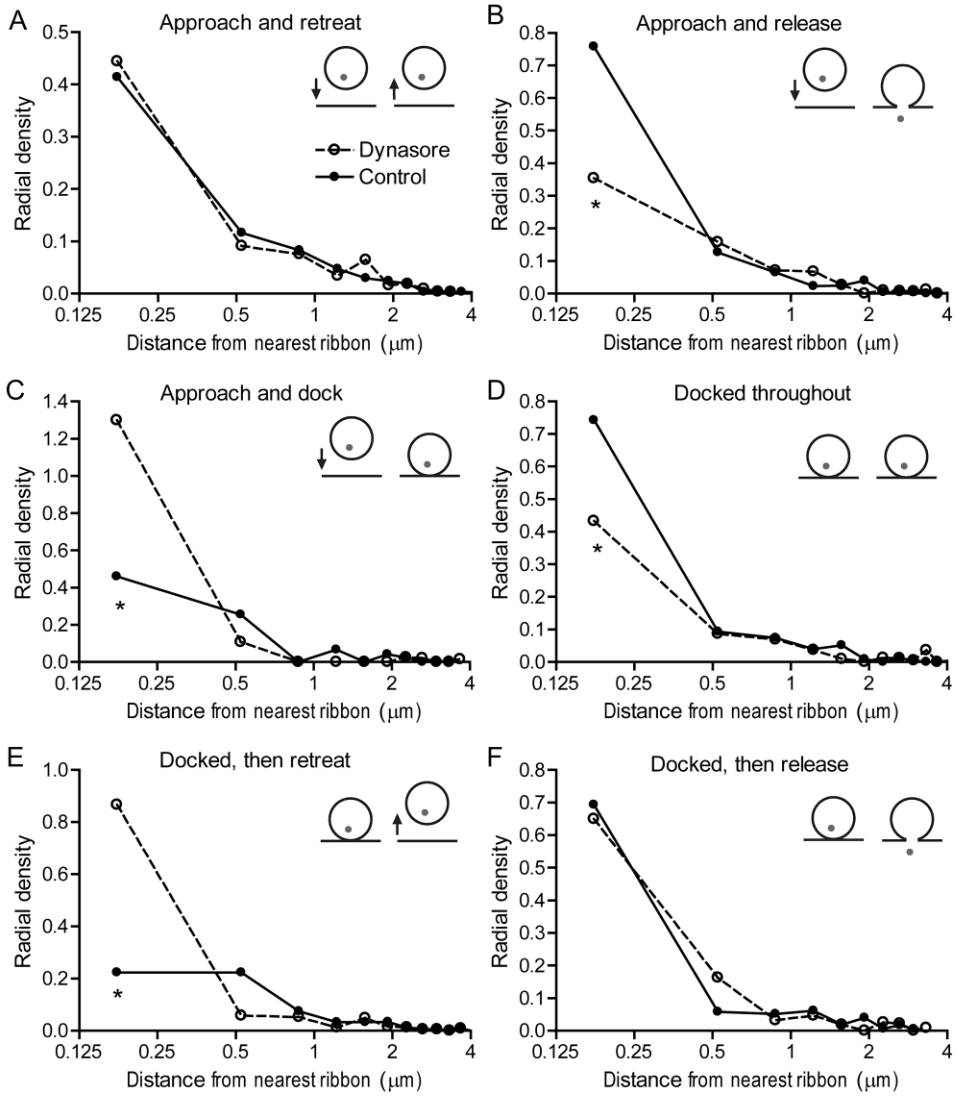

Figure 14. Comparisons of the radial density distributions of vesicle behaviors in control (0.1% DMSO) vs. dynasore-treated (80 μM) rods.

As in the previous figure, the relative frequency of vesicle events as a function of distance from the nearest ribbon was binned at 350 nm intervals and adjusted for radial density. (A) Spatial distribution of vesicles that approached the membrane and then retreated without fusion did not differ between control and dynasore-treated rods (N=157 events from 8 rods, control; N=76 events from 9 rods, dynasore). (B) Distribution of

vesicles that approached the membrane and then fused during the trial. In dynasore-treated rods, there was a significant decline in fusion of vesicles in the bin closest to the ribbon (N=48, control; N=22, dynasore; $p<0.0001$, z-test). (C) In the bin closest to the ribbon, there was also a significant increase in the likelihood that a newly arriving vesicle would remain at the membrane for the remainder of the trial in dynasore-treated rods (N=17, control; N=8, dynasore; $p<0.0001$). (D) However, among vesicles that were docked at the membrane at the beginning of the trial, fewer remained at the membrane in the bin closest to the ribbon for the entire 6 s trial in dynasore-treated rods (N=28, control; N=30, dynasore; $p<0.0001$). (E) In the bin closest to the ribbon, a larger fraction of membrane-associated vesicles retreated from the membrane without fusion in dynasore-treated rods (N=35, control; N=30, dynasore; $p<0.0001$). (F) The likelihood of release for membrane-associated vesicles was similarly high with both control and dynasore-treated rods (N=30, control; N=16, dynasore) in the bin closest to the ribbon.

V. Discussion

In addition to its role in recycling vesicles, endocytosis is important for restoring release site function following prior release (Kawasaki et al, 2000; Hosoi et al., 2009; Neher, 2010; Hua et al., 2013; Lipstein et al., 2013; Mahapatra et al., 2016). Our results show that the restoration of release site function by endocytosis is crucial for allowing continued release at photoreceptor ribbon synapses. The greater sensitivity to endocytic restoration at photoreceptor ribbon synapses may derive from the fact that photoreceptor ribbons release multiple vesicles at the same active zone whereas release at the calyx of Held occurs at hundreds of active zones but with each active zone releasing only one or two vesicles at a time (Taschenberger et al., 2002). Inhibiting endocytosis significantly slowed recovery from paired pulse depression of fast, ribbon-related release from rods.

A number of different lines of evidence indicate that the impairment of fast, ribbon-mediated release that occurs in response to inhibition of endocytosis is due to a reduced availability of functional ribbon release sites. First, several studies showed that

inhibition of endocytic processes rapidly leads to inhibition of vesicle exocytosis (Chen et al., 2003; Ferguson et al., 2007; Hosoi et al., 2009; Kawasaki et al., 2000; Shupliakov et al., 1997); this effect cannot be readily explained by a depletion of the releasable pool of vesicles. Further evidence for impaired replenishment of ribbon release sites came from the finding that inhibiting endocytosis with dynasore, dynamin inhibitory peptide or dyngo-4A slowed the rate at which fast, ribbon-mediated release at rod synapses, but not slow release, recovered from paired pulse depression. Finally, TIRFM experiments showed that the fusion of vesicles at or near ribbons was directly impaired by dynasore treatment.

The relatively large size of rods in salamander retina allowed us to perform paired recordings, TIRFM, and single particle tracking experiments that we could not perform using mouse rods, but use of salamander retina precluded the use of genetic models. For most of these experiments, we used the small molecule dynasore to inhibit synaptic endocytosis in rods. In paired pulse replenishment experiments, we introduced dynasore through a patch pipette to limit effects to the presynaptic rod. However, in addition to inhibiting endocytic retrieval of synaptic vesicles, dynasore can inhibit other forms of endocytosis and influence other aspects of cell behavior (Park et al., 2013; Girard et al., 2011; Preta et al., 2015). We therefore also tested effects on paired pulse depression of a more potent inhibitor dyngo-4A and a dynamin inhibitory peptide. It is unlikely that off-target effects of dynasore on dynamin-independent processes are shared with dynamin inhibitory peptide. Thus, the finding that all three compounds caused a similar slowing of recovery from paired pulse depression argues that impaired vesicle replenishment was a consequence of impaired dynamin-mediated endocytosis and not to other effects of dynasore. For TIRFM experiments, we only tested dynasore and cannot rule out the possibility that some of dynasore's effects might reflect actions

on targets other than dynamin. However, taken together, our results suggest that the synaptic changes we observed were likely due to effects of these inhibitors on dynamin-dependent, synaptic vesicle endocytosis.

The present results showed that ribbon-mediated release in rods recovered from paired pulse depression with a bi-exponential time course similar to that observed in cones (Van Hook et al., 2014; Thoreson et al., 2016). Under normal circumstances, the principal rate-limiting step that limits synaptic transmission to HCs during sinusoidal stimulation of cones is the fast component of this replenishment process that has a time constant of 600-800 ms (Innocenti and Heidelberger, 2008; Van Hook et al., 2014; Thoreson et al., 2016; Grabner et al., 2016). In both rods and cones, this fast replenishment process involves actions of Ca^{2+} operating through calmodulin to enhance vesicle attachment to the ribbon and thereby speed replenishment of ribbon release sites (Van Hook et al., 2014; Van Hook and Thoreson, 2015). The present results indicate that while vesicles may be returned to ribbons by this process, newly delivered vesicles cannot be efficiently released from ribbons until endocytosis has restored release sites to fusion competence. Thus, when endocytosis is inhibited, the process of release site clearance becomes the rate-limiting step in replenishment, slowing the time constant for replenishment three or fourfold to 2.5-3.2 s.

The need to quickly restore release site function may provide a rationale for the rapid rate of endocytosis observed at photoreceptor synapses with time constants of a few hundred milliseconds (Van Hook and Thoreson, 2012; Cork and Thoreson, 2014; Wen et al., 2017). Simply restoring the cytoplasmic vesicle pool would not necessitate such rapid retrieval since refilling newly retrieved vesicles with glutamate is considerably slower, with a time constant of ~15 s (Hori and Takahashi, 2012). Rapid endocytosis in photoreceptors appears to involve significant contributions from kiss-and-run release in

which vesicles fuse transiently with the plasma membrane through a narrow fusion pore (Wen et al., 2017). The preferential retention of 10-kDa AlexaFluor488 near the membrane in TIRFM experiments is consistent with the presence of kiss-and-run events that preferentially release small 3-kDa dyes over 10-kDa dyes. In addition to facilitating rapid retrieval, kiss-and-run may minimize changes to the surface area and contents of the plasma membrane that would be caused by insertion of vesicle lipids and proteins during full-collapse fusion.

Unlike fast ribbon-mediated release, slow release from rods involves significant contributions from non-ribbon sites that can be triggered by CICR (Chen et al., 2013, 2014). The locations of non-ribbon release events vary from trial to trial, suggesting that ectopic release sites are not fixed in location or, alternatively, that they are fixed but show extremely low release probability (Chen et al., 2014). With either scenario, prior release at a non-ribbon site should have little impact on subsequent release. Consistent with this, recovery of slow release from paired pulse depression was not significantly altered. TIRFM experiments also showed that dynasore treatment caused more significant changes in release at ribbon than non-ribbon sites. It might involve obstructions created by the accumulation of hemifused vesicles in perisynaptic membrane that occurs during dynasore treatment (Logiudice et al., 2009). This might also account for the observation in TIRFM experiments that fewer vesicles advanced towards the membrane in dynasore-treated rods.

TIRFM experiments provided insights into the behavior of vesicles at ribbons and how that behavior was altered by inhibition of endocytosis. One possible concern is that some fusion events may have been mis-categorized as retreat events or vice versa. Such mis-categorization would obscure differences between release and retreat events observed under various experimental conditions. For example, consider Figures 12C

and D in which dynasore caused a significant decline in the number of fusion events among membrane-associated vesicles. If some fusion events were not accurately identified, but were instead mis-categorized as retreat events, then this might account for the small decline in retreat events that was seen in this same experiment (Fig. 12). And if so, this would also suggest that dynasore had even greater effects on the likelihood of fusion. While some events may have been mis-categorized, it is clear that our criteria were at least moderately successful in separating release and retreat events. If these criteria were completely incapable of distinguishing these events, then it would not be possible to distinguish any differences whatsoever in dynasore's effects on release vs. retreat. Therefore, the data in Figures 12 and 14 showing that dynasore had significantly different effects on release and retreat events supports conclusions from other evidence (Chen et al., 2013; Wen et al., 2017) that release events can be reliably distinguished from retreat events.

In control rods, TIRFM results showed that most vesicles fused soon after arriving at the membrane near ribbons. The short period of time that vesicles generally spend at the membrane prior to fusion is consistent with the idea that vesicles are primed during descent down the ribbon and therefore ready for almost immediate release (Snellman et al., 2011; Mehta et al., 2013). Fewer newly arriving vesicles docked at the membrane or retreated without fusion. For those vesicles that successfully docked, very few retreated from the membrane without fusing. These results are consistent with experiments from bipolar cells suggesting that vesicles almost always exit ribbons at their base and rarely return up the ribbon (Vaithianathan and Matthews, 2014).

While the number of newly approaching vesicles was reduced in dynasore-treated rods, the number of membrane-associated or docked vesicles was not (Fig. 12).

This suggests that vesicles which successfully reach the membrane can initiate early steps in docking. Unlike control rods where ribbon-associated vesicles often fused soon after reaching the membrane, vesicles located near ribbons in dynasore-treated rods were more likely to retreat soon after arrival or to dock at the membrane for a time and then retreat. These results suggest that, after inhibiting endocytosis, vesicles descending the ribbon are more likely to encounter non-functional release sites at the ribbon base and are therefore less likely to be released immediately after reaching the membrane, but instead linger near the membrane. While some of these membrane-associated vesicles may ultimately fuse, others simply retreat from the membrane.

We initially hypothesized that perhaps the reduction in the number of vesicles that approach the membrane in dynasore-treated rods may occur because vesicle approach might be obstructed by an accumulation of un-retrieved hemifused vesicles resulting from the inhibition of vesicle fission by dynasore. However, endocytosis in photoreceptors is thought to occur primarily in perisynaptic regions (Wahl et al., 2013; Fuchs et al., 2014) and we did not see a greater impairment of vesicle approach at non-ribbon sites compared to ribbon sites. Furthermore, we examined electron micrographs of rod and cone terminals treated with dynasore and did not see an obvious accumulation of vesicles at the membrane surface (unpublished observations). Instead, perhaps local changes in active zone structure caused by inhibition of endocytosis may propagate into the surrounding protein network and impede vesicle approach.

Our results show that rod ribbons are particularly sensitive to inhibition of endocytosis and subsequent disruption of release site function. This sensitivity likely involves the structure of synaptic ribbons where many vesicles are clustered closely together along the base, separated from one another by as little as 10 nm (Lasansky, 1978; Thoreson et al., 2004). Similar to photoreceptors, bipolar cells are capable of a

rapid form of endocytosis with time constants of 1-2 s that would support rapid restoration of release site function (Von Gersdorff and Matthews, 1994a). However, while endocytic restoration of release site competence may be important at retinal ribbon synapses, it does not appear to be as critical to for sustained release at hair cell ribbon synapses. These synapses are capable of sustaining release of large numbers of synaptic vesicles during maintained depolarization (Schnee et al., 2011; Graydon et al., 2011) but utilize relatively slow forms of endocytosis (Parsons et al., 1994; Moser and Beutner, 2000). Cones can follow higher frequencies than rods but fast endocytosis was not inhibited in cones as effectively by dynasore (Van Hook and Thoreson, 2012) and so we did not have the pharmacological tools to test the role of endocytosis in these cells.

Although ribbon-mediated fusion was disrupted, early steps in docking were not impaired by treatment with dynasore. This argues against the idea that prior vesicle release events impede subsequent fusion primarily by impairing vesicle docking (e.g., as a consequence of the accumulation of "used" vesicular proteins, such as cis-SNARE complexes; Hosoi et al., 2009; Kim and von Gersdorff, 2009). Instead, our results suggest that endocytosis maintains fusion competence by acting at later steps in the fusion process. Inhibiting endocytosis is more likely to disrupt the arrangement of plasma membrane-associated proteins than vesicle-associated proteins. Plasma membrane-associated t-SNAREs are therefore good candidates for proteins rendered dysfunctional by inhibition of endocytosis. The t-SNARE, syntaxin, is needed for both docking and release (Sudhof, 2013). Syntaxin is located on the presynaptic plasma membrane where it tends to cluster at active zones (Lang et al., 2001; Sieber et al., 2007; Barg et al., 2010; Ribrault et al., 2011; Bar-On et al., 2012). This clustering requires phosphatidylinositol 3,4,5 trisphosphate ($PI(3,4,5)P_3$) (van den Bogaart et al., 2011; Khuong et al., 2013). Deposition of lipids and proteins from a prior vesicle fusion event

might transiently disrupt this clustering by altering the local distribution of $PI(3,4,5)P_3$ and syntaxin (Ullrich et al., 2015). SNAP-25 clusters (Lang et al., 2001; Bar-On et al., 2012) might also be disrupted by prior fusion. The presence of specific protein isoforms shape the processes of docking, priming and fusion at different synapses (Kasai et al., 2012) and so the particular proteins expressed at rod ribbon synapses might contribute to their particular sensitivity to inhibition of endocytosis. For example, unlike conventional synapses that typically utilize syntaxin-1, photoreceptor ribbons use syntaxin-3B (Curtis et al., 2008, 2010) and SNARE complex formation at retinal ribbon synapses is regulated by phosphorylation of syntaxin 3B by Ca^{2+}/calmodulin-dependent kinase II (Curtis et al., 2010). If inhibiting endocytosis were to somehow disrupt this critical interaction, it would impair SNARE complex formation.

The relatively depolarized, resting membrane potential maintained by rod photoreceptors promotes continuous multivesicular release. The sensitivity to inhibition of endocytosis indicates that this process of multivesicular release from rod ribbons occurs at focal sites within a compact active zone. The proximity of many release sites to one another beneath a ribbon makes the need for rapid and robust endocytosis particularly critical in maintaining the integrity and structure of the active zone at photoreceptor ribbon synapses. This is in turn essential for accurately regulating synaptic release rates in response to illumination-dependent changes in rod membrane potential, thereby encoding the visual information collected by phototransduction in rod outer segments.

Chapter 3 Kiss-and-run is a significant contributor to synaptic exocytosis and endocytosis in photoreceptors

I. Abstract:

Accompanying sustained release in darkness, rod and cone photoreceptors exhibit rapid endocytosis of synaptic vesicles. Membrane capacitance measurements indicated that rapid endocytosis retrieves at least 70% of the exocytotic membrane increase. One mechanism for rapid endocytosis is kiss-and-run fusion where vesicles briefly contact the plasma membrane through a small fusion pore. Release can also occur by full-collapse in which vesicles merge completely with the plasma membrane. We assessed relative contributions of full-collapse and kiss-and-run in salamander photoreceptors using optical techniques to measure endocytosis and exocytosis of large vs. small dye molecules. Incubation with small dyes (SR101, 1 nm; 3-kDa dextran-conjugated Texas Red, 2.3 nm) loaded rod and cone synaptic terminals much more readily than larger dyes (10-kDa Texas Red, 4.6 nm; 10-kDa pHrodo, 4.6 nm; 70-kDa Texas Red, 12 nm) consistent with significant uptake through 2.3-4.6 nm fusion pores. By using total internal reflection fluorescence microscopy (TIRFM) to image individual vesicles, when rods were incubated simultaneously with Texas Red and AlexaFluor-488 dyes conjugated to either 3-kDa or 10-kDa dextran, more vesicles loaded small molecules than large molecules. Using TIRFM to detect release by the disappearance of dye-loaded vesicles, we found that SR101 and 3-kDa Texas Red were released from individual vesicles more readily than 10-kDa and 70-kDa Texas Red. Although 10-kDa pHrodo was endocytosed poorly like other large dyes, the fraction of release events was similar to SR101 and 3-KDa Texas Red. We hypothesize that while 10-kDa pHrodo may not exit through a fusion pore, release of intravesicular protons can promote detection of fusion events by rapidly quenching fluorescence of this pH-sensitive dye. Assuming that large molecules can only be released by full-collapse whereas small molecules can be

released by both modes, our results indicate that 50-70% of release from rods involves kiss-and-run with 2.3-4.6 nm fusion pores. Rapid retrieval of vesicles by kiss-and-run may limit disruption of release site function during ongoing release at photoreceptor ribbon synapses.

II. Introduction:

Vertebrate photoreceptors maintain a relatively depolarized membrane potential in darkness near -40 mV, allowing the continuous release of glutamate-filled vesicles at ribbon-style synapses. Photoreceptors do not generate sodium-dependent action potentials but instead respond to light with graded changes in membrane potential. Release slows when photoreceptors hyperpolarize to light. To assist with continuous release, photoreceptors possess a large vesicle pool and a specialized complement of synaptic proteins (Duncan et al., 2010; Magupalli et al., 2008; Morgans et al., 1996; Reim et al., 2005; Schmitz et al., 2000; Thoreson et al., 2004). However, even the large pool of 216,000 vesicles in a salamander cone synapse would be emptied in <15 min by sustained release in darkness if not replenished by endocytosis (Sheng et al., 2007). Mechanisms for rapid and robust endocytic retrieval are therefore essential to maintain continuous release.

Exocytosis and endocytosis of synaptic vesicles can be coupled in two general ways (Alabi and Tsien, 2013; Wu et al., 2014). In the full-collapse model, the vesicle membrane merges completely with the plasma membrane and vesicles must be fully reconstructed and retrieved during endocytosis. In the kiss-and-run model, a vesicle briefly contacts the plasma membrane through a small fusion pore that permits release of small molecules but the vesicle does not flatten into the plasma membrane. The vesicle with its complement of proteins is quickly recycled to the cytoplasm after closure

of the fusion pore. By speeding vesicle recycling, kiss-and-run can provide an efficient mechanism to facilitate sustained release.

Kiss-and-run fusion events have been observed in both neurons and neuroendocrine cells (Albillos et al., 1997; Fulop and Smith, 2006; He et al., 2006; Holroyd et al., 2002; Vardjan et al., 2007; Wang et al., 2003). In neuroendocrine cells, kiss-and-run allows selective release of small molecules while retaining larger peptides (Liang et al., 2017). The fraction of release events that arise from kiss-and-run in neurons may vary with experimental preparations and conditions. Some studies have suggested that kiss-and-run in neurons is quite rare (Balaji and Ryan, 2007; Chen et al., 2008; Granseth et al., 2006; He et al., 2006; Zenisek et al., 2002) while others have suggested that it can contribute to a majority of release events in certain preparations or under certain conditions (Gandhi and Stevens, 2003; Photowala et al., 2006; Richards et al., 2005; Zhang et al., 2009).

Characteristics used to distinguish kiss-and-run from full-collapse fusion include rapid endocytic kinetics and the small size of the fusion pore formed during kiss-and-run. Whole-cell capacitance measurements showed that vesicles can be retrieved in rods and cones by a rapid form of endocytosis (Cork and Thoreson, 2014; Van Hook and Thoreson, 2012). Although rapid endocytosis is consistent with contributions from kiss-and-run, it can also arise from other mechanisms (Watanabe et al., 2013; Watanabe and Boucrot, 2017). To assess the frequency of kiss-and-run and full-collapse events in salamander rods and cones, we measured both exocytosis and endocytosis of synaptic vesicles using multiple fluorescent dyes ranging from 1-12 nm diameter (Takahashi et al., 2002). Use of optical techniques allowed us to measure the properties of release and retrieval in many vesicles. We assessed endocytosis by measuring changes in whole-

terminal fluorescence and by imaging individual vesicles using electron microscopy and total internal reflection fluorescence microscopy (TIRFM). We measured exocytosis by using TIRFM to image release of individual vesicles. We also used membrane capacitance measurements to assess contributions from rapid and slow modes of endocytosis. We found that small molecules (≤2.3 nm) were both released and retrieved much more readily than large molecules (≥4.6 nm). Together with capacitance measurements, these results suggest that kiss-and-run events with a fusion pore diameter between 2.3 and 4.6 nm contribute to at least 50% of vesicle release and recycling in photoreceptor terminals. By limiting possible disruption of neighboring release sites along the ribbon base that can be produced by prior fusion events, rapid retrieval by kiss-and-run may be particularly useful for maintaining release at continuously active photoreceptor ribbon synapses.

III. Materials and Methods:

a. Animal care and use

Aquatic tiger salamanders (Ambystoma tigrinum, 18-25 cm; Sullivan Company, Nashville, TN) were maintained on a 12-h light/dark cycle and sacrificed after ≥1 h of dark adaptation. Salamanders were anaesthetized by immersion in 0.25 g/L tricaine methanesulfonate (Western Chemical) for >15 min, decapitated with heavy shears, and pithed. Procedures were approved by the University of Nebraska Medical Center Institutional Animal Care and Use Committee.

b. Reagents

Unless otherwise noted, reagents were from Sigma-Aldrich Chemicals.

c. Photoreceptor isolation

After enucleation and removal of the anterior segment, the eyecup was cut in half and the retina isolated in Ca^{2+}-free, high-Mg^{2+} amphibian saline consisting of (in mM): 116 NaCl, 2.5 KCl, 5 $MgCl_2$, 5 glucose, and 10 HEPES (pH 7.4). Retinal pieces were incubated with 30 units/ml papain (Worthington) activated with 0.2 mg/ml cysteine in Ca^{2+}-free high-Mg^{2+} saline solution for 35 min at room temperature. Afterwards, retinal pieces were transferred to ice-cold Ca^{2+}-free high-Mg^{2+} saline with 1% bovine serum albumin for 3 min. Retinal pieces were washed another 3 min in ice-cold Ca^{2+}-free, high-Mg^{2+} saline and then incubated in ice-cold Ca^{2+}-free, high-Mg^{2+} saline containing DNase (4000 u/ml; Worthington) for another 5 min. Photoreceptors were isolated by gently triturating the tissue ~10 times through the tip of a fire-polished, bent Pasteur pipette. Isolated cells were plated on glass coverslips with a refractive index of 1.52 (#1 Coverslips, Warner Instruments) or 1.78 (Olympus) and coated with 3.5 µg/cm^2 Cell-Tak (BD Biosciences).

d. Capacitance measurements of endocytosis

Whole-cell recordings for capacitance measurements were obtained from isolated photoreceptors and photoreceptors in retinal slices. For electrophysiological recording, isolated cells were plated on glass slides coated with 1 mg/ml concanavalin A.

Retinal slice preparation has been detailed elsewhere (Van Hook and Thoreson, 2012). Briefly, a piece of eyecup was placed vitreal surface down onto nitrocellulose membrane (5×10 mm, 0.8 µm pores; Millipore), the retina was isolated, and then cut into

125 µm thick slices using a razor blade tissue slicer (Stoelting). Slices were viewed through an upright fixed-stage microscope (Olympus BH2-WI) and superfused at room temperature at ~1 ml min^{-1} with oxygenated amphibian saline containing (in mM): 116 NaCl, 2.5 KCl, 1.8 $CaCl_2$, 0.5 $MgCl_2$, 5 glucose, and 10 HEPES (pH 7.8).

Whole-cell capacitance measurements were described previously (Van Hook and Thoreson, 2012). Borosilicate glass pipettes (1.2 mm OD, 0.9 mm ID, with internal filament; World Precision Instruments) were pulled with a vertical pipette puller (Narishige). Pipette shafts were coated with dental wax. Pipettes were filled with (Cin mM): 50 CsGluconate, 40 CsGlutamate, 10 TEACl, 3.5 NaCl, 1 $CaCl_2$, 1 $MgCl_2$, 9.4 MgATP, 0.5 GTP-Na, 5 EGTA (pH 7.2). Membrane capacitance was measured with phase tracking hardware integrated into the Optopatch amplifier (Cairn Research), acquired with Clampex 10.4 software (Molecular Devices), and analyzed with Clampfit 10.4 software. Series resistance (R_s), membrane resistance (R_m), and capacitance (C_m) averaged: 29.6±1.5 MΩ (R_s), 200.3±20.4 MΩ (R_m) and 58.7±2.9 pF (C_m) for cones (N=7) in slices; 35.0±4.1 MΩ, 225.5±48.2 MΩ, and 23.5±1.6 pF for rods (N=6) in slices; 38.0±5.1 MΩ, 1102.0±238.8 MΩ, and 15.1±0.7 pF for isolated cones (N=7); and 34.5±3.4 MΩ, 410.3±80.4 MΩ and 15.1±1.3 pF for isolated rods (N=12). Charging curves of rods and cones are well fit by single exponentials indicating a compact electrotonic structure (Van Hook and Thoreson, 2012; Warren et al., 2016a). Responses were excluded if holding currents exceeded 250 pA, access resistance exceeded 50 MΩ, or if there were large changes in R_s during the test step. Photoreceptors were depolarized with a 25 ms step from -70 mV to -10 mV. Capacitance measurements were begun after tail currents had subsided completely, typically ~250 ms after terminating the test step. Rates of endocytosis were determined by fitting

capacitance declines with a single exponential function.

e. Whole-terminal fluorescence measurements

After letting cells settle onto coverslips, isolated photoreceptors were incubated with SR101, 3-, 10-, 70-kDa dextran-conjugated Texas Red, or 10-kDa dextran-conjugated pHrodo (Molecular Probes, Invitrogen, 7 μM) in amphibian saline for 3 or 10 min. Basal release was measured by incubating photoreceptors for 10 min with dye in Ca^{2+}-free, high-Mg^{2+} solution containing 0.1 mM Cd^{2+}. Cells were superfused with oxygenated amphibian saline for at least 10 min before measurements.

In experiments with dynasore (Abcam) and pitstop-2, retinal pieces were pre-treated with drug in Ca^{2+}-free high-Mg^{2+} saline for 20 min and then transferred to a solution containing dye (67 μM 3-kDa Texas Red or 50 μM 10-kDa Texas Red) and drug for 10 min. Photoreceptors were isolated and plated after dye loading.

Whole-terminal fluorescence was measured on an inverted microscope (Olympus IX71) through a 1.45 NA/60X, oil-immersion objective. Fluorescence emission was collected with 40-ms exposure times by an EMCCD camera (Hamamatsu ImageEM) through a 609 nm (54 nm wide) bandpass filter (Semrock). Background fluorescence was measured in adjacent regions outside the cell and subtracted from measurements of terminal fluorescence. Data were acquired and analyzed using MetaMorph software (Molecular Devices).

f. In vitro dye fluorescence measurements

To compare intraterminal fluorescence measured with different dyes, the brightness of each dye was measured in vitro at three points along the shaft of a dye-filled patch pipette (0.25 NA/10X objective; Olympus). The molar fluorescent brightness (F'/μM) for each dye was: SR101: 25,040 arbitrary fluorescence units (a.u.)/μM, 3-kDa dextran-conjugated Texas Red: 2,084 a.u./μM, 10- kDa Texas Red: 10,716 a.u./μM, 70-kDa Texas Red: 22,837 a.u./μM, and pHrodo: 12,882 a.u./μM (pH=5.5); 6901 a.u./μM (pH=7.8). Dextran-conjugated 3-, 10-, 70-kDa Texas Red are sulfonyl derivatives of SR101. Dextran-conjugated 10-kDa pHrodo is a pH sensitive form of rhodamine that is brighter in acidic environments. Fluorescence of pHrodo was measured at both pH 5.5 and 7.8. To calculate relative fluorescence values in Figure 16C, we used pHrodo fluorescence measured at pH 5.5.

g. Dye release measurements in retinal slices

For studies of release from retinal slices, pieces of isolated retina were loaded by incubation in darkness with SR 101 (83 μM, 30 min), 3-kDa Texas Red (133 μM, 45 min), 10-kDa Texas Red (100 μM, 60 min), or 70-kDa Texas Red (36 μM, 60 min). After incubation, retina pieces were washed in Ca^{2+}-free high-Mg^{2+} saline and slices were prepared as described above. The recording chamber was placed on an upright fixed-stage microscope (Nikon E600 FN) equipped with a spinning disk laser confocal scan head (PerkinElmer UltraView LCI). Dyes were excited at 568 nm with an Ar/Kr laser. Emitted light was captured through 600 nm interference filters by a cooled CCD camera (Hamamatsu OrcaER). Excitation and emission were controlled by a Lambda 10-2 filter wheel and controller (Sutter Instrument). Images were acquired once per minute and analyzed with NIS-Elements AR software (Nikon). After collecting baseline data for 5

min, release was stimulated by applying 50 mM KCl saline (in mM: 68.6 NaCl, 50 KCl, 1.8 $CaCl_2$, 0.5 $MgCl_2$, 5 glucose, and 10 HEPES, pH 7.8) for another 15 min.

h. Electron microscopy

For electron microscopy, retinal pieces were loaded with 3- or 10-kDa Texas Red (7 μM, lysine fixable) in Ca^{2+}-free, high-Mg^{2+} saline for 2 min and then incubated in a solution containing 1.8 mM Ca^{2+} and 20 mM K^+ saline with the same dyes for 8 additional minutes. Retinal pieces were then washed with Ca^{2+}-free, high-Mg^{2+} saline 3 times for 3 min apiece. Retinal pieces were fixed overnight at 4 deg C in 2% glutaraldehyde, 2% paraformaldehyde, and 0.1 M Sorensen's phosphate buffer (pH=7.4). After fixation, retinas were washed in 0.1 M Tris buffer (pH=7.6) for 2 min and then incubated in 0.01% 3,3′-diaminobenzidine tetrahydrochloride (DAB) in 0.1 M Tris buffer for 10 min. Dyes were photoconverted for 30 min in the presence of DAB (Maranto, 1982; Schmued and Snavely, 1993) by 609 nm light through a 0.25 NA, 10X objective. After photoconversion, retinal pieces were washed twice in phosphate-buffered saline and then placed in 1% osmium tetroxide. Samples were dehydrated through a graded ethanol series, followed by three washes with 100% propylene oxide. Samples were left overnight in a 1:1 mixture of Araldite embedding medium and propylene oxide, embedded in fresh Araldite in silicon rubber molds, and then placed in an oven at 65 deg C overnight. Resulting blocks were thin sectioned on a Leica UC6 ultramicrotome and placed on 200 mesh copper grids. Sections were stained with 1% uranyl acetate and Reynold's lead citrate. Sections were examined in a FEI Tecnai G2 TEM operated at 80 kV.

i. TIRFM experiments

Individual synaptic vesicles were visualized in rod terminals using total internal reflection fluorescence microscopy (TIRFM) as described previously (Chen et al., 2013). Solid-state lasers (561 nm or 488 nm; Melles Griot) were focused off-axis through the objective (100X, 1.65 N.A., oil immersion, Olympus) so that the beam underwent total internal reflection at the interface between the coverslip and overlying cell membrane or aqueous solution. We used an incident angle of ~60 deg that generates an evanescent wave with this objective exhibiting length constants of ~65 and ~57 nm for 561 and 488 nm lasers, respectively. Fluorescent emission was collected through 609 nm bandpass (54 nm wide, Semrock) or 500-545 nm/575-710 nm bandpass (Chroma) filters using an EMCCD camera (Hamamatsu ImageEM) at 40 ms/frame with a pixel size of 80 nm/pixel. TIRFM data were acquired using MetaMorph software and analyzed using MetaMorph and ImageJ.

To load dye for TIRFM experiments on release, tissue was dissected and retinas were isolated in darkness using GenIII image intensifiers (Nitemate NAV3, Litton Industries) mounted on a dissecting microscope. Maintaining retinae in a dark-adapted state keeps photoreceptors at a resting membrane potential of approximately -40 mV and thus promotes vesicle recycling. Retinal pieces were typically incubated in dye for a short time to load only a small percentage of vesicles: SR101 (8.3 μM, 1.5 min), 3-kDa Texas Red (133.3 μM, 1.5 min), 10-kDa Texas Red (50 μM, 3 min), and pHrodo (50 μM, 3 min). We incubated tissue with 70-kDa Texas Red (14.3 μM) for 30 min because it loaded quite poorly.

Synaptic vesicle release was stimulated by depolarizing rod terminals with a 2-s puff of 50 mM KCl delivered from a glass patch pipette using a pressure valve system (Toohey Company; 8 psi). The pipette tip was positioned 10-20 µm from rod terminals. For TIRFM experiments on endocytosis we loaded red and green dyes simultaneously in various combinations--3- or 10-kDa Texas Red (7 µM, zwitterionic) with 3- or 10-kDa AlexaFluor-488 (7 µM, anionic)--by incubating pieces of whole retina in dye solution prior to cell isolation. When we incubated isolated cells in dye after plating, many dye molecules adhered to coverslips, making it difficult to distinguish dye molecules within synaptic vesicles from extracellular dye molecules stuck to the glass. To limit vesicle cycling as dyes diffused through the retina, we first loaded the two dyes in Ca^{2+}-free, high-Mg^{2+} saline for two min. To further limit vesicle cycling during this period, we also strongly light-adapted retinas by illuminating them with bright white light for 10 min before dye incubation. As a basal measurement of endocytosis in Ca^{2+}-free conditions, we loaded one sample of retinas for another 2 min (for a total of 4 min) in Ca^{2+}-free, high-Mg^{2+} saline. In a second sample, we followed the first 2 min of incubation in Ca^{2+}-free, high-Mg^{2+} saline with 2 min incubation in a solution containing 1.8 mM Ca^{2+} and 20 mM K^{+} saline. After isolating and plating, rods were examined in the presence of Cd^{2+} (0.1 mM) to block Ca^{2+} channels and limit further vesicle cycling. Excitation was alternated between 561 and 488 nm (30 frames apiece, 40-ms/ frame) at 140-ms intervals. We used ImageJ to identify the terminal footprint and local maxima in average TIRFM images that were used to count the number of dye-loaded vesicles.

For release experiments, only vesicles with a signal-to-noise ratio >4:1 in a 7x7 pixel region of interest were analyzed. As described in the results, we compared the rise in fluorescence as vesicles approached the membrane to rates of fluorescence decline

to distinguish release events from departure of vesicles from the membrane without release.

j. Statistical Analysis

Unless otherwise noted, data were analyzed by Prism 4.0 (GraphPad Software) and results are presented as mean ± standard error of the mean (SEM).

IV. Results:

a. Rapid endocytosis in photoreceptors.

Whole-cell capacitance measurements suggested the presence of rapid endocytosis in rod and cone photoreceptors (Cork and Thoreson, 2014; Van Hook and Thoreson, 2012). However, we were concerned that the time course of endocytosis in these earlier studies may have been influenced by I_h currents or by anion currents associated with the activity of presynaptic glutamate transporters. To address this, we measured exocytotic capacitance changes while bath applying CsCl (3 mM) to block I_h and DL-TBOA (100 μM) to block glutamate transporters. We measured capacitance changes in rods and cones from retinal slices evoked by depolarizing steps (-70 to -10 mV, 25 ms) to stimulate exocytosis. Step-evoked capacitance jumps averaged 80.1±11.9 fF in cones (N=10) and 54.3±18.6 fF (N=6) in rods. Non-ribbon release from rods was minimized by using brief 25 ms steps (Chen et al., 2013). Consistent with a synaptic origin, we observed paired pulse depression of capacitance jumps (Rabl et al., 2006). Other evidence that depolarization-evoked capacitance responses in salamander rods and cones derive from synaptic release include matches between the amplitude and kinetics of capacitance changes and the amplitude and kinetics of synaptic currents

measured in paired photoreceptor/horizontal cell recordings (Rabl et al., 2005; Thoreson et al., 2004). Exocytotic capacitance jumps also ran down more quickly than calcium-activated chloride tail currents (Bartoletti et al., 2010; Cork and Thoreson, 2014; Rabl et al., 2005; Thoreson et al., 2004; Van Hook and Thoreson, 2013).

The rate of endocytic membrane retrieval was assessed by fitting the decline in membrane capacitance with a single exponential curve (Fig. 15). To avoid possible contamination by membrane conductance changes, fitting was begun after the end of any tail currents, typically ~250 ms after termination of the step. As illustrated in Figure 15A and B, depolarization-evoked jumps in capacitance showed an initial decline with time constants of 570±109 ms in cones (N=10) and 492±78 ms (N=6) in rods. After this initial rapid phase of retrieval, membrane capacitance often leveled out above baseline. This suggests the presence of an additional slower component of endocytosis similar to that observed previously in salamander cones (Innocenti and Heidelberger, 2008). In cones, particularly in retinal slices, membrane capacitance sometimes overshot baseline, consistent with the excess endocytosis observed by (Van Hook and Thoreson, 2012). During the 5 s trial, the initial rapid phase of endocytosis recovered 78.8±5.3% and 67.6±7.6% of the exocytotic capacitance increase in cones and rods from retinal slices, respectively.

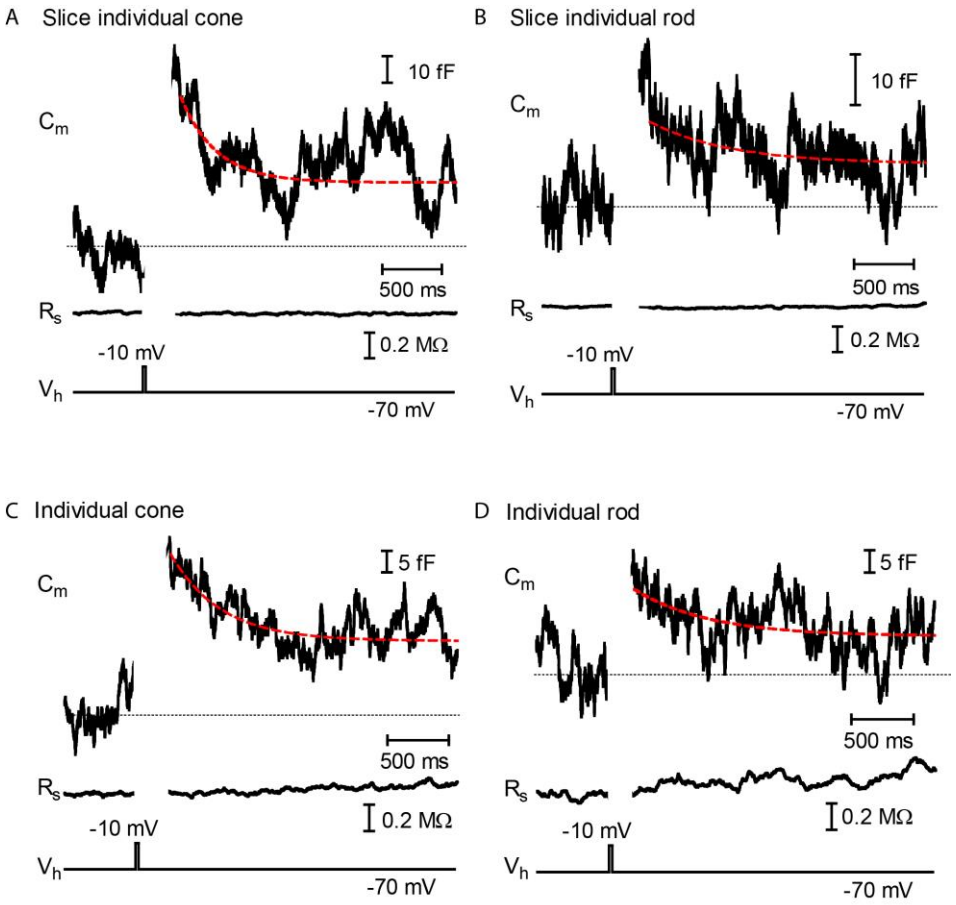

Figure 15. Fast endocytosis in photoreceptors.

Whole-cell capacitance measured in photoreceptors from retinal slices (A,B) and isolated cells (C,D) in the presence of DL-TBOA (100 μM) and CsCl (3 mM). (A) and (B) show responses from a cone and rod, respectively, measured in retinal slices. (C) and (D) show responses from an isolated cone and rod, respectively. Depolarization (-70 mV to -10 mV, 25 ms) stimulated an increase in membrane capacitance that subsequently returned to baseline due to endocytosis. Endocytic capacitance decays were fit by single exponential curves (red lines): (A) tau=297.8 ms, amplitude (a)=0.0320308 pF, plateau amplitude (c)=0.026172 pF; (B) tau=608.3, a=0.0081128, c=-0.43617; (C) tau=602.7, a=0.028183, c=0.011441; (D) tau=599.9, a=0.010456, c=0.099100. Dashed line shows the initial baseline of each trace.

We further minimized the potential impact of glutamate transporter activity by measuring capacitance responses in the presence of TBOA and Cs^+ using enzymatically-isolated cones and rods. Capacitance jumps evoked by 25 ms steps averaged 26.7±4.0 fF in isolated cones (N=7) and 53.3±8.6 fF in isolated rods (N=12). As illustrated in Figure 15, rates of endocytosis in isolated rods and cones were similar to those observed in retinal slices. Endocytosis in rods and cones showed an initial rapid decline that recovered 66.3±7.2% and 71.5±6.4% of the exocytotic capacitance increase, respectively, and exhibited time constants averaging 649±86 ms and 672±142 ms. In addition to showing that glutamate transporter activity is unlikely to be responsible for the fast capacitance decline, measurements from isolated cells indicate that enzymatic isolation and plating of photoreceptors did not greatly distort their synaptic function. The presence of rapid endocytosis is consistent with significant contributions from kiss-and-run fusion, but it can also be explained by other forms of rapid retrieval (Watanabe et al., 2013). We therefore turned to optical methods to help distinguish contributions of kiss-and-run from full-collapse fusion.

b. Small dyes were loaded preferentially into synaptic terminals.

Because kiss-and-run involves smaller fusion pores than full-collapse fusion, we made optical measurements of exocytosis and endocytosis using a range of different size dyes. We used SR101 and its sulfonyl derivative Texas Red conjugated to dextrans of 3-, 10-, and 70-kDa (7 μM) with Stokes' diameters of 1, 2.3, 4.6, and 12 nm, respectively (Armstrong et al., 2004; Choi et al., 2010; Erickson, 2009) (https://www.sigmaaldrich.com/content/dam/sigma-aldrich/docs/Sigma/Product_Information_Sheet/1/fd250spis.pdf). We also tested 10-kDa dextran conjugated to a pH-sensitive dye, pHrodo.

We began by studying the ability of isolated rods and cones to endocytose different dyes. After incubating isolated cells in dye for 3 or 10 min, fluorescent intensities of isolated rod and cone terminals were measured by epi-fluorescence. Uptake during this time was presumably due to endocytosis accompanying spontaneous vesicle release. Dye was concentrated in terminals as expected by uptake into synaptic vesicles (Fig. 16B). Intraterminal fluorescence was significantly reduced (unpaired t-tests; see figure legend) by incubating rods and cones for 10 min with dye in the presence of Ca^{2+}-free, high-Mg^{2+} solution containing 0.1 mM Cd^{2+} to block Ca^{2+} channels. This can be seen in the insets of Figure 16C showing measurements at low fluorescent intensities made after 10 min. Uptake of 3-kDa Texas Red after blocking Ca^{2+} channels was slightly greater than the other four dyes, but was still substantially lower than uptake in control conditions. This suggests a slightly greater propensity for uptake of 3-kDa Texas Red by Ca^{2+}-independent vesicle cycling (Cork et al., 2016) or other mechanisms.

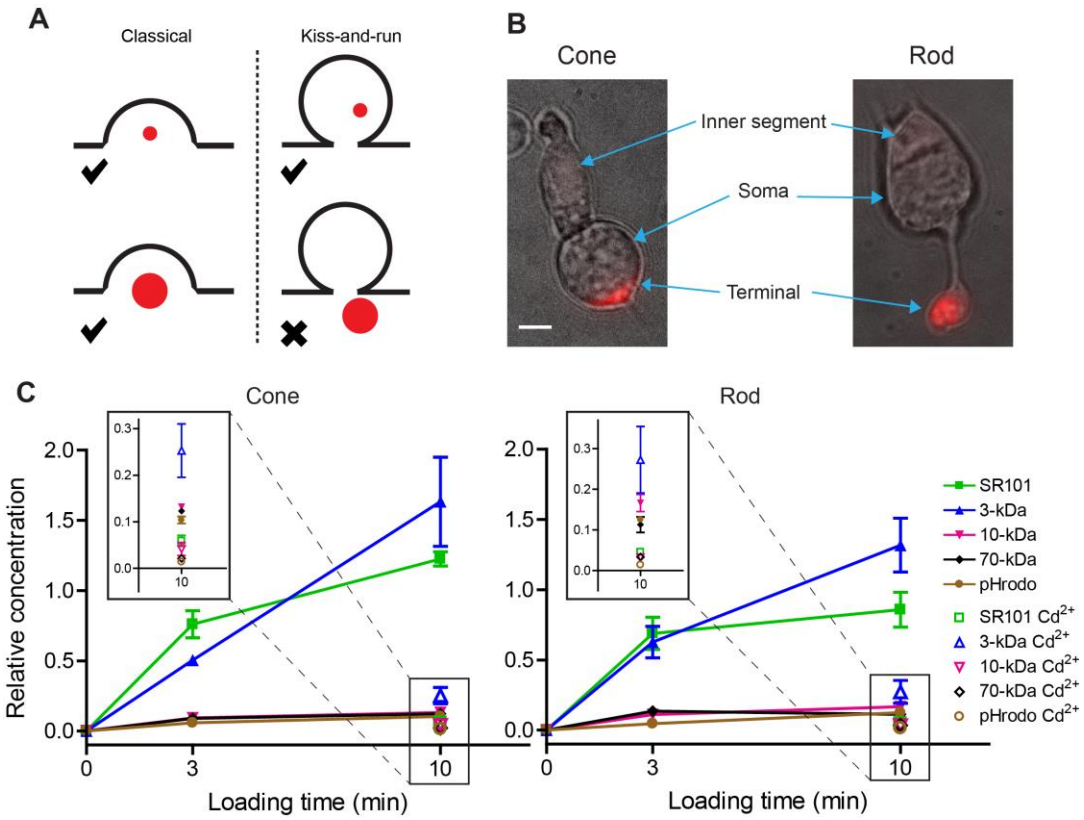

Figure 16. Small dyes were loaded preferentially into photoreceptor terminals over large dyes.

(A) Schematic image illustrating the idea that small dyes can be endocytosed by both classical and kiss-and-run endocytosis, whereas large dyes can be engulfed by classical endocytosis but would be rejected by kiss-and-run. (B) Examples of an isolated salamander cone and rod loaded by incubation with SR101 (7 µM, 3 min). Inner segments, cell somas, and brightly fluorescent synaptic terminals are indicated by arrows. Scale bar: 5 µm. (C) SR101, 3-kDa Texas Red, 10-kDa Texas Red, 70-kDa Texas Red, and 10-kDa pHrodo (7 µM) were loaded by incubating isolated cones and rods for 3 or 10 min. Basal loading was measured by incubating cells for 10 min in Ca^{2+}-free, high-Mg^{2+} saline solution with 0.1 mM Cd^{2+}. Specific brightness of each dye (F') relative to its concentration was measured in vitro. The relative intra-terminal concentration for each dye was calculated as follows: $\text{Relative concentration} = \frac{F}{F'/\mu M}$ where F is whole terminal fluorescence. Insets show data measured after 10-min loading at low relative concentration. Each data point is the average±SEM from three replicates.

For each replicate, we measured intraterminal fluorescence from 5-70 cells (average of 48 cones/replicate and 22 rods/replicate). Basal loading in Ca^{2+}-free, Cd^{2+}-containing solution was significantly lower than loading for 10 min in control saline (unpaired t-tests: SR101: cones, P<0.0001; rods, P=0.0029. 3-kDa Texas Red: cones, P=0.0128; rods, P=0.0074. 10-kDa Texas Red: cones, P=0.0031; rods, P=0.0034. 70-kDa Texas Red: cones, P<0.0001; rods, P=0.015. pHrodo, cones, P=0.0003; rods, P<0.0001).

Fluid phase indicators enter vesicles during endocytosis by passive diffusion. Given an internal vesicle diameter of 30 nm and dye concentration of 7 μM, an average of 0.06 dye molecules should be present within an intra-vesicular volume of $1.4x10^{-20}$ L. Most vesicles should therefore be retrieved with either a single dye molecule or no dye. Consistent with this, single vesicle fluorescence measured by TIRFM after loading with 7 μM 70-kDa Texas Red (560.7±334.9 [S.D.] fluorescence units, N=168 vesicles) was not significantly (P=0.063, F-test) greater than single 70-kDa Texas Red molecules (486.4±166.9 units, N=230). Thus, regardless of dye size, the overall intra-terminal concentrations of different dyes in this experiment should more closely reflect the number of dye-loaded vesicles than the concentration of dye within each vesicle.

Relative intra-terminal dye concentrations were calculated by dividing whole terminal fluorescence by the molar fluorescence of each dye measured in vitro. The fluorescence of pHrodo increases during vesicle re-acidification but terminal fluorescence was measured 3 and 10 min after loading, much longer than the time required for vesicle re-acidification (Gandhi and Stevens, 2003). Thus, like the other dyes, terminal fluorescence with pHrodo was determined by the rate of uptake, not re-acidification. The data fell into two distinct groups in both cones and rods: smaller dyes (0.6-kDa SR101 and 3-kDa Texas Red) were loaded equally well, whereas larger 10-kDa Texas Red, 10-kDa pHrodo, and 70-kDa Texas Red were loaded more poorly

(Figure 2C). The differences between these two groups increased as the loading period was increased from 3 to 10 min. Preferential uptake of the small dyes over large dyes is consistent with the idea that small dyes can be retrieved by two modes--kiss-and-run and conventional endocytosis--whereas uptake of large dyes is restricted to conventional mechanisms of endocytosis.

c. Dyes were loaded into synaptic vesicles.

To test whether dyes were loaded into synaptic vesicles, we incubated retinas with the various dyes and then measured their ability to be released by depolarizing stimulation with high KCl saline. For this experiment, we used higher dye concentrations and longer incubation times than the previous experiment (detailed in the legend for Figure 17). We found that all of the dyes (SR101, 3-kDa Texas Red, 10-kDa Texas Red, 70-kDa Texas Red, and 10-kDa pHrodo) were released from rod and cone terminals by depolarizing stimulation with 50 mM K^+ solution (Fig. 17A,B) indicating that they were loaded into synaptic vesicles. We also confirmed that 3- and 10-kDa Texas Red could be released from terminals of isolated rods and cones by 50 mM K^+ (data not shown).

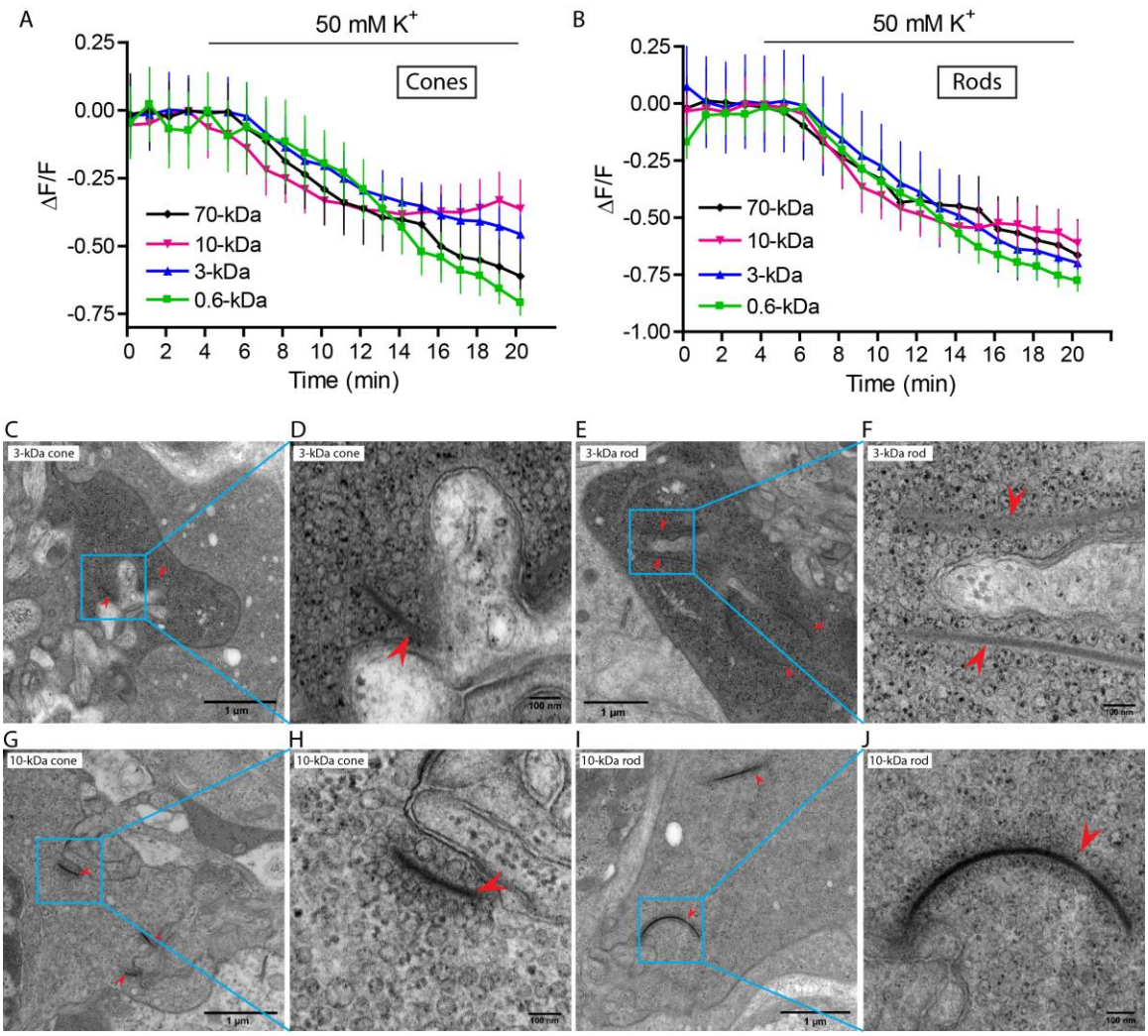

Figure 17. Dyes were loaded into synaptic vesicles.

(A,B) Fluorescence (ΔF/F) of SR101, 3-, 10-, and 70-kDa Texas Red declined upon application of 50 mM K^+ in both cones (A) and rods (B). Slices were incubated with SR 101 (83 μM, 30 min), 3-kDa Texas Red (133 μM, 45 min), 10-kDa Texas Red (100 μM, 60 min), and 70-kDa Texas Red (36 μM, 60 min). Each experiment was repeated three times and each data point shows the average ± SEM from 8-44 terminals. The capability of dyes to be released from retinal slices by depolarizing stimulation indicates they were loaded into releasable synaptic vesicles. (C-J) Electron micrographs of photoreceptor terminals loaded with lysine-fixable, 3-kDa Texas Red (7 μM). After photoconversion in the presence of DAB, electron dense precipitate can be seen in vesicles throughout the terminals. A cone terminal with its characteristically small ribbons (arrowheads) is shown in (C) and a rod terminal with its larger ribbons (arrowheads) in (E). Panels D and F

show magnified views of the square regions in C and E, respectively. (G-J) Electron micrograph of a photoreceptor terminal loaded with 10-kDa Texas Red (7 μM). (G) and (I) show a cone and a rod terminal, respectively. (H) and (J) show magnified views of the square regions in (G) and (I).

As further confirmation that dyes were loaded into synaptic vesicles, we photoconverted 3- and 10-kDa Texas Red and examined their distribution within photoreceptor terminals by EM. We loaded retinal pieces with 3- or 10-kDa lysine-fixable Texas Red at a concentration of 7 μM for 2 min in Ca^{2+} free solution to allow dye levels to equilibrate throughout the retina and then stimulated vesicle turnover by incubating the retinal pieces in dye for another 8 min in 20 mM K^{+} solution. After fixation, we photoconverted dyes in the presence of DAB to generate an electron-opaque, osmiophilic precipitate for EM images (Maranto, 1982; Schmued and Snavely, 1993). Electron-dense particles were concentrated in synaptic vesicles of photoreceptor terminals loaded with either 3- or 10-kDa Texas Red (Fig. 17). Photoreceptor terminals in the outer plexiform layer were identified by the presence of electron-dense ribbons (arrowheads). Rods were distinguished from cones by their much longer ribbons (Lasansky, 1978). For both dyes, we illustrate an example of a rod and cone terminal at low and high magnification. Figures 17C-D show a cone terminal at low (C) and high (D) magnification after loading with 3-kDa Texas Red. Figures 17G-H show a cone terminal loaded with 10-kDa Texas Red. Figures 17E-F show a rod terminal loaded with 3-kDa Texas Red. Figures 17I-J show a rod terminal loaded with 10-kDa Texas Red. Electron-dense particles were observed in vesicles both near and far from synaptic ribbons consistent with previous studies suggesting mixing of vesicles throughout the cytoplasmic and ribbon pools (Ripps et al., 1976; Schacher et al., 1976; Schaeffer and Raviola, 1978; Townes-Anderson et al., 1985; Townes-Anderson et al., 1988). Particles

were heavily concentrated in photoreceptor terminals and rarely seen in other parts of photoreceptors or neighboring processes of horizontal and bipolar cells. As in an earlier study of endocytosis in salamander rods using horseradish peroxidase (Townes-Anderson et al., 1985), electron-dense particles were occasionally observed in larger vacuoles, but the vast majority were located in synaptic vesicles. These experiments confirmed that the dyes used in our experiments are endocytosed into synaptic vesicles. In addition, more vesicles appeared to contain particles in terminals loaded with 3-kDa Texas Red than in terminals loaded with 10-kDa Texas Red (Figure 17C-J), consistent with preferential endocytosis of smaller molecules.

d. Impact of endocytosis inhibitors on uptake of large and small dyes

Different modes of synaptic endocytosis depend differently on clathrin and dynamin in different cells (Artalejo et al., 1995; Ferguson et al., 2007; Granseth et al., 2006; Kononenko and Haucke, 2015). Uptake of 3-kDa Texas Red into cone and rod terminals was significantly inhibited (see Figure 18 legend for statistics) by the dynamin inhibitor, dynasore (80 μM), and clathrin inhibitor, pitstop-2 (25 μM), with dynasore producing somewhat greater inhibition than pitstop-2. Uptake of 10-kDa Texas Red was inhibited to a similar extent by both dynasore and pitstop-2 (Fig. 18E-H). A larger fraction of 3-kDa Texas Red uptake into rod and cone terminals was inhibited by dynasore treatment than 10-kDa Texas Red uptake (Fig. 18). This may be partly due to the finding in Figure 2 that a larger fraction of the total uptake of 3-kDa Texas Red appears to be synaptic in origin--and is thus more likely to be sensitive to dynasore--than uptake of 10-kDa Texas Red.

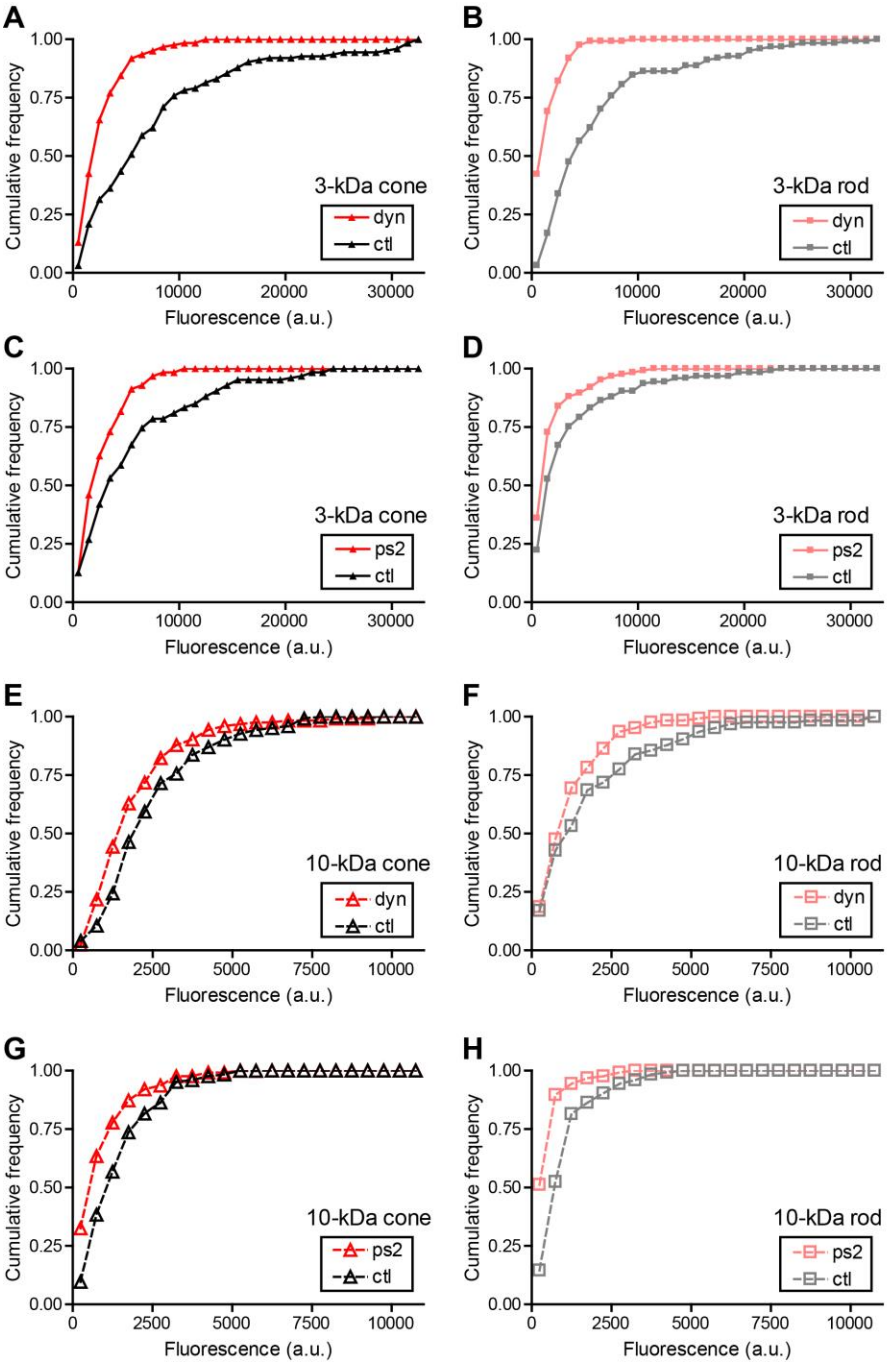

Figure 18. Sensitivity of small and large dyes to endocytic inhibitors.

Cumulative frequency histograms of whole-terminal fluorescence measured in rods and cones after incubation with 3-kDa or 10-kDa Texas Red. Retinas were incubated for 20 min in a test solution (dynasore, pitstop-2, or vehicle control) and then another 10 min in test solution supplemented with 3-kDa (67 μM) or 10-kDa Texas Red (50 μM). Retinal cells were then isolated and plated onto coverslips. Data in each condition were

obtained from multiple cells in three replicate experiments. (A) Cones loaded with 3-kDa Texas Red and treated with dynasore (80 μM, N=122 cells) or vehicle control (0.1% DMSO, N=124). The cumulative distributions of intraterminal fluorescence differed significantly by a Kolmogorov–Smirnov test (P<0.0001). (B) Rods loaded with 3-kDa Texas Red and treated with dynasore (N=123) or vehicle control (N=124; P<0.0001, Kolmogorov–Smirnov test). (C) Cones loaded with 3-kDa Texas Red and treated with pitstop-2 (25 μM, N=126) or vehicle control (0.2% DMSO, N=126; P<0.0001). (D) Rods loaded with 3-kDa Texas Red and treated with pitstop-2 (N=125) or vehicle control (N=125; P=0.002). (E) Cones loaded with 10-kDa Texas Red and treated with dynasore (N=124) or vehicle control (N=123; P<0.0001). (F) Rods loaded with 10-kDa Texas Red and treated with dynasore (N=124) or vehicle control (N=124; P=0.035). (G) Cones loaded with 10-kDa Texas Red and treated with pitstop-2 (N=126) or vehicle control (N=125; P<0.0001). (H) Rods loaded with 10-kDa Texas Red and treated with pitstop-2 (N=125) or vehicle control (N=124; P<0.0001).

e. Comparisons of endocytosis in individual vesicles.

Whole-terminal fluorescence measurements and ultrastructural images both indicated that a larger number of vesicles endocytosed small dyes than large dyes when exposed to similar concentrations. To compare the ability of vesicles to take up large and small dyes more directly, we used TIRFM techniques (Chen et al., 2013) to examine uptake into individual vesicles that were incubated simultaneously in 10-kDa and 3-kDa dyes.

We first incubated rods simultaneously with both red 3-kDa Texas Red and green 10-kDa AlexaFluor-488 (Fig. 19B). Salamander rods possess relatively large synaptic terminals that, when flattened onto the coverslip, can produce a region of membrane contact that is sufficiently large for TIRFM imaging. A faint fluorescent footprint reveals the region of contact between the coverslip and synaptic terminal membrane in the

average images. We used rods for these experiments because cones rarely exhibited synaptic terminal footprints that were suitable for TIRFM imaging. Individual bright spots could be seen in this footprint region (Fig. 19B), representing dye-loaded vesicles that advanced to the membrane and entered the evanescent field of illumination during the acquisition period. The evanescent wave in TIRFM decays with a length constant of ~60 nm, somewhat longer than the diameter of a single vesicle. The x-y resolution has a full-width half maximum of ~350 nm, but the incubation protocol loads only a small percentage of vesicles and so most individual bright spots were likely to represent the fluorescence of single vesicles (Chen et al., 2013). As discussed above, the low dye concentration (7 μM) and small intravesicular volume limited the likelihood that two dye particles were loaded into the same vesicle. We interleaved 488 and 565 nm excitation (30 frames apiece at 40 ms/frame and 140-ms intervals). In average images from this sequence (e.g., Fig. 19B), the brightness of a fluorescent spot was largely a function of the residence time of a dye-loaded vesicle at the membrane rather than the concentration of dye in each individual vesicle. The low percentage of loaded vesicles explains the limited overlap of red and green fluorescence in the average image (Fig. 19B).

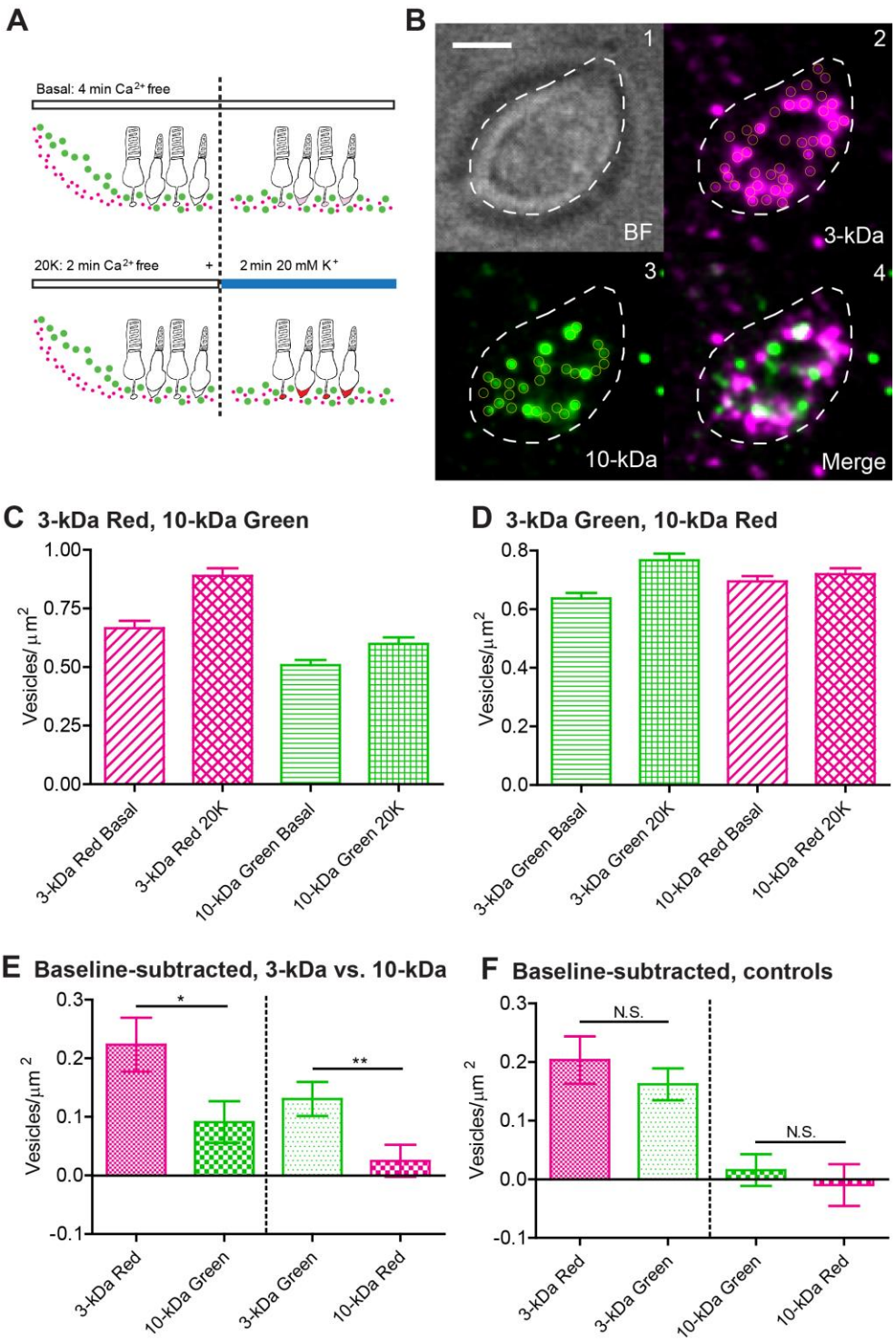

Figure 19. By incubating rods simultaneously in red and green dyes, TIRFM imaging of individual synaptic vesicles showed that more vesicles were loaded with small dyes than large dyes.

(A) Loading protocol: We incubated retinal pieces for 2 min in Ca^{2+}-free, high-Mg^{2+} saline to equilibrate dye throughout the retina. To measure basal loading, we maintained retinas for another 2 min in Ca^{2+}-free saline. To measure depolarization-evoked loading, we incubated retinas for the final 2 min in 20 mM K^+/1.8 mM Ca^{2+}. (B1) Bright-field image of an isolated rod terminal. (B2) Average TIRFM image (30x40 ms/frame, 140-ms intervals) of the same terminal showed many fluorescent vesicles (yellow circles) after incubation with 3-kDa Texas Red. Vesicle brightness in these average images was largely a function of the time each vesicle spent in the evanescent field near the membrane during the trial. (B3) Simultaneous incubation with 10-kDa AlexaFluor-488 loaded fewer vesicles. (B4) Merged image of 3-kDa Texas Red (magenta) and 10-kDa AlexFluor-488 (green) dyes. Scale bar: 2.5 µm. (C,D) Bar graphs show vesicles/μm^2 observed using TIRFM under basal Ca^{2+}-free and 20 mM high-K^+ conditions. 3-kDa Texas Red vs. 10-kDa AlexaFluor-488 in C (basal: N=83 terminals; 20-K^+: N=108); 3-kDa AlexaFluor-488 vs. 10-kDa Texas Red in D (basal: N=132; 20-K^+: N=109). (E,F) Bar graphs show vesicles/μm^2 observed with high-K^+ stimulation after subtracting basal loading. Panel E compares loading of 3-kDa vs. 10-kDa dyes. Panel F shows control experiments comparing loading of 3-kDa Texas Red vs. 3-kDa AlexFluor-488 (basal: N=132; 20-K^+: N=116) and 10-kDa Texas Red vs. 10-kDa AlexFluor-488 dyes (basal: N=113; 20-K^+: N=122). *P<0.05, **P<0.01, N.S. P>0.05 (t-test).

We collected a single trial for each rod terminal and identified local maxima in the average image (yellow circles in Fig. 19B) to count the number of vesicles loaded with red and green dyes. We typically saw 20-30 dye-labeled vesicles per terminal footprint (33.5±0.5 μm^2, N=914 terminals). To eliminate differences in loading that could arise from differences in the rate of dye diffusion through the retina, we began both control and test trials by loading the retina for 2 min in Ca^{2+}-free saline. In control trials, we then kept retinas in Ca^{2+}-free saline for another 2 min (for a total of 4 min). In test trials, after the first 2 min in Ca^{2+}-free saline, we incubated retinas for another 2 min in 20 mM K^+ saline with 1.8 mM Ca^{2+} to stimulate vesicle cycling and measure the attendant synaptic endocytosis. The number of vesicles loaded with 3-kDa Texas Red averaged 0.67±0.29

vesicles/μm^2 (N=83 terminals) in basal conditions and 0.89±0.34 vesicles/μm^2 (N=108) following high-K^+ stimulation (Fig. 19C). Rods are capable of considerable Ca^{2+}-independent spontaneous release that can account for much of the loading under basal, Ca^{2+}-free conditions (Cork et al., 2016). After subtracting basal loading, the net high-K^+-evoked increase in endocytosis averaged 0.22±0.05 vesicles/μm^2 with 3-kDa Texas Red. Significantly fewer vesicles were loaded with 10-kDa AlexaFluor-488 in the same synaptic terminals, with a net high-K^+-evoked increase in loading of 0.09±0.04 vesicles/μm^2 (P=0.024, unpaired t-test). Although the smaller 3-kDa dye has fewer fluorophore moieties attached to each dextran molecule, more vesicles were loaded with 3-kDa dye (Fig. 19B) and so we observed greater background fluorescence with this dye than with 10-kDa dye. This worsened the signal-to-noise ratio and so we may have under-counted the number of vesicles loaded with 3-kDa dyes. To control for differences in loading or detection arising from properties of the fluorophore other than molecule size, we swapped the fluorophores to measure endocytosis into vesicles that were incubated simultaneously in 10-kDa Texas Red and 3-kDa AlexaFluor-488 (Fig. 19D). As with the previous comparison of small red dye vs. large green dye, the net high K^+-evoked increase in vesicles loaded with the small green dye, 3-kDa AlexaFluor-488, was significantly greater than the increase in vesicles loaded with large 10-kDa Texas Red (N=109, P=0.0085; Figure 5E). As additional controls, we compared loading of 3-kDa Texas Red with 3-kDa AlexaFluor-488 and 10-kDa Texas Red with 10-kDa AlexaFluor-488 (Fig. 19F). We found no significant differences in net loading between red and green dyes of the same size (3-kDa, N=116, P=0.40; 10-kDa, N=122, P=0.57). Thus, consistent with whole-terminal fluorescence measurements of endocytosis and EM experiments, these data show that individual vesicles take up 2.3 nm 3-kDa dyes more frequently than 4.6 nm 10-kDa dyes.

f. Two modes of synaptic vesicle exocytosis.

The greater uptake of small dyes compared to large dyes suggests there are at least two modes of endocytosis in photoreceptors, with one mode favoring uptake of small molecules with diameter <4.6 nm. If the endocytic mode that preferentially takes up small molecules involves kiss-and-run, then we should also see differences in exocytosis since the processes of release and re-uptake are intrinsically coupled to one another during kiss-and-run. While full-collapse fusion should release large and small molecules equally, kiss-and-run should be incapable of releasing molecules that are larger than the fusion pore (Fig. 21A).

We examined release of various dyes by studying exocytosis of individual vesicles in rods using TIRFM (Chen et al., 2013). As a vesicle approaches the membrane, it becomes progressively brighter at a rate determined by its advance through the exponentially increasing evanescent field intensity (Fig. 20A,B). If, after contacting the membrane, a vesicle retreats from the membrane without fusion, then it should decline in brightness at a rate paralleling the rate at which vesicle brightness increases during approach (Fig. 20A). Figure 20A shows a non-release event for a vesicle loaded with SR101 in which vesicle fluorescence increased in a roughly exponential fashion as it approached the membrane and then decreased at a similar rate as it departed the membrane. If on the other hand, a vesicle releases its contents, then its fluorescence should decline almost instantly, as illustrated by the example in Figures 20B and C. Assuming a diffusion coefficient in water of 5.8×10^{-7} cm^2/s, a single 70-kDa Texas Red molecule should diffuse an average of 2.2 μm (27 pixels) within a single 40-ms frame and therefore disappear from view almost immediately after release. For TIRFM experiments on release, we used higher dye concentrations than for endocytosis experiments: SR101 (8.3 μM), 3-kDa Texas Red (133.3 μM), 10-kDa Texas Red (50

μM), pHrodo (50 μM), and 70-kDa Texas Red (14.3 μM). This increased the likelihood that a vesicle may contain more than a single dye molecule. By selecting the brightest vesicles for imaging, we also may have preferentially selected vesicles from the sub-population that contained more than a single dye molecule.

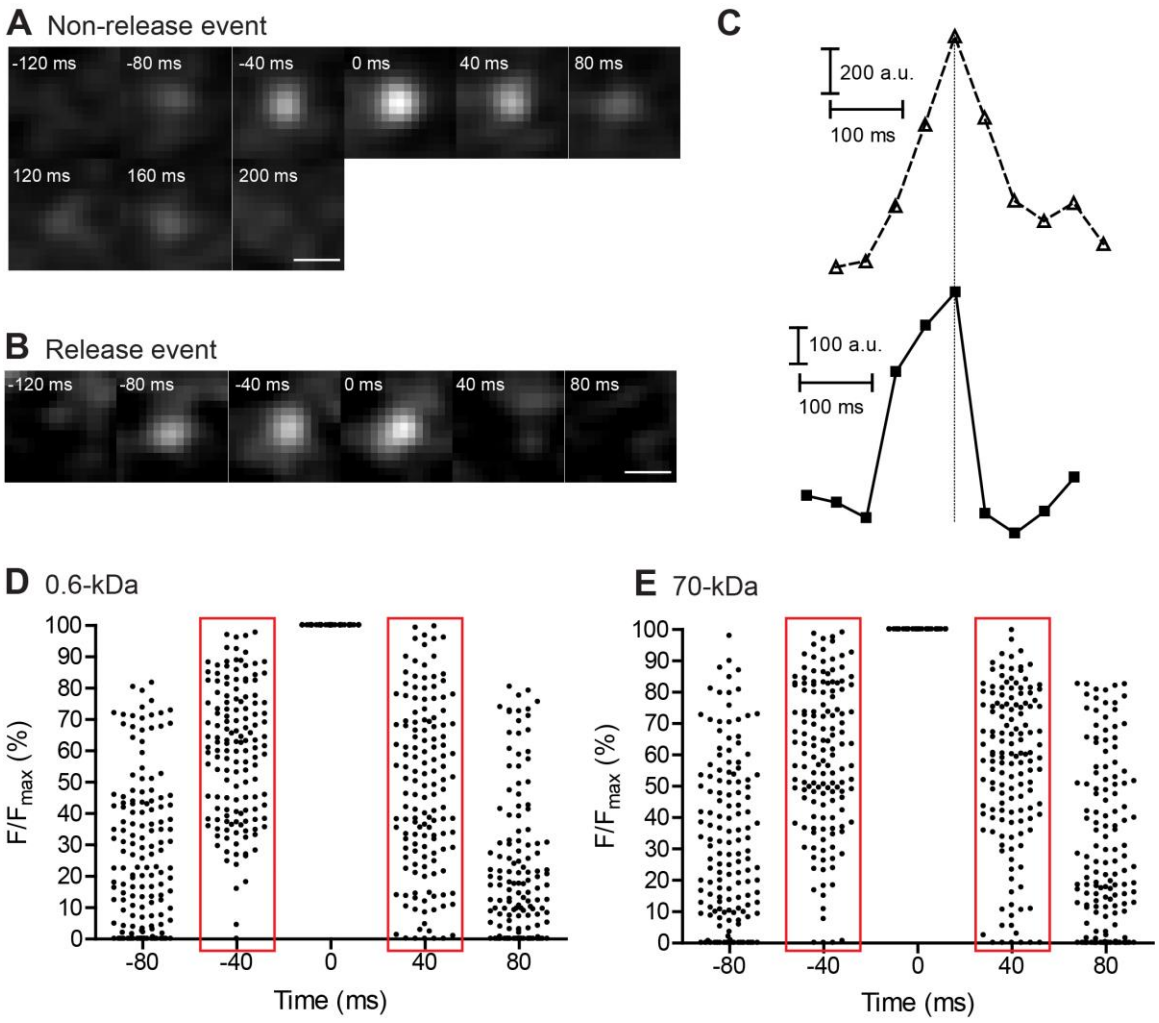

Figure 20. Imaging of individual vesicle release events using TIRFM in rods.

Consecutive 40-ms images showing a non-release event (A) and release event (B) in individual synaptic vesicles loaded with SR101. Scale bars: 0.5 μm. (C) Fluorescence changes were measured within a 7x7 pixel region of interest enclosing the vesicles in A (top) and B (bottom) and plotted as a function of time. Vertical line aligns the peak fluorescence values. Vesicle fluorescence declined more rapidly during release than

during non-release events in which fluorescence declined at a rate similar to the rate of increase observed as a vesicle approached the membrane. (D,E) Scatter plots of normalized fluorescence values measured in individual vesicles during the final two 40-ms frames of vesicle approach to the membrane and the first two frames during fluorescence decline. Data show vesicles loaded with SR101 (N=143 events) (D) and 70-kDa Texas Red (N=142) (E) during 50 mM K^+ puff.

From differences in the kinetics of appearance and disappearance, we distinguished release events from non-release events where vesicles departed the membrane without fusion. Figures 20D and E show scatter plots of relative fluorescence intensities (normalized to peak fluorescence) measured in individual vesicles during depolarizing stimulation with a puff of 50 mM K^+. We illustrate fluorescence changes in vesicles loaded with 0.6-kDa SR101 (Fig. 20D) and 70-kDa Texas Red (Fig. 20E). With both dyes, vesicle brightness increased gradually during the final two 40-ms frames of membrane before attaining peak fluorescence (Fig. 20). The relative fluorescence of a vesicle as it approaches the membrane can be converted to vesicle position within the submembrane evanescent field and then used to calculate approach velocity. Approach velocities calculated from vesicle position in the penultimate frame during membrane approach were similar (P=0.30; Student's t-test) for both SR101 (537±40 nm/s, N=143 events) and 70-kDa Texas Red (612±60 nm/s, N=142) and similar to earlier measurements made with other dyes (Chen et al., 2013; Zenisek et al., 2000). After reaching the membrane, vesicle fluorescence typically remained elevated for a short time and then declined in intensity (Chen et al., 2013). When analyzing vesicles that remained stably associated with the membrane for two or more frames, we measured the increase in fluorescence relative to the initial peak attained during approach and measured the decline in fluorescence relative to the final peak intensity just before it began to fall. For vesicles loaded with 70-kDa Texas Red (Fig. 20E), fluorescence

intensity generally declined at a similar rate as it rose during membrane approach suggesting most of these vesicles disappeared because of membrane departure, not fusion. Thus, for vesicles loaded with 70-kDa Texas Red, apparent velocities calculated from the rate of vesicle disappearance in one frame (736±74 nm/s, N=142) did not differ significantly from approach velocities (P=0.19, unpaired t-test). Similar approach and departure kinetics for non-release events was also seen with pHrodo-loaded vesicles by Chen et al. (2013) and may reflect high vesicle mobility at photoreceptor ribbon synapses (Holt et al., 2004; Rea et al., 2004). Many more of the vesicles loaded with the small dye, SR101 (Fig. 20D), showed rapid fluorescence declines. For example, during membrane approach, only 5 of 143 SR101-loaded vesicles exhibited an intensity <25% of its peak value by the penultimate frame. By contrast, six times as many vesicles (32) had fallen to <25% peak fluorescence by the first frame during the decline phase. Because of the greater number of release events in which fluorescence declined precipitously, the average apparent velocity calculated from the decline in fluorescence of SR101-loaded vesicles by the first frame after the peak (928±80 nm/s, N=143 events) was significantly faster than the approach velocity calculated from the rise in the fluorescence during the final frame (P<0.0001).

To assess the frequency of release events, we compared cumulative frequency histograms of relative fluorescence changes during the final 40-ms frame of membrane approach and the first frame of the decline phase (Fig 20D,E). For 70-kDa Texas Red, the two histograms were nearly identical indicating that rates of vesicle appearance and disappearance were very similar and therefore that most disappearance events were due to membrane departure rather than fusion (Fig. 21F). Histograms for 10-kDa Texas Red were also similar to one another (Fig. 21E). However, with SR101, 3-kDa Texas

Red, and 10-kDa pHrodo, there were noticeably larger differences between the histograms of fluorescence increase and decrease (Fig. 21B-D), suggesting many more release events. To determine the fraction of vesicles that disappeared more rapidly than they appeared during approach, we calculated differences between the cumulative histograms for fluorescence increase and decrease with each dye (Fig. 21G). From the peak differences between these cumulative histograms, we determined that 20% of the vesicles loaded with SR101 (N=143 events) or 3-kDa Texas Red (N=315) disappeared more rapidly than they appeared and were thus identified as release events (Fig. 21G,H). 25% of pHrodo-loaded vesicles were classified as release events in this way. By contrast, for 70-kDa (N=142) and 10-kDa Texas Red (N=213), only 6-9% of the events showed faster disappearance and were categorized as release events (Fig. 21G,H). Thus, similar to uptake experiments, release fell into two distinct groups with 10-kDa and 70-kDa Texas Red showing significantly less release than the other dyes (see figure legend for statistics).

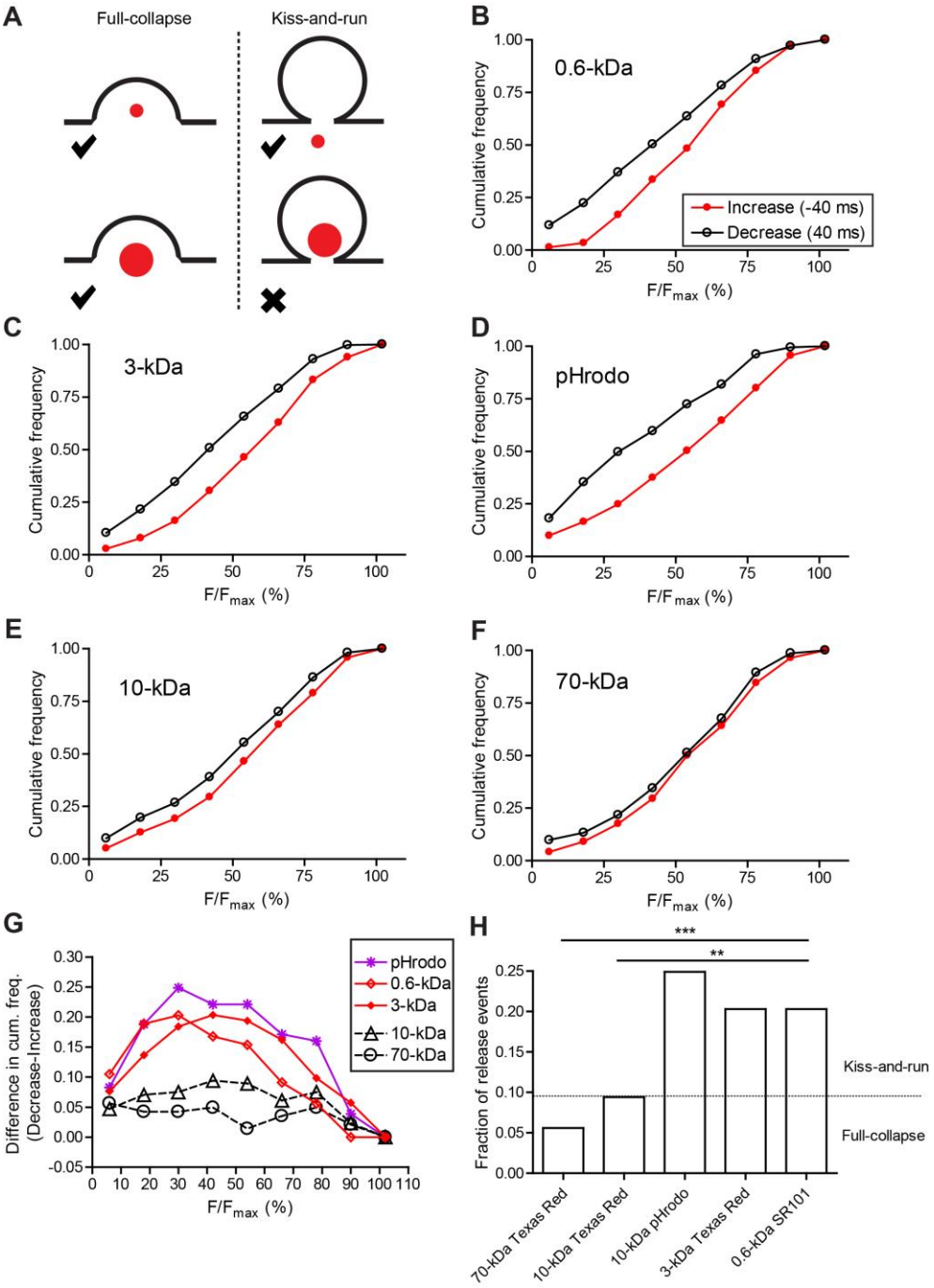

Figure 21 Two modes of synaptic vesicle exocytosis.

(A) Schematic image illustrating that small dyes can be released by both full-collapse and kiss-and-run exocytosis, whereas large dyes can only be released by full-collapse. (B-F) Cumulative histograms of relative fluorescence values measured in individual vesicles one 40-ms frame before the peak (increase; red filled circles) and one frame

after peak fluorescence was attained (decrease; black open circles). (G) Differences in cumulative frequency between fluorescence decrease and increase from B-F used to assess the fraction of events due to release. (H) Bar graph of release fractions determined from the maximum difference in cumulative frequency for each dye in G. Fractions of release events seen with SR101 (N=143 events), 3-kDa Texas Red (N=315), and pHrodo (N=181) were significantly greater than fractions of release events seen with 10-kDa (N=213) and 70-kDa Texas Red (N=142). **P<0.01, ***P<0.001 (z-test: pHrodo vs. 10-kDa Texas Red: P<0.0001; pHrodo vs. 70-kDa Texas Red: P<0.0001; SR101 vs. 10-kDa Texas Red: P=0.0034; SR101 vs. 70-kDa Texas Red: P=0.0002; 3-kDa Texas Red vs. 10-kDa Texas Red: P=0.0008; 3-kDa Texas Red vs. 70-kDa Texas Red: P<0.0001.)

The use of 10-kDa pHrodo provided a useful test of the hypothesis that differences in uptake and release between large and small molecules involve significant contributions from kiss-and-run. Recall that in uptake experiments, 10-kDa pHrodo was endocytosed poorly like 10-kDa and 70-kDa Texas Red. On the other hand, pHrodo behaved like smaller dyes in release experiments. What can explain this difference? Unlike Texas Red, pHrodo fluoresces more brightly in the acidic environment of the vesicle interior and is quenched by alkaline extracellular pH (https://www.thermofisher.com/us/en/home/brands/molecular-probes/key-molecular-probes-products/phrodo-indicators.html). Thus, while 10-kDa pHrodo itself may be retained within a vesicle during kiss-and-run, protons can readily exit the vesicle through a small fusion pore, causing pHrodo fluorescence to decline abruptly. An abrupt decline in fluorescence would classify this as a fusion event. The finding that the percentage of pHrodo-loaded vesicles classified as release events was similar to the percentage of release events for SR101 and 3-kDa Texas Red supports the conclusion that kiss-and-run contributes to a large fraction of release events. If large molecules (10-kDa and 70-kDa Texas Red) can only be released by full-collapse whereas small molecules (SR101,

3-kDa Texas Red, and intravesicular protons) can be released by both full-collapse and kiss-and-run, then these data indicate that full-collapse contributes to 24-45% of release events identified by our criteria (6-9%/20-25%) and kiss-and-run contributes to the remaining 55-66% (Fig. 21H).

V. Discussion:

a. Kiss-and-run is favored in photoreceptors.

A key property of kiss-and-run is the transient opening of a small fusion pore that allows release of vesicle contents without complete fusion with the plasma membrane. We found that molecules $\leq$2.3 nm diameter were released and retrieved much more readily than molecules $\geq$4.6 nm. This suggests there are two modes of release and re-uptake: one involving kiss-and-run fusion with a pore diameter of 2.3-4.6 nm and a second involving full-collapse followed by conventional endocytosis in which large and small dyes are released and retrieved equally well. We found that 10-kDa pHrodo loaded poorly like 10-kDa and 70-kDa Texas Red, but exhibited release properties similar to smaller dyes in TIRFM release experiments. This can be explained by the pH-dependence of pHrodo in which departure of intravesicular protons through a fusion pore during kiss-and-run can rapidly quench pHrodo fluorescence even while the dye itself is retained within the vesicle. Because loading of 10-kDa pHrodo likely occurs by conventional endocytic mechanisms, this suggests that vesicles retrieved by conventional endocytosis can subsequently participate in kiss-and-run release. Consistent with mixing of vesicles after retrieval as suggested by earlier studies (Ripps et al., 1976; Schacher et al., 1976; Schaeffer and Raviola, 1978; Townes-Anderson et al., 1985; Townes-Anderson et al., 1988). photoconversion experiments showed that

vesicles loaded with both 3- and 10-kDa Texas Red were dispersed throughout the terminal.

CNS neurons can retrieve synaptic vesicles by fast and slow forms of endocytosis (Delvendahl et al., 2016; Jockusch et al., 2005; Liang et al., 2017; Van Hook and Thoreson, 2012; von Gersdorff and Matthews, 1994b; Watanabe et al., 2013; Watanabe and Boucrot, 2017). While there are exceptions, vesicle fission typically requires the GTPase dynamin. Slower forms of endocytosis also typically involve formation of a clathrin protein lattice whereas faster forms can proceed without clathrin (Soykan et al., 2016). We observed inhibition of uptake with dynasore and pitstop-2 indicating the presence of both dynamin- and clathrin-dependent retrieval processes. Measurements of membrane capacitance in rods and cones suggested the presence of both fast and slow forms of endocytosis with the rapid form (τ~600 ms) accounting for at least 70% of membrane retrieval. Although other forms of endocytosis can also produce rapid declines in membrane capacitance (Elhamdani et al., 2006; He et al., 2006; Watanabe and Boucrot, 2017; Wu and Wu, 2007), the initial rapid decline in capacitance that we observed is consistent with TIRFM results suggesting that kiss-and-run contributes to a majority of release events.

We confirmed that the rapid decline in capacitance seen after depolarizing stimulation in rods and cones found by Van Hook and Thoreson (2012) was not an artefact of conductance changes accompanying glutamate transporter anion channels or activation of I_h channels by blocking these channels. Van Hook and Thoreson (2012) found that ultrafast endocytosis in cones, but not rods, was dynamin-independent. By contrast, our imaging studies did not show any obvious differences between rods and cones in their sensitivity to dynasore . In the study by Van Hook and Thoreson (2012),

release was stimulated by strong, brief depolarizing steps. On the other hand, photoreceptors in the present study were incubated in dye for many minutes without any depolarizing stimulation. This may favor slower forms of endocytosis that are more likely to show sensitivity to dynasore in both cones and rods

To identify release events using TIRFM, we developed stringent criteria to exclude events in which vesicle disappearance might be due to retreat from the membrane without fusion. Because we compared release event ratios and not absolute numbers, the larger percentage of release events observed with SR101, 3-kDa Texas Red, and pHrodo in TIRFM experiments was not a result of differences in dye loading. Furthermore, pHrodo exhibited a similar release percentage to smaller dyes even though it was endocytosed much more poorly. All vesicles analyzed for TIRFM release experiments showed similar signal-to-noise properties and so noise-related errors should be similar among dyes. Differences in diffusion kinetics among dyes were not large enough to significantly impact rates of vesicle disappearance. For example, 3-kDa and 10-kDa dye particles should depart a 7x7 pixel region of interest in 0.88 and 1.36 ms, respectively, creating only 0.6% difference in probability of detecting release by our criteria. It is therefore unlikely that the criteria used to identify release events selectively favored detection of release when using SR101, 3-kDa Texas Red, or pHrodo.

While the most parsimonious explanation for our data involves two modes of release, full-collapse and kiss-and-run, we also considered alternatives that might require only full-collapse. A possible alternative explanation for preferential detection of release with small molecules that involves only full-collapse could be that the fusion pore dilates very slowly to allow release of small molecules many milliseconds before release

of larger molecules. While such a mechanism could promote faster disappearance of vesicles loaded with small dyes, it should also cause a graded increase in the likelihood of detecting release events with decreasing molecular size. Instead, we found that release clustered into two distinct groups. This hypothetical full-collapse mechanism would also have to incorporate preferential uptake of small dyes during endocytosis. This could be achieved if, during endocytic retrieval of vesicles after full collapse, the vesicle lumen remained in contact with the extracellular space through a narrow neck for an extended time prior to fission. However, once again, this mechanism would predict a graded increase in uptake efficiency with decreasing molecular size, not the two distinct groups that we observed. This mechanism also predicts that increasing the persistence of vesicles at the membrane should increase the preferential uptake of small dyes. An increase in the persistence of hemifused vesicles at the membrane can be achieved by inhibiting dynamin GTPase activity (Logiudice et al., 2009; Newton et al., 2006). However, contrary to this prediction, we found that inhibiting dynamin with dynasore reduced uptake of small dyes rather than promoting their preferential uptake. Thus, the preferential release and re-uptake of small molecules cannot be explained by a single full-collapse mechanism and is instead more likely due to significant contributions from kiss-and-run.

Consistent with our findings, capacitance measurements from large secretory vesicles in neuroendocrine cells (Albillos et al., 1997; Fulop et al., 2005; Spruce et al., 1990) and small synaptic vesicles in neurons (He et al., 2006) have found that fusion pores formed during the first few milliseconds of fusion or during stand-alone kiss-and-run events can have a diameter of 1-3 nm. On the other hand, fusion pores of 0.3 nm diameter or smaller have been observed in synaptic-like microvesicles of pituitary cells

(Klyachko and Jackson, 2002) and small secretory granules of neutrophils (Lollike et al., 1995; Lollike et al., 1998). Lollike et al. (1998) suggested that further dilation of a pore beyond its initial small size may lead irreversibly to fusion of small secretory granules. On the other hand, imaging of large dense core granules in chromaffin cells suggests that the fusion pore connecting a hemifused vesicle to the plasma membrane may never fully dilate (Chiang et al., 2014; Zhao et al., 2016). Electron tomography has shown omega figures characteristic of hemifused vesicles at rod synapses in mouse retina (Zampighi et al., 2011).

b. Functional significance for retinal processing and vision.

Cones release vesicles exclusively from ribbons (Snellman et al., 2011; Van Hook and Thoreson, 2015) at a steady rate in darkness of ~2 vesicles/s per ribbon release site (Heidelberger et al., 2005). Rods release vesicles at slower rates, with release occurring at both ribbon and non-ribbon release sites (Chen et al., 2013; Sheng et al., 2007). We only examined release with TIRFM techniques in rods, but the similar capacitance responses and behavior in endocytosis assays of rods and cones suggests that retrieval in both cell types likely involves kiss-and-run. One advantage of kiss-and-run is that it provides a mechanism to return synaptic vesicles rapidly to the releasable pool. However, re-loading of vesicles with glutamate is slow, with a time constant of ~15 s (Hori and Takahashi, 2012), and so rapid endocytosis may not greatly speed the return of vesicles to a fully functional status. Instead, the fast rate of vesicle retrieval in photoreceptors may be more important for clearing used synaptic proteins and lipids from the active zone to restore release site function (Hosoi et al., 2009; Hua et al., 2013; Kawasaki et al., 2000; Lipstein et al., 2013; Mahapatra et al., 2016; Neher, 2010). This role for endocytosis may be particularly important in photoreceptors where release

occurs continuously at numerous closely adjacent sites along the base of the ribbon. Another potential advantage of kiss-and-run is that it could limit changes to the active zone membrane that might otherwise be caused by the merger of vesicle membrane proteins and lipids during full-collapse fusion.

What are the post-synaptic effects of kiss-and-run release? The 10-90% rise time of miniature excitatory postsynaptic currents (mEPSCs) at rod and cone synapses averages ~0.7 ms (Cadetti et al., 2008; Cork et al., 2016; Feigenspan and Babai, 2015), slower than many synapses. Synaptic cleft glutamate levels reach ~1 mM (Cadetti et al., 2008; Kim and Miller, 1993). Modeling suggests that glutamate released through a 2-nm pore can attain a concentration of >3 mM at a distance of 20 nm within 0.7 ms (Jackson, 2007). Thus, glutamate release through kiss-and-run pores can account for properties of mEPSCs observed in second-order retinal neurons.

Release at photoreceptor ribbon synapses involves a number of specialized synaptic proteins. In addition to the ribbon protein RIBEYE (Schmitz et al., 2000), other specialized proteins include syntaxin 3b (Mazelova et al., 2009; Morgans et al., 1996) and complexins 3 and 4 (Reim et al., 2005). The Ca^{2+} sensor that mediates release from photoreceptors has not been identified but shows a higher Ca^{2+} affinity and lower cooperativity than synaptotagmin 1 (Duncan et al., 2010; Thoreson et al., 2004). Syntaxin, complexin and synaptotagmin have all been implicated in regulating fusion pore size and duration (Archer et al., 2002; Dhara et al., 2014; Han et al., 2004; Rao et al., 2017; Wang et al., 2003; Zhang et al., 2011). The protein isoforms employed at photoreceptor synapses may favor kiss-and-run, although a number of these isoforms are also present at bipolar cell ribbon synapses where kiss-and-run appears to be rare (Zenisek et al., 2002). Identifying the particular specializations that promote kiss-and-run

in photoreceptors may help to identify factors regulating release mode in other CNS neurons.

The amount of kiss-and-run release found at CNS synapses varies among preparations and even between studies using the same preparation. Studies in retinal bipolar cells, hippocampal neurons, and the calyx of Held suggest that kiss-and-run is a relatively rare occurrence (Balaji and Ryan, 2007; Chen et al., 2008; Granseth et al., 2006; He et al., 2006; Zenisek et al., 2002). However, other studies from hippocampal neurons (Gandhi and Stevens, 2003; Richards et al., 2005; Zhang et al., 2009) and studies in lamprey reticulospinal synapses (Photowala et al., 2006) suggest that it can sometimes be quite common. The preferential uptake and release of small molecules, along with the rapid kinetics of endocytic retrieval, suggest that kiss-and-run mechanisms contribute significantly to vesicle cycling at photoreceptor synapses. This efficient mode of retrieval may promote rapid recycling that is particularly important at photoreceptor ribbon synapses to maintain the structure and function of release sites during continuous release.

Chapter 4 Glutamate transporter currents and calcium-activated chloride currents contribute to feedback signals from horizontal cells to cone photoreceptors

I. Introduction:

Light signals received by photoreceptors are transmitted to retinal bipolar cells which then pass them on to retinal ganglion cells and finally to higher visual centers in the brain. If the retina projected feedforward signals to higher centers without modification, visual images reaching our brain would be much more coarse and blurry. To sharpen images, enhance edge detection, and separate colors, the retina modifies light responses by negative feedback in the outer retina via horizontal cells (HCs) and in the inner retina via amacrine cells. HCs receive visual signals from photoreceptors and then send a sign-inverted feedback signal back to photoreceptors (Thoreson and Mangel, 2012). Thus, while a cone hyperpolarizes to light, negative feedback from HCs can depolarize the cone membrane potential (Baylor et al., 1971).

Central to this negative feedback, hyperpolarization of HCs by light cause both an increase in peak amplitude and a negative activation shift in voltage-dependence of I_{Ca} in cones (Verweij et al., 1996). The combined effects of this negative activation shift and increase in peak amplitude increases I_{Ca} within the normal physiological range of cone membrane potentials (ca. -40 to -60 mV). This increase in Ca^{2+} influx will also increase the release of glutamate-laden synaptic vesicles from cones, countering the reduction in glutamate release that accompanies light-evoked hyperpolarization of cones. The mechanisms by which negative feedback from HCs alter cone I_{Ca} remain unclear, but they appear to involves extracellular pH changes (Cadetti and Thoreson, 2006; Thoreson and Mangel, 2012; Vroman et al., 2014; Wang et al., 2014; Warren et al., 2016a).

The increase in Ca^{2+} influx in cones caused by HC feedback can depolarize the cone. Ca^{2+} entry will also act on the Ca^{2+}-dependent K^+ and Cl^- channels found in cones. In addition to exerting a hyperpolarizing influence on membrane potentials, Ca^{2+}-activated K^+ currents in salamander rods directly facilitate Ca^{2+} influx and glutamate release (Xu and Slaughter, 2005). However, blocking K^+ channels does not appear to alter feedback responses of cones (Thoreson and Burkhardt, 1991). Ca^{2+}-activated Cl^- currents ($I_{Cl(Ca)}$) are particularly prominent in cones and blocking these Cl^- channels with niflumic acid can reduce the feedback-induced depolarization in cones (Barnes and Deschenes, 1992; Kraaij et al., 2000; Packer et al., 2010; Thoreson and Burkhardt, 1991; Verweij et al., 2003). Cl^- channel activity may influence feedback by effects of Cl^- flux on cone membrane potential, changes in ephaptic currents (Endeman et al., 2012) and by direct effects on I_{Ca} (Thoreson et al., 1997). Another Cl^- conductance in cones is the anion conductance associated with glutamate transporter activity (Eliasof and Werblin, 1993; Picaud et al., 1995a; Rauen and Kanner, 1994; Vandenbranden et al., 1996). In some glutamate transporters, when glutamate is transported, this also causes a chloride-permeable pore in the transporter to open. Cones possess two EAAT2 splice variants (Eliasof et al., 1998; Rauen et al., 2004; Reye et al., 2002; Rowan et al., 2010; Schneider et al., 2014). While some EAAT2 isoforms exhibit little anion current, the retina-specific variant of EAAT2 shows prominent anion currents (Schneider et al., 2014). Glutamate released from a cone can act locally on itself to stimulate glutamate transporter activity and the associated anion conductance (Picaud et al., 1995b). Glutamate can also diffuse to neighboring cones where uptake by EAAT glutamate transporters can activate anion channels (Arriza et al., 1997; Szmajda and Devries, 2011). Vroman and Kamermans (2015) showed that activation of glutamate-associated Cl^- currents in neighboring cones by diffusion of glutamate can help to bring their membrane potential back into the range where I_{Ca} is active. However, these earlier

studies used surround illumination to stimulate HC feedback and were not therefore able to assess the role of locally released glutamate on feedback currents. We therefore investigated the relative contributions of $I_{Cl(Ca)}$ and glutamate transporter anion currents on feedback-induced currents in cones. To study negative feedback from HCs to cones, we obtained simultaneous whole-cell patch clamp recordings from both cones and HCs. This allowed us to study the effects of changes in HC membrane potential on cone membrane currents directly. We found that glutamate-transporter coupled Cl^- currents contributed to a larger fraction of feedback currents than $I_{Cl(Ca)}$ and thus play a more prominent role in HC to cone feedback than previously recognized.

II. Methods:

a. Animal care and use

Aquatic tiger salamanders (Ambystoma tigrinum, 18 to 25 cm; Sullivan Company, Nashville, TN, USA) were maintained on a 12-h light/dark cycle and sacrificed after $\geq$1 h of dark adaptation. Salamanders were anaesthetized by immersion in 0.25 g/L Tricaine-S (tricaine methanesulfonate, Western Chemical, WA, USA) for >15 min, decapitated with heavy shears, and then pithed. Procedures were approved by the University of Nebraska Medical Center Institutional Animal Care and Use Committee.

b. Retinal slices

A detailed description of retinal slice preparation and whole cell recording techniques has been described previously (Van Hook and Thoreson, 2013). Briefly, after enucleation, the front of the eye was removed and the resulting eyecup was cut into 2-4 pieces. A piece of retina was placed vitreal side down on a piece of nitrocellulose membrane (5 x 10 mm; type AAWP, 0.8 μm pores; EMD Millipore). The filter paper was

then submerged in cold amphibian saline and the sclera peeled away, leaving the retina attached to the membrane. The retina was cut into 125-μm slices using a razor blade tissue slicer (Stoelting Co, Wood Dale, IL, USA). Slices were rotated 90 degrees to view retinal layers and anchored in the recording chamber by embedding the ends of the nitrocellulose membrane in vacuum grease. For recording, the recording chamber was mounted on an upright fixed-stage microscope (Olympus BH2-WI, Shinjuku, Tokyo, Japan) and slices were superfused at ~1 ml min^{-1} with bicarbonate-buffered amphibian saline solution (in mM): 101 NaCl, 22 $NaHCO_3$, 2.5 KCl, 2.0 $CaCl_2$, 0.5 $MgCl_2$, 11 glucose (pH 7.4). Solutions were bubbled continuously with 95% O_2/5% CO_2.

c. Patch-clamp electrophysiology

Patch pipettes were fabricated with borosilicate glass (1.2 mm OD, 0.9 mm ID, with an internal filament; World Precision Instruments, Sarasota, FL, USA) using a PC-10 or PP-830 vertical puller (Narishige, Tokyo, Japan). Patch pipettes had tip diameters of ~1 μm and resistances of 10-15 MΩ.

We used a number of different pipette solutions that differed in anion levels and Ca2+ buffering. In many experiments, we used a Cs-Gluconete/CsGlutamate-based pipette solution for cones that contained (CsGluc/Glut; in mM): 50 Cs-gluconate, 40 Cs-glutamate, 10 TEA-Cl, 3.5 NaCl, 1 $CaCl_2$, 1 $MgCl_2$, 10 ATP-Mg, 0.5 GTP-Na, 10 HEPES, and 5 EGTA. The addition of glutamate to the presynaptic pipette solution enhances post-synaptic currents in HCs during paired whole-cell recording (Bartoletti and Thoreson, 2011). The CsGluc pipette solution omitted glutamate and consisted of (in mM): 90 Cs-gluconate, 10 TEA-Cl, 3.5 NaCl, 1 $CaCl_2$, 1 $MgCl_2$, 10 ATP-Mg, 0.5 GTP-Na, 10 HEPES, and 5 EGTA. Another cone pipette solution replaces gluconate and glutamate with chloride (CsCl) and contained (in mM): 90 CsCl, 10 TEA-Cl, 3.5 NaCl, 1

$CaCl_2$, 1 $MgCl_2$, 9.4 ATP-Mg, 0.5 GTP-Na, 10 HEPES, and 5 EGTA.

Synaptic transmission was monitored using paired whole-cell recordings from cones and HCs using a Multiclamp 700B amplifier, pClamp 10.7 software, and Digidata 1440A digitizer (Molecular Devices, Sunnyvale, CA, USA). Cones were identified by their morphology. HCs were identified by their morphology, position in the slice, and electrophysiological characteristics (Van Hook and Thoreson 2013). HCs were voltage-clamped at -60 mV and cones at -70 mV.

After obtaining whole cell recordings from a cone and HC, we held cones at a variety of different membrane potentials from -30 to +50 mV while feedback currents were evoked by hyperpolarizing the HC from -30 to -90 mV. Test solutions were bath applied.

d. Reagents

DL-TBOA, Ani9, 6-cyano-7-nitroquinoxaline-2,3-dione (CNQX) were from Tocris (Bristol, UK). Unless otherwise noted, other reagents were from Sigma-Aldrich Chemicals (St. Louis, MO, USA).

III. Results:

a. Chloride currents contributes to inward feedback currents in cones.

Using an approach described previously (Warren et al., 2016b), we evoked inward feedback currents in voltage-clamped cones by simultaneously voltage-clamping a HC at -30 mV (similar to its membrane potential in darkness) and then hyperpolarizing it to -90 mV, to mimic the effect of a saturating bright flash of light. We tested the effects of this change in HC membrane potential on cone membrane currents while holding the cone at different membrane potentials ranging from -50 to +30 mV (Fig. 22A-B). As

illustrated in Figure 22D and E, hyperpolarizing the HC from -30 to -90 mV introduces a feedback signal to the cone that shifts cone I_{Ca} voltage dependence leftward towards more negative voltages and increases the peak amplitude of I_{Ca} (Cadetti and Thoreson, 2006; Verweij et al., 1996). Figure 22E plots the difference between I_{Ca} measured in a cone while the HC was voltage-clamped at -30 mV and I_{Ca} measured when the HC was held at -90 mV. Because the leftward voltage shift enhances currents at voltages more negative potentials (left of the peak current), the maximal change in I_{Ca} produced by HC feedback occurs at voltages left of the peak value for I_{Ca} (Fig. 22E). When the cone is held steadily at membrane potentials from -50 to +10 mV, hyperpolarizing the HC typically stimulated an inward current in the cone due to an increase in cone I_{Ca}. The peak amplitude of this inward feedback current in the cone was plotted against the cone holding potential (Fig. 22F). At a cone holding potential of -50 mV, there is little I_{Ca} activity and thus minimal feedback currents. Holding the cone at -30 mV or higher stimulated greater activation of I_{Ca} and larger feedback currents (Fig. 22F). However, the voltage-dependence of inward feedback currents did not match the increase in I_{Ca} determined by measuring the change in the current/voltage relationship of I_{Ca} produced by hyperpolarizing the HC from -30 to -90 mV. Although HC feedback caused only a slight increase in I_{Ca} at the cone membrane potential of -30 mV (Fig. 22E), there was a more pronounced increase in inward feedback currents at this potential (Fig. 22F). This suggests that the inward feedback currents produced in cones by HC hyperpolarization are not simply the result of changes in I_{Ca} but likely involve other currents.

The increase in intracellular Ca^{2+} accompanying the increase in I_{Ca} stimulates an increase in $I_{Cl(Ca)}$ and can stimulate glutamate release which can in turn activate glutamate transporter-associated chloride channels. To test for a contribution of Cl^- currents to the inward feedback currents evoked in cones by HC hyperpolarization, we

switched from a pipette solution with E_{Cl} ~ -46 mV to one with higher intracellular Cl^- levels where E_{Cl} was predicted to be ~ 0 mV. Consistent with a contribution from Cl^- currents, this change led to an increase in the amplitude of inward feedback currents when evoked in cones held at -30 mV (P=0.0127) or -50 mV (P=0.0164) (Fig. 22F).

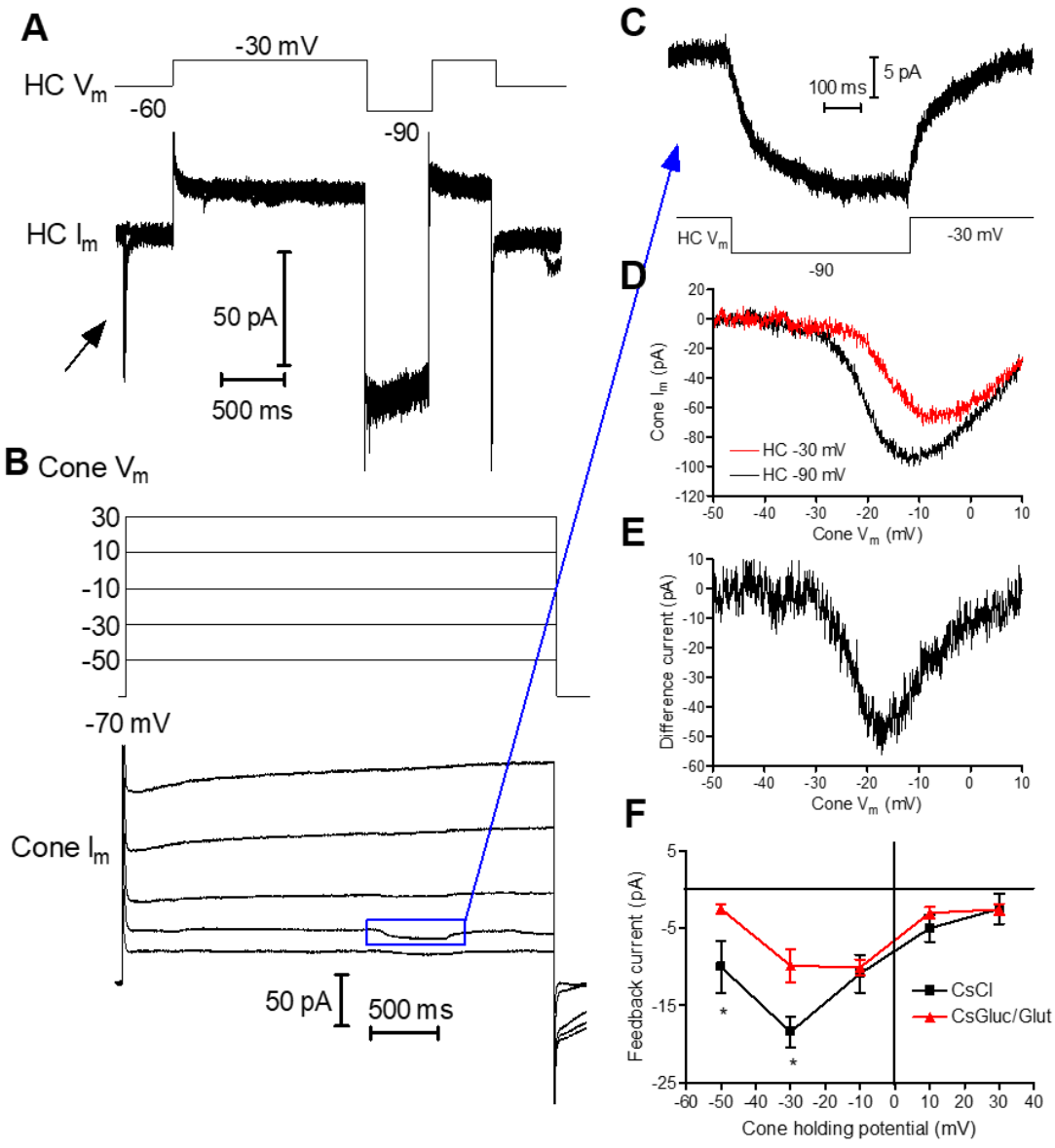

Figure 22. Testing for inward feedback currents in cone/HC pairs.

(A) The voltage step waveform applied to the voltage-clamped HC is shown at the top (HC V_m), and the resulting HC membrane currents accompanying the five different test steps applied to cones are overlaid below (HC I_m). The presence of excitatory postsynaptic currents (EPSCs) evoked in the HC when the cone was depolarized to at least -30 mV (arrow), shows that the HC and cone were synaptically connected. (B) Voltage step protocol applied to a simultaneously voltage-clamped cone (Cone V_m) is shown at the top and the resulting cone membrane currents shown below (Cone I_m). The maximal inward feedback current evoked by hyperpolarizing the HC from -30 to -90 mV was observed when the cone was held at -30 mV (blue rectangular). (C) Magnified view of the inward feedback current evoked when the cone was voltage-clamped at -30 mV. (D) Leak-subtracted cone I_{Ca} plotted against the cone holding potential measured using CsGluc/Glut pipette solution while a post-synaptic HC was simultaneously voltage-clamped at either -30 (red trace) or -90 mV (black trace). (E) Difference current showing the increase in cone I_{Ca} caused by changing the HC holding potential from -30 to -90 mV. (F) The peak amplitude of inward feedback currents in cones plotted against cone holding potential using the CsGluc/Glut (triangle, red line, N=11 pairs) and CsCl (square, black line, N=7). Each data points show average ± SEM. * $P<0.05$.

It has been proposed that currents flowing through post-synaptic glutamate receptors into HC dendrites might contribute to feedback by generating extracellular, ephaptic voltage changes (Byzov and Shura-Bura, 1986; Kamermans et al., 2001). When feedback from HCs to cones is evoked by light, blocking AMPA/KA receptors on HCs blocks feedback by blocking the feedforward effects of glutamate released by cones onto HCs and thus blocking the light-evoked hyperpolarization of HCs (Thoreson and Burkhardt, 1990; Verweij et al., 1996). With paired cone/HC recordings, we bypassed feedforward glutamate release from cones, allowing us to test directly for contributions from postsynaptic glutamate receptors at the feedback synapses from HCs onto cones. With superfusion of CNQX (100 μM), a competitive AMPA/KA glutamate receptor antagonist, we saw a slight increase in feedback currents but this was also

seen in vehicle control experiments using 0.3% DMSO and is therefore likely due to run-up (Fig. 23B). The evidence that CNQX did not significantly alter feedback currents in cones suggests that glutamate receptors on HC dendrites do not play a direct role in feedback (Fig. 23A).

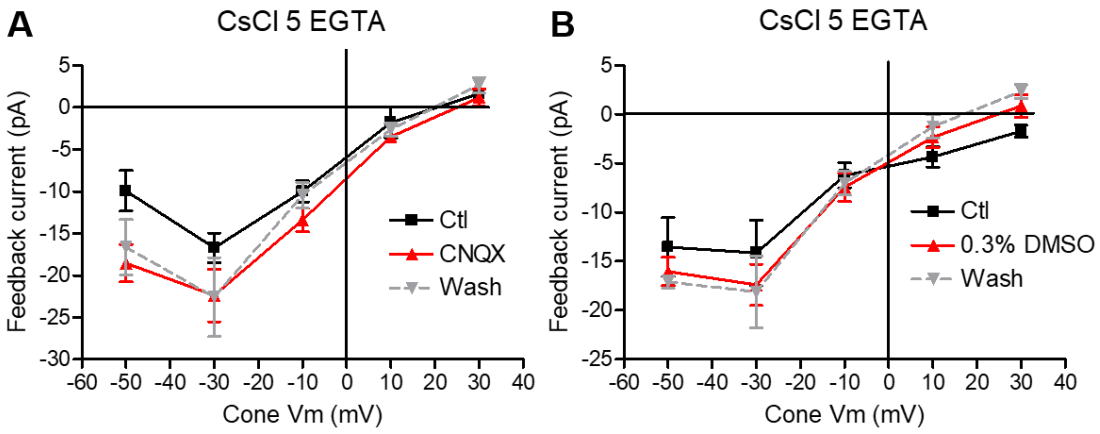

Figure 23. Inhibiting glutamate receptors at the HC to cone feedback synapse did not alter inward feedback currents in cones.

Inward feedback currents in cones are plotted against cone holding potential. Cone pipette solution contained CsCl (E_{Cl} = 0 mV). (A) The AMPA/KA antagonist CNQX (100 μM) was bath applied for 3 min. Feedback currents were measured in control conditions (square, black line); 4th minute of bath application of CNQX (upward triangle, red line), and 3-5 min. after washout of the drug (downward triangle, gray line) (N= 5 pairs.). (B) Effects of vehicle control solution (0.3% DMSO) on feedback currents (N= 3).

b. Calcium-activated chloride currents are not a major component of feedback currents in cones.

To identify the chloride currents contributing to inward feedback currents in cones, we turned to pharmacology. $I_{Cl(Ca)}$ have been suggested to contribute to feedback (Barnes and Deschenes, 1992; Kraaij et al., 2000; Packer et al., 2010;

Thoreson and Burkhardt, 1991; Verweij et al., 1996; Verweij et al., 2003). This conclusion was largely based on the ability of niflumic acid to block $I_{Cl(Ca)}$ in cones, but this compound can also inhibit I_{Ca} directly (Barnes and Deschenes, 1992; Thoreson et al., 2003). There is evidence for two types of Ca^{2+}-activated Cl^- channels in cones: both anoctamin-1 (Ano1/ TMEM16a) and anoctamin-2 (Ano2/ TMEM16b) (Mercer et al., 2011b); (Dauner et al., 2013; Jeon et al., 2013). We tested a Ca^{2+}-activated chloride channel antagonist, Ani9 that is reportedly selective for Ano1 over Ano2 for its ability to block $I_{Cl(Ca)}$ in cones. Activation of $I_{Cl(Ca)}$ by strong depolarizing steps results in a large inward tail current at the end of the step (Mercer et al., 2011b). We measured the tail current amplitude 150 ms after the end of the test pulse relative to baseline currents when the cone was held at -70 mV. We measured currents evoked by steps to -10 mV which evoked the largest amplitude tail current. In recordings with a CsCl-based cone pipette solution where E_{Cl} = 0 mV, bath application of Ani9 (1 μM) inhibited ~81% of these tail currents (N=4, P= 0.007, one sample t-test). (Fig. 24A-B). Tail currents did not recover 3-5 min after returning to the control solution indicating that Ani9 does not washout very quickly.

We also tested whether Ani9 might inhibit $I_{Cl(Ca)}$ by directly inhibiting I_{Ca} in cones. Rather than inhibiting I_{Ca}, Ani9 (1 μM) caused a small but statistically insignificant increase in the peak amplitude of I_{Ca} (Fig. 24C, N= 3 cells, P=0.2651, one sample t-test). This indicates that, unlike niflumic acid, the inhibitory effects of Ani9 on $I_{Cl(Ca)}$ does not involve inhibition of I_{Ca}.

We next tested effects of Ani9 on cone feedback currents evoked with in cones using a pipette solution where E_{Cl} was set at ~ 0 mV. We found that bath application of Ani9 (1 μM) caused no significant changes in feedback current at any of the holding potentials in cones (Fig. 24D). In contrast, to conclusions from earlier studies (Barnes

and Deschenes, 1992; Endeman et al., 2012; Kraaij et al., 2000; Packer et al., 2010; Thoreson and Burkhardt, 1991; Verweij et al., 2003), these results suggest that $I_{Cl(Ca)}$ contributes very little to inward feedback currents, at least under our experimental conditions.

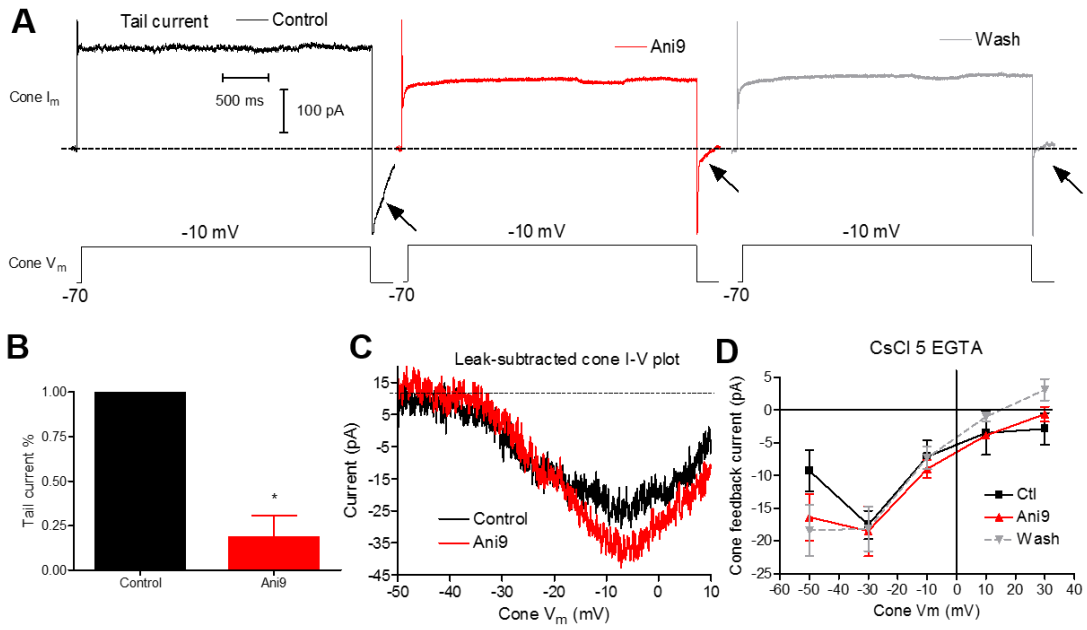

Figure 24. Ani9 blocks $I_{Cl(Ca)}$ tail currents but not cone I_{Ca} or inward feedback currents.

(A) Cone membrane currents (Cone I_m) evoked by a strong depolarizing test step (-70 to -10 mV, 3.2 s) show a large inward $I_{Cl(Ca)}$ tail current at offset of the step (arrow). After bath application of Ani9 (1 μM) for 3 min, this tail current was strongly inhibited (middle panel). Tail currents did not recover after 3 min. washout. (B)The percentage of tail current decrease significantly after treatment of Ani9 (1 μM) (N=4, *: P= 0.007, one sample t-test). (C) Examples of leak-subtracted I_{Ca} plotted against cone holding potential measured before (black trace) and after (red trace) treatment with Ani9 (1 μM). (D) Inward cone feedback currents plotted as a function of cone holding potential before, during and after treatment with Ani9 (1 μM) using CsCl pipette solution (N= 5 pairs). Control: square with black line; Ani9: upward triangle with red line; wash: downward triangle with grey dashed line.

c. Glutamate transporter chloride currents contribute significantly to feedback currents in cones.

In addition to stimulating $I_{Cl(Ca)}$, Ca^{2+} influx into cones stimulates the release of glutamate into the synaptic cleft. After release, glutamate molecules are recycled by excitatory amino acid transporters (EAAT) on the plasma membrane of glial Müller cells and photoreceptors. Activation of EAATs in cones by glutamate is accompanied by the opening of transporter-associated anion channels (Eliasof and Werblin, 1993). We tested a role for EAAT anion currents in feedback by using a glutamate transporter inhibitor, DL-TBOA (300 μM). TBOA can inhibit EAAT1-5, but is particularly effective in blocking EAAT2 (Shimamoto et al., 1998) which is the subtype found in cones (Eliasof et al., 1998; Rowan et al., 2010; Schneider et al., 2014). Glutamate-transporter currents appear to be inhibited completely by a concentration of 300 μM TBOA (Szmajda and Devries, 2011). As above, we first tested feedback with a cone pipette solution containing CsGluc/Glut and E_{Cl} ~-46 mV. With this pipette solution, inhibiting glutamate transporter anion currents ($I_{Cl(Glut)}$) reduced feedback currents at -30 mV (N= 7 pairs; P=0.0043), but increased inward feedback currents at more positive potentials (Fig. 25A) suggesting that it inhibited a current that reversed from inward to outward at ~-20 mV, above the predicted value for E_{Cl}. We used a pipette solution containing 40 mM glutamate because the presence of this additional glutamate in the cone increases post-synaptic currents in horizontal cells and slows rundown of those currents in paired cone/HC recordings (Bartoletti et al., 2010). We were concerned about possible effects of intracellular glutamate on glutamate transporter activity and thus on feedback currents. However, we found that application of TBOA had similar effects when using

CsGluconate-based pipette solution without glutamate (Fig. 25B). Thus, addition of glutamate to the cone pipette solution did not significantly affect feedback currents.

We then tested TBOA on feedback currents when using a cone pipette solution in which E_{Cl} ~ 0 mV. As before, this pipette solution increased inward feedback currents at -50 and -30 mV. Consistent with contributions from $I_{Cl(Glut)}$, blocking glutamate transporters with TBOA significantly reduced inward feedback currents at potentials below -10 mV (Fig. 25C) (N=5 pairs; -50 mV: P=0.0472; -30 mV: P=0.0011).

Inward feedback currents often show a two-phase time course that can be fit by a sum of two exponentials (Warren et al., 2016b). Our data also present a two-phase decline. However, the residual inward currents that remained after TBOA treatment were often too small to be well fit with two exponentials. To compare release kinetics before and after TBOA treatment, we fit feedback currents at -30 mV with a single exponential. When we did so, we found that the time constant (τ) averaged 102 ± 25 ms in control and 79 ± 20 ms after TBOA treatment with no significant difference (N= 5 pairs, P=0.5146, paired t-test) when using the CsCl pipette solution. With the CsGluc/Glut pipette solution, time constants averaged 179 ± 25 ms in control and 129 ± 16 ms in TBOA with no significant difference (N= 7 pairs, P=0.1047, paired t-test) With the CsGluc pipette solution, time constants averaged 124 ± 39 ms in control and 82 ± 31 ms in TBOA with no significant difference (N= 4 pairs, P=0.3743, paired t-test). Together, these results indicate that glutamate transporter currents are a much more significant contributor to inward feedback currents than $I_{Cl(Ca)}$, contrary to suggestions from earlier studies.

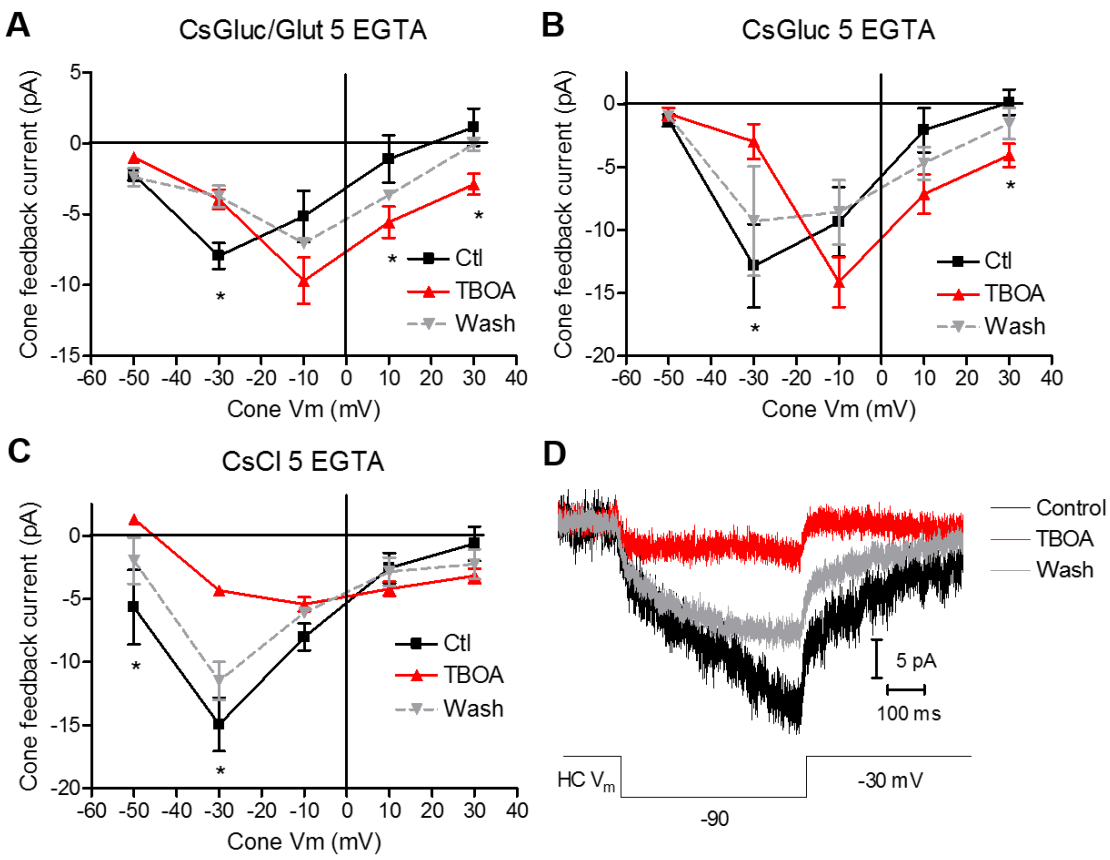

Figure 25. Inward feedback currents in cones are inhibited significantly by blocking glutamate transporters with TBOA (300 μM).

After rupturing into both the cone and HC, control feedback currents were measured. TBOA was superfused into the bath for 3 min and then currents were measured again. Drugs were washed for 3-5 min with control superfusate and then currents were measured again. Control: square with black line; TBOA (300 μM). (A) Inward cone feedback currents plotted as a function of cone holding potential before, during and after treatment with TBOA measured using CsGluc/Glut pipette solution. (N= 7 pairs; * -30 mV P=0.0043; +10 mV P=0.0469; +30 mV P=0.0202) (B) Effects of TBOA on cone feedback currents measured using a cone pipette solution containing CsGlu without any added glutamate (N= 4 pairs; * -30 mV P=0.0330; +30 mV P=0.0218). (C) Effects of TBOA on cone feedback currents measured using a cone pipette solution containing CsCl. Inward feedback currents were reduced significantly at potentials below -10 mV. (N=5 pairs; * -50 mV: P=0.0472; -30 mV: P=0.0011.) (D) Example current traces measured at -30 mV

using CsCl pipette solution. Black trace represents the control current measured before treatment with TBOA; red trace represents the current measured after treatment with TBOA for 3 min; grey trace represents the current measured after washing out TBOA for 3-5 min.

IV. Discussion:

The negative shift of voltage-dependence of VGCCs in cones and the increased amplitude of I_{Ca} are key mechanisms in lateral inhibition at OPL. Earlier studies had suggested that inward feedback currents could be amplified by activation of $I_{Cl(Ca)}$ accompanying the increase in Ca^{2+} influx (Barnes and Deschenes, 1992; Endeman et al., 2012; Kraaij et al., 2000; Thoreson and Burkhardt, 1991; Verweij et al., 2003). However, we found that while $I_{Cl(Ca)}$ may contribute, there is a much more significant contribution to inward feedback currents from Cl^- channels coupled to the glutamate transporter.

In salamander photoreceptors, antibodies to anoctamin 1 (Ano1 or TMEM16A) label rod and cone terminals (Mercer et al., 2011). In mammalian retina, there is evidence for both Ano1 and Ano2 (TMEM16B) (Dauner et al., 2013; Jeon et al., 2013). Ani9 is reported to be selective for Ano1 channels (Seo et al., 2016) and so our finding that Ani9 strongly inhibited $I_{Cl(Ca)}$ in cones supports immunohistochemical evidence that Ano1 is the major subtype responsible for $I_{Cl(Ca)}$ currents in cones.

Strongly inhibiting $I_{Cl(Ca)}$ with Ani9 (1 μM) did not significantly reduce inward feedback currents in cones, even after we enhanced Cl^- currents by using a cone pipette solution that set E_{Cl} at ~0 mV. This differs from earlier studies suggesting a more significant contribution from $I_{Cl(Ca)}$. One contributor to differences with our study is that earlier conclusions were largely based on the finding that niflumic acid reduced negative

feedback (Barnes and Deschenes, 1992; Endeman et al., 2012; Kraaij et al., 2000). However, niflumic acid not only inhibits $I_{Cl(Ca)}$, but also inhibits I_{Ca} directly (Barnes and Deschenes, 1992; Thoreson et al., 2003). It is possible that a larger contribution from $I_{Cl(Ca)}$ might be revealed if we were to test HC to cone feedback using a lower concentration of the Ca^{2+} buffer, EGTA, in the cone pipette solution to enhance Ca^{2+}-associated currents. However, under our conditions with 5 mM EGTA as the principle Ca^{2+} buffer, we found that $I_{Cl(Ca)}$ is not a major component of feedback currents.

$I_{Cl(Glut)}$ was found to contribute to inward feedback currents when cones were held at a very negative membrane potential, e.g. under strong light, in goldfish. It was suggested that this current arose from spillover following release by neighboring cones and that these feedback currents helped to depolarize the cone when it was hyperpolarized by strong light (Vroman and Kamermans, 2015). Unlike earlier experiments using surround illumination to evoke feedback signals in cones, we used simultaneous paired whole cell recordings from HCs and cones to bypass feedforward signals from cones to HCs and study feedback signals directly. We found that using TBOA to block $I_{Cl(Glut)}$ significantly reduced cone feedback currents evoked by changes in HC membrane potential when the cone was voltage clamped at membrane potentials above -50 mV where I_{Ca} is active. This suggests that, in addition to activation by spillover from neighboring cones, activation of $I_{Cl(Glut)}$ by locally released glutamate also contributes to feedback currents. Our results suggest that the feedback-induced increase in I_{Ca} stimulates additional glutamate release that in turn activates $I_{Cl(Glu)}$. E_{Cl} in cones appears to be close to the cone dark resting membrane potential (Thoreson and Bryson, 2004). When cones are hyperpolarized by light, E_{Cl} would thus be more positive than the resting membrane potential and so the activation of Cl^- currents would depolarize the cone membrane. However, when we tested feedback with a cone pipette

solution where E_{Cl} = -46 mV, close to endogenous values, we saw inward feedback currents even when cones were held at -30 mV. So even at potentials above E_{Cl}, activation of glutamate transporters may contribute to inward, depolarizing currents in cones. This is consistent with other findings that the net reversal potential for transporter currents is typically 15-20 mV more positive than E_{Cl} due to the inward counter-transport of glutamate anions (Wadiche and Kavanaugh, 1998).

In previous studies, inward feedback currents were often evoked by an annulus of light (Verweij et al., 1996; Vroman and Kamermans, 2015). With this protocol, annular illumination hyperpolarizes cones in the receptive field surround to reduce feed-forward glutamate release onto HCs. This reduction in glutamate release hyperpolarizes HCs which in turn stimulates inward, depolarizing feedback in cones. Thus, when studied with light, postsynaptic glutamate receptor antagonists will block feedback by blocking effects of glutamate on HCs (Verweij et al., 1996; Vroman and Kamermans, 2015). By using paired recordings from cones and HCs to study feedback directly, we were able to test whether glutamate receptors also participate directly in feedback at the synapse from HCs back onto cones. It has been suggested that currents flowing through post-synaptic glutamate receptors into HC dendrites might contribute to feedback by generating extracellular, ephaptic voltage changes (Byzov and Shura-Bura, 1986; Kamermans et al., 2001). Our results showing that feedback currents in cones were not be affected by blockade of AMPA receptors with CNQX show that this is not likely to be the case.

Our results show a surprisingly large role for glutamate transporter currents and smaller than expected role for $I_{Cl(Ca)}$ in contributing to feedback currents in cones. Because these currents are activated by Ca^{2+} influx, we predicted that the contributions from glutamate transporter currents would be slower than changes in I_{Ca}. We did not see any significant change in the overall kinetics of feedback currents when we applied

TBOA, but feedback current kinetics often changed during the course of recording even in untreated control cell pairs, so further studies will be needed to address definitively whether glutamate transporter activity shapes the kinetics of feedback currents in cones.

Chapter 5 Appendices

I. Appendix A: Abbreviations:

Ano1/ TMEM16a	anoctamin-1
Ano2/ TMEM16b	anoctamin-2
Arr1	arrestin
calmodulin	CaM
Ca_v	voltage-gated Ca^{2+} channel
cGMP	cyclic guanosine monophosphate
CICR	calcium-induced calcium release
C_m	capacitance
cMFB	cerebellar mossy fiber boutons
CNQX	6-cyano-7-nitroquinoxaline-2,3-dione
CNS	central neural system
CtBP2	C-terminal binding peptide 2
DMSO	dimethyl sulfoxide
Dnase	deoxyribonuclease
Dyn	dynasore
EAAT	excitatory amino acid transporter
E_{Cl}	chloride equilibrium potential

EGTA	ethylene glycol-bis(β-aminoethyl ether)-N,N,N',N'-tetraacetic acid
EM	electron microscope
EPSC	excitatory post-synaptic current
ER	endoplasmic reticulum
FM1-43	N-(3-Triethylammoniumpropyl)-4-(4-(Dibutylamino) Styryl) Pyridinium Dibromide
FRAP	fluorescence recovery after photobleaching
GABA	gamma-Aminobutyric acid
GAP	GTPase activating protein
GDP	guanosine diphosphate
GPCR	G-protein coupled receptor
GTP	guanosine triphosphate
Gβ5-L	long form of Gβ5 subunit
HC	horizontal cell
HEPES	4-(2-hydroxyethyl)-1-piperazineethanesulfonic acid
I_{Ca}	calcium current
$I_{Cl(Ca)}$	Ca^{2+}-activated chloride currents
$I_{Cl(Glut)}$	glutamate-associated Cl- current
iGluR	ionotropic glutamate receptors

INL	inner nuclear layer
IP3	inositol 1,4,5-trisphosphate
IPL	inner plexiform layer
IS	inner segment
mEPSC	miniature excitatory post-synaptic current
mGluR6	type 6 metabotropic glutamate receptors
mV	millivolt
NHEs	Na^+ /H^+ exchangers
ONL	outer nuclear layer
OPL	outer plexiform layer
OS	outer segment
PDE	phosphodiesterase
pF	picofarad
PI(3,4,5)P_3	phosphatidylinositol 3,4,5 trisphosphate
Ps2	pitstop2
Q_{Ca}	calcium current charge transfer
R9AP	membrane anchor protein
Rec	recoverin
RGC	retinal ganglion cell
RGS9-1	regulator-of-G-protein-signaling proteins

R_m	membrane resistance
RRP	readily release pool
R_s	series resistance
SEM	the standard error of the mean
SNARE	soluble NSF attachment protein receptors
Syt	synaptotagmin
TBOA	threo-β-Benzyloxyaspartic acid
TEA	tetraethylammonium
TIRFM	total internal reflection fluorescence microscopy
TRPM1	transient receptor potential 1
VGCC	voltage-gated Ca^{2+} channel

II. Appendix B: References

Alabi, A.A., and Tsien, R.W. (2013). Perspectives on kiss-and-run: role in exocytosis, endocytosis, and neurotransmission. Annu. Rev. Physiol. 75, 393-422.

Albillos, A., Dernick, G., Horstmann, H., Almers, W., Alvarez de Toledo, G., and Lindau, M. (1997). The exocytotic event in chromaffin cells revealed by patch amperometry. Nature 389, 509-512.

Allman, J., Miezin, F., and McGuinness, E. (1985). Stimulus specific responses from beyond the classical receptive field: neurophysiological mechanisms for local-global comparisons in visual neurons. Annu. Rev. Neurosci. 8, 407-430.

Archer, D.A., Graham, M.E., and Burgoyne, R.D. (2002). Complexin regulates the closure of the fusion pore during regulated vesicle exocytosis. J. Biol. Chem. 277, 18249-18252.

Arikawa, K., Molday, L.L., Molday, R.S., and Williams, D.S. (1992). Localization of peripherin/rds in the disk membranes of cone and rod photoreceptors: relationship to disk membrane morphogenesis and retinal degeneration. J. Cell Biol. 116, 659-667.

Armstrong, J.K., Wenby, R.B., Meiselman, H.J., and Fisher, T.C. (2004). The hydrodynamic radii of macromolecules and their effect on red blood cell aggregation. Biophys. J. 87, 4259-4270.

Arriza, J.L., Eliasof, S., Kavanaugh, M.P., and Amara, S.G. (1997). Excitatory amino acid transporter 5, a retinal glutamate transporter coupled to a chloride conductance. Proc. Natl. Acad. Sci. U. S. A. 94, 4155-4160.

Arshavsky, V.Y., Lamb, T.D., and Pugh, E.N.,Jr. (2002). G proteins and phototransduction. Annu. Rev. Physiol. 64, 153-187.

Artalejo, C.R., Henley, J.R., McNiven, M.A., and Palfrey, H.C. (1995). Rapid endocytosis coupled to exocytosis in adrenal chromaffin cells involves Ca2+, GTP, and dynamin but not clathrin. Proc. Natl. Acad. Sci. U. S. A. 92, 8328-8332.

Arvanitaki, A. (1942). Effects evoked in an axon by the activity of a contiguous one. J. Neurophysiol. 5, 89-108.

Babai, N., and Thoreson, W.B. (2009). Horizontal cell feedback regulates calcium currents and intracellular calcium levels in rod photoreceptors of salamander and mouse retina. J. Physiol. 587, 2353-2364.

Babai, N., Bartoletti, T.M., and Thoreson, W.B. (2010a). Calcium regulates vesicle replenishment at the cone ribbon synapse. J. Neurosci. 30, 15866-15877.

Babai, N., Morgans, C.W., and Thoreson, W.B. (2010b). Calcium-induced calcium release contributes to synaptic release from mouse rod photoreceptors. Neuroscience 165, 1447-1456.

Bader, C.R., Bertrand, D., and Schwartz, E.A. (1982). Voltage-activated and calcium-activated currents studied in solitary rod inner segments from the salamander retina. J. Physiol. 331, 253-284.

Baehr, W., Devlin, M.J., and Applebury, M.L. (1979). Isolation and characterization of cGMP phosphodiesterase from bovine rod outer segments. J. Biol. Chem. 254, 11669-11677.

Balaji, J., and Ryan, T.A. (2007). Single-vesicle imaging reveals that synaptic vesicle exocytosis and endocytosis are coupled by a single stochastic mode. Proc. Natl. Acad. Sci. U. S. A. 104, 20576-20581.

Barg S, Knowles MK, Chen X, Midorikawa M, Almers W. (2010) Syntaxin clusters assemble reversibly at sites of secretory granules in live cells. Proc Natl Acad Sci U S A. 107:20804-20809.

Barnes, S., and Deschenes, M.C. (1992). Contribution of Ca and Ca-activated Cl channels to regenerative depolarization and membrane bistability of cone photoreceptors. J. Neurophysiol. 68, 745-755.

Barnes, S., and Hille, B. (1989). Ionic channels of the inner segment of tiger salamander cone photoreceptors. J. Gen. Physiol. 94, 719-743.

Bar-On D, Wolter S, van de Linde S, Heilemann M, Nudelman G, Nachliel E, Gutman M, Sauer M, Ashery U. (2012) Super-resolution imaging reveals the internal architecture of nano-sized syntaxin clusters. J Biol Chem. 287:27158-27167.

Bartoletti TM, Thoreson WB. (2011) Quantal amplitude at the cone ribbon synapse can be adjusted by changes in cytosolic glutamate. Mol Vis. 17:920-931.

Bartoletti, T.M., Babai, N., and Thoreson, W.B. (2010). Vesicle pool size at the salamander cone ribbon synapse. J. Neurophysiol. 103, 419-423.

Bartoletti, T.M., Jackman, S.L., Babai, N., Mercer, A.J., Kramer, R.H., and Thoreson, W.B. (2011). Release from the cone ribbon synapse under bright light conditions can be controlled by the opening of only a few Ca(2+) channels. J. Neurophysiol. 106, 2922-2935.

Baylor, D.A., Fuortes, M.G., and O'Bryan, P.M. (1971). Receptive fields of cones in the retina of the turtle. J. Physiol. 214, 265-294.

Baylor, D.A., Nunn, B.J., and Schnapf, J.L. (1987). Spectral sensitivity of cones of the monkey Macaca fascicularis. J. Physiol. 390, 145-160.

Berntson, A., Taylor, W.R., and Morgans, C.W. (2003). Molecular identity, synaptic localization, and physiology of calcium channels in retinal bipolar cells. J. Neurosci. Res. 71, 146-151.

Berntson, A.K., and Morgans, C.W. (2003). Distribution of the presynaptic calcium sensors, synaptotagmin I/II and synaptotagmin III, in the goldfish and rodent retinas. J. Vis. 3, 274-280.

Blot, A., and Barbour, B. (2014). Ultra-rapid axon-axon ephaptic inhibition of cerebellar Purkinje cells by the pinceau. Nat. Neurosci. 17, 289-295.

Borst, J.G., and Soria van Hoeve, J. (2012). The calyx of Held synapse: from model synapse to auditory relay. Annu. Rev. Physiol. 74, 199-224.

Bowmaker, J.K., Astell, S., Hunt, D.M., and Mollon, J.D. (1991). Photosensitive and photostable pigments in the retinae of Old World monkeys. J. Exp. Biol. 156, 1-19.

Burkhardt, D.A. (1993). Synaptic feedback, depolarization, and color opponency in cone photoreceptors. Vis. Neurosci. 10, 981-989.

Byzov, A.L., and Shura-Bura, T.M. (1986). Electrical feedback mechanism in the processing of signals in the outer plexiform layer of the retina. Vision Res. 26, 33-44.

Cadetti, L., and Thoreson, W.B. (2006). Feedback effects of horizontal cell membrane potential on cone calcium currents studied with simultaneous recordings. J. Neurophysiol. 95, 1992-1995.

Cadetti, L., Bartoletti, T.M., and Thoreson, W.B. (2008). Quantal mEPSCs and residual glutamate: how horizontal cell responses are shaped at the photoreceptor ribbon synapse. Eur. J. Neurosci. 27, 2575-2586.

Cadetti, L., Bryson, E.J., Ciccone, C.A., Rabl, K., and Thoreson, W.B. (2006). Calcium-induced calcium release in rod photoreceptor terminals boosts synaptic transmission during maintained depolarization. Eur. J. Neurosci. 23, 2983-2990.

Ceccarelli, B., Hurlbut, W.P., and Mauro, A. (1973). Turnover of transmitter and synaptic vesicles at the frog neuromuscular junction. J. Cell Biol. 57, 499-524.

Chen, M., Krizaj, D., and Thoreson, W.B. (2014). Intracellular calcium stores drive slow non-ribbon vesicle release from rod photoreceptors. Front. Cell. Neurosci. 8, 20.

Chen, M., Van Hook, M.J., and Thoreson, W.B. (2015). Ca2+ Diffusion through Endoplasmic Reticulum Supports Elevated Intraterminal Ca2+ Levels Needed to Sustain Synaptic Release from Rods in Darkness. J. Neurosci. 35, 11364-11373.

Chen, M., Van Hook, M.J., Zenisek, D., and Thoreson, W.B. (2013). Properties of ribbon and non-ribbon release from rod photoreceptors revealed by visualizing individual synaptic vesicles. J. Neurosci. 33, 2071-2086.

Chen, X., Barg, S., and Almers, W. (2008). Release of the styryl dyes from single synaptic vesicles in hippocampal neurons. J. Neurosci. 28, 1894-1903.

Chen, Y., Deng, L., Maeno-Hikichi, Y., Lai, M., Chang, S., Chen, G., and Zhang, J.F. (2003). Formation of an endophilin-Ca2+ channel complex is critical for clathrin-mediated synaptic vesicle endocytosis. Cell 115, 37-48.

Chiang, H.C., Shin, W., Zhao, W.D., Hamid, E., Sheng, J., Baydyuk, M., Wen, P.J., Jin, A., Momboisse, F., and Wu, L.G. (2014). Post-fusion structural changes and their roles in exocytosis and endocytosis of dense-core vesicles. Nat. Commun. 5, 3356.

Choi, J.J., Wang, S., Tung, Y.S., Morrison, B.,3rd, and Konofagou, E.E. (2010). Molecules of various pharmacologically-relevant sizes can cross the ultrasound-induced blood-brain barrier opening in vivo. Ultrasound Med. Biol. 36, 58-67.

Chung, C., Barylko, B., Leitz, J., Liu, X., and Kavalali, E.T. (2010). Acute dynamin inhibition dissects synaptic vesicle recycling pathways that drive spontaneous and evoked neurotransmission. J. Neurosci. 30, 1363-1376.

Clayton, E.L., Evans, G.J., and Cousin, M.A. (2008). Bulk synaptic vesicle endocytosis is rapidly triggered during strong stimulation. J. Neurosci. 28, 6627-6632.

Clements, J.D., and Silver, R.A. (2000). Unveiling synaptic plasticity: a new graphical and analytical approach. Trends Neurosci. 23, 105-113.

Corey, D.P., Dubinsky, J.M., and Schwartz, E.A. (1984). The calcium current in inner segments of rods from the salamander (Ambystoma tigrinum) retina. J. Physiol. 354, 557-575.

Cork, K.M., and Thoreson, W.B. (2014). Rapid kinetics of endocytosis at rod photoreceptor synapses depends upon endocytic load and calcium. Vis. Neurosci. 31, 227-235.

Cork, K.M., Van Hook, M.J., and Thoreson, W.B. (2016). Mechanisms, pools, and sites of spontaneous vesicle release at synapses of rod and cone photoreceptors. Eur. J. Neurosci.

Craxton, M. (2010). A manual collection of Syt, Esyt, Rph3a, Rph3al, Doc2, and Dblc2 genes from 46 metazoan genomes--an open access resource for neuroscience and evolutionary biology. BMC Genomics 11, 37-2164-11-37.

Curtis L., Datta P., Liu X., Bogdanova N., Heidelberger R., Janz R. (2010) Syntaxin 3B is essential for the exocytosis of synaptic vesicles in ribbon synapses of the retina. Neuroscience. 166:832-841.

Curtis L.B., Doneske B., Liu X., Thaller C., McNew J.A., Janz R. (2008) Syntaxin 3b is a t-SNARE specific for ribbon synapses of the retina. J Comp Neurol. 510:550-559.

Dacey, D.M., and Lee, B.B. (1994). The 'blue-on' opponent pathway in primate retina originates from a distinct bistratified ganglion cell type. Nature 367, 731-735.

Dauner, K., Mobus, C., Frings, S., and Mohrlen, F. (2013). Targeted expression of anoctamin calcium-activated chloride channels in rod photoreceptor terminals of the rodent retina. Invest. Ophthalmol. Vis. Sci. 54, 3126-3136.

Davenport, C.M., Detwiler, P.B., and Dacey, D.M. (2008). Effects of pH buffering on horizontal and ganglion cell light responses in primate retina: evidence for the proton hypothesis of surround formation. J. Neurosci. 28, 456-464.

Delvendahl, I., and Hallermann, S. (2016). The Cerebellar Mossy Fiber Synapse as a Model for High-Frequency Transmission in the Mammalian CNS. Trends Neurosci. 39, 722-737.

Delvendahl, I., Vyleta, N.P., von Gersdorff, H., and Hallermann, S. (2016). Fast, Temperature-Sensitive and Clathrin-Independent Endocytosis at Central Synapses. Neuron 90, 492-498.

Dhara, M., Yarzagaray, A., Schwarz, Y., Dutta, S., Grabner, C., Moghadam, P.K., Bost, A., Schirra, C., Rettig, J., Reim, K., et al. (2014). Complexin synchronizes primed vesicle exocytosis and regulates fusion pore dynamics. J. Cell Biol. 204, 1123-1140.

Dick, O., Hack, I., Altrock, W.D., Garner, C.C., Gundelfinger, E.D., and Brandstatter, J.H. (2001). Localization of the presynaptic cytomatrix protein Piccolo at ribbon and conventional synapses in the rat retina: comparison with Bassoon. J. Comp. Neurol. 439, 224-234.

Dick, O., tom Dieck, S., Altrock, W.D., Ammermuller, J., Weiler, R., Garner, C.C., Gundelfinger, E.D., and Brandstatter, J.H. (2003). The presynaptic active zone protein bassoon is essential for photoreceptor ribbon synapse formation in the retina. Neuron 37, 775-786.

Dmitriev, A.V., and Mangel, S.C. (2006). Electrical feedback in the cone pedicle: a computational analysis. J. Neurophysiol. 95, 1419-1427.

Douthitt H.L., Luo F., McCann S.D., Meriney S.D. (2011) Dynasore, an inhibitor of dynamin, increases the probability of transmitter release. Neuroscience. 172:187-195.

Dowling, J.E., and Boycott, B.B. (1966). Organization of the primate retina: electron microscopy. Proc. R. Soc. Lond. B. Biol. Sci. 166, 80-111.

Duncan, G., Rabl, K., Gemp, I., Heidelberger, R., and Thoreson, W.B. (2010). Quantitative analysis of synaptic release at the photoreceptor synapse. Biophys. J. 98, 2102-2110.

Eggermann E., Bucurenciu I., Goswami S.P., Jonas P. (2011) Nanodomain coupling between Ca^{2+} channels and sensors of exocytosis at fast mammalian synapses. Nat Rev Neurosci. 13:7-21.

Elhamdani, A., Azizi, F., and Artalejo, C.R. (2006). Double patch clamp reveals that transient fusion (kiss-and-run) is a major mechanism of secretion in calf adrenal chromaffin cells: high calcium shifts the mechanism from kiss-and-run to complete fusion. J. Neurosci. 26, 3030-3036.

Eliasof, S., and Werblin, F. (1993). Characterization of the glutamate transporter in retinal cones of the tiger salamander. J. Neurosci. 13, 402-411.

Eliasof, S., Arriza, J.L., Leighton, B.H., Kavanaugh, M.P., and Amara, S.G. (1998). Excitatory amino acid transporters of the salamander retina: identification, localization, and function. J. Neurosci. 18, 698-712.

Endeman, D., Fahrenfort, I., Sjoerdsma, T., Steijaert, M., Ten Eikelder, H., and Kamermans, M. (2012). Chloride currents in cones modify feedback from horizontal cells to cones in goldfish retina. J. Physiol. 590, 5581-5595.

Erickson, H.P. (2009). Size and shape of protein molecules at the nanometer level determined by sedimentation, gel filtration, and electron microscopy. Biol. Proced. Online 11, 32-51.

Feigenspan, A., and Babai, N. (2015). Functional properties of spontaneous excitatory currents and encoding of light/dark transitions in horizontal cells of the mouse retina. Eur. J. Neurosci. 42, 2615-2632.

Ferguson, S.M., Brasnjo, G., Hayashi, M., Wolfel, M., Collesi, C., Giovedi, S., Raimondi, A., Gong, L.W., Ariel, P., Paradise, S., et al. (2007). A selective activity-dependent requirement for dynamin 1 in synaptic vesicle endocytosis. Science 316, 570-574.

Firth, S.I., Morgan, I.G., Boelen, M.K., and Morgans, C.W. (2001). Localization of voltage-sensitive L-type calcium channels in the chicken retina. Clin. Exp. Ophthalmol. 29, 183-187.

Fox, M.A., and Sanes, J.R. (2007). Synaptotagmin I and II are present in distinct subsets of central synapses. J. Comp. Neurol. 503, 280-296.

Francis A.A., Mehta B., Zenisek D. (2011) Development of new peptide-based tools for studying synaptic ribbon function. J Neurophysiol. 106:1028-1037.

Fuchs M., Brandstätter J.H., Regus-Leidig H. (2014) Evidence for a Clathrin-independent mode of endocytosis at a continuously active sensory synapse. Front Cell Neurosci. 8:60.

Fulop, T., and Smith, C. (2006). Physiological stimulation regulates the exocytic mode through calcium activation of protein kinase C in mouse chromaffin cells. Biochem. J. 399, 111-119.

Fulop, T., Radabaugh, S., and Smith, C. (2005). Activity-dependent differential transmitter release in mouse adrenal chromaffin cells. J. Neurosci. 25, 7324-7332.

Gaffield, M.A., Romberg, C.F., and Betz, W.J. (2011). Live imaging of bulk endocytosis in frog motor nerve terminals using FM dyes. J. Neurophysiol. 106, 599-607.

Gandhi, S.P., and Stevens, C.F. (2003). Three modes of synaptic vesicular recycling revealed by single-vesicle imaging. Nature 423, 607-613.

Gerschenfeld, H.M., and Piccolino, M. (1980). Sustained feedback effects of L-horizontal cells on turtle cones. Proc. R. Soc. Lond. B. Biol. Sci. 206, 465-480.

Girard E., Paul J.L., Fournier N., Beaune P., Johannes L., Lamaze C., Védie B. (2011) The dynamin chemical inhibitor dynasore impairs cholesterol trafficking and sterol-sensitive genes transcription in human HeLa cells and macrophages. PLoS One 6:e29042.

Goetze, B., Schmidt, K.F., Lehmann, K., Altrock, W.D., Gundelfinger, E.D., and Lowel, S. (2010). Vision and visual cortical maps in mice with a photoreceptor synaptopathy: reduced but robust visual capabilities in the absence of synaptic ribbons. Neuroimage 49, 1622-1631.

Grabner C.P., Ratliff C.P., Light A.C., DeVries S.H. (2016) Mechanism of high-frequency signaling at a depressing ribbon synapse. Neuron. 91:133-145.

Grabs D., Slepnev V.I., Songyang Z., David C., Lynch M., Cantley L.C., De Camilli P. (1997) The SH3 domain of amphiphysin binds the proline-rich domain of dynamin at a single site that defines a new SH3 binding consensus sequence. J Biol Chem. 272:13419-13425.

Granseth, B., Odermatt, B., Royle, S.J., and Lagnado, L. (2006). Clathrin-mediated endocytosis is the dominant mechanism of vesicle retrieval at hippocampal synapses. Neuron 51, 773-786.

Graydon, C.W., Cho, S., Li, G.L., Kachar, B., and von Gersdorff, H. (2011). Sharp Ca(2)(+) nanodomains beneath the ribbon promote highly synchronous multivesicular release at hair cell synapses. J. Neurosci. 31, 16637-16650.

Haeseleer, F., Williams, B., and Lee, A. (2016). Characterization of C-terminal Splice Variants of Cav1.4 Ca2+ Channels in Human Retina. J. Biol. Chem. 291, 15663-15673.

Han, X., Wang, C.T., Bai, J., Chapman, E.R., and Jackson, M.B. (2004). Transmembrane segments of syntaxin line the fusion pore of Ca2+-triggered exocytosis. Science 304, 289-292.

HARTLINE, H.K., WAGNER, H.G., and RATLIFF, F. (1956). Inhibition in the eye of Limulus. J. Gen. Physiol. 39, 651-673.

Haverkamp, S., Grunert, U., and Wassle, H. (2001). The synaptic architecture of AMPA receptors at the cone pedicle of the primate retina. J. Neurosci. 21, 2488-2500.

He, L., Wu, X.S., Mohan, R., and Wu, L.G. (2006). Two modes of fusion pore opening revealed by cell-attached recordings at a synapse. Nature 444, 102-105.

Heidelberger, R., Thoreson, W.B., and Witkovsky, P. (2005). Synaptic transmission at retinal ribbon synapses. Prog. Retin. Eye Res. 24, 682-720.

Heidelberger, R., Wang, M.M., and Sherry, D.M. (2003). Differential distribution of synaptotagmin immunoreactivity among synapses in the goldfish, salamander, and mouse retina. Vis. Neurosci. 20, 37-49.

Hering, E. (1964). Outlines of a Theory of the Light Sense.(Cambridge, Mass: Harvard University Press).

Heuser, J.E., and Reese, T.S. (1973). Evidence for recycling of synaptic vesicle membrane during transmitter release at the frog neuromuscular junction. J. Cell Biol. 57, 315-344.

Hirasawa, H., and Kaneko, A. (2003). pH changes in the invaginating synaptic cleft mediate feedback from horizontal cells to cone photoreceptors by modulating Ca2+ channels. J. Gen. Physiol. 122, 657-671.

Hirokawa, N., and Takemura, R. (2004). Kinesin superfamily proteins and their various functions and dynamics. Exp. Cell Res. 301, 50-59.

Holroyd, P., Lang, T., Wenzel, D., De Camilli, P., and Jahn, R. (2002). Imaging direct, dynamin-dependent recapture of fusing secretory granules on plasma membrane lawns from PC12 cells. Proc. Natl. Acad. Sci. U. S. A. 99, 16806-16811.

Holt, M., Cooke, A., Neef, A., and Lagnado, L. (2004). High mobility of vesicles supports continuous exocytosis at a ribbon synapse. Curr. Biol. 14, 173-183.

Holt, M., Cooke, A., Wu, M.M., and Lagnado, L. (2003). Bulk membrane retrieval in the synaptic terminal of retinal bipolar cells. J. Neurosci. 23, 1329-1339.

Hori, T., and Takahashi, T. (2012). Kinetics of synaptic vesicle refilling with neurotransmitter glutamate. Neuron 76, 511-517.

Hosoi, N., Holt, M., and Sakaba, T. (2009). Calcium dependence of exo- and endocytotic coupling at a glutamatergic synapse. Neuron 63, 216-229.

Hua, Y., Woehler, A., Kahms, M., Haucke, V., Neher, E., and Klingauf, J. (2013). Blocking endocytosis enhances short-term synaptic depression under conditions of normal availability of vesicles. Neuron 80, 343-349.

HURVICH, L.M., and JAMESON, D. (1957). An opponent-process theory of color vision. Psychol. Rev. 64, Part 1, 384-404.

Innocenti, B., and Heidelberger, R. (2008). Mechanisms contributing to tonic release at the cone photoreceptor ribbon synapse. J. Neurophysiol. 99, 25-36.

Jackman, S.L., Babai, N., Chambers, J.J., Thoreson, W.B., and Kramer, R.H. (2011). A positive feedback synapse from retinal horizontal cells to cone photoreceptors. PLoS Biol. 9, e1001057.

Jackman, S.L., Choi, S.Y., Thoreson, W.B., Rabl, K., Bartoletti, T.M., and Kramer, R.H. (2009). Role of the synaptic ribbon in transmitting the cone light response. Nat. Neurosci. 12, 303-310.

Jackson, M.B. (2007). In search of the fusion pore of exocytosis. Biophys. Chem. 126, 201-208.

Jacobs, G.H. (1996). Primate photopigments and primate color vision. Proc. Natl. Acad. Sci. U. S. A. 93, 577-581.

Jacobs, G.H. (2018). Photopigments and the dimensionality of animal color vision. Neurosci. Biobehav. Rev. 86, 108-130.

Jeon, J.H., Paik, S.S., Chun, M.H., Oh, U., and Kim, I.B. (2013). Presynaptic Localization and Possible Function of Calcium-Activated Chloride Channel Anoctamin 1 in the Mammalian Retina. PLoS One 8, e67989.

Jockusch, W.J., Praefcke, G.J., McMahon, H.T., and Lagnado, L. (2005). Clathrin-dependent and clathrin-independent retrieval of synaptic vesicles in retinal bipolar cells. Neuron 46, 869-878.

Johnson S.L., Olt J., Cho S., von Gersdorff H., Marcotti W. (2017) The coupling between Ca^{2+} channels and the exocytotic Ca^{2+} sensor at hair cell ribbon synapses varies tonotopically along the mature cochlea. J Neurosci. 37:2471-2484.

Kamermans, M., Fahrenfort, I., Schultz, K., Janssen-Bienhold, U., Sjoerdsma, T., and Weiler, R. (2001). Hemichannel-mediated inhibition in the outer retina. Science 292, 1178-1180.

Kaneko, A., and Tachibana, M. (1986). Effects of gamma-aminobutyric acid on isolated cone photoreceptors of the turtle retina. J. Physiol. 373, 443-461.

Kasai H., Takahashi N., Tokumaru H. (2012) Distinct initial SNARE configurations underlying the diversity of exocytosis. Physiol Rev. 92:1915-1964.

Kawasaki, F., Hazen, M., and Ordway, R.W. (2000). Fast synaptic fatigue in shibire mutants reveals a rapid requirement for dynamin in synaptic vesicle membrane trafficking. Nat. Neurosci. 3, 859-860.

Khuong T.M., Habets R.L., Kuenen S., Witkowska A., Kasprowicz J., Swerts J., Jahn R., van den Bogaart G., Verstreken P. (2013) Synaptic PI(3,4,5)P3 is required for Syntaxin1A clustering and neurotransmitter release. Neuron. 77:1097-1108.

Kim, H.G., and Miller, R.F. (1993). Properties of synaptic transmission from photoreceptors to bipolar cells in the mudpuppy retina. J. Neurophysiol. 69, 352-360.

Kim, J.H., and von Gersdorff, H. (2009). Traffic jams during vesicle cycling lead to synaptic depression. Neuron 63, 143-145.

Klaassen, L.J., Sun, Z., Steijaert, M.N., Bolte, P., Fahrenfort, I., Sjoerdsma, T., Klooster, J., Claassen, Y., Shields, C.R., Ten Eikelder, H.M., et al. (2011). Synaptic

transmission from horizontal cells to cones is impaired by loss of connexin hemichannels. PLoS Biol. 9, e1001107.

Kleinschmidt, J., and Dowling, J.E. (1975). Intracellular recordings from gecko photoreceptors during light and dark adaptation. J. Gen. Physiol. 66, 617-648.

Klyachko, V.A., and Jackson, M.B. (2002). Capacitance steps and fusion pores of small and large-dense-core vesicles in nerve terminals. Nature 418, 89-92.

Kolb, H. (1970). Organization of the outer plexiform layer of the primate retina: electron microscopy of Golgi-impregnated cells. Philos. Trans. R. Soc. Lond. B. Biol. Sci. 258, 261-283.

Kondo, S., Sato-Yoshitake, R., Noda, Y., Aizawa, H., Nakata, T., Matsuura, Y., and Hirokawa, N. (1994). KIF3A is a new microtubule-based anterograde motor in the nerve axon. J. Cell Biol. 125, 1095-1107.

Kononenko, N.L., and Haucke, V. (2015). Molecular mechanisms of presynaptic membrane retrieval and synaptic vesicle reformation. Neuron 85, 484-496.

Koschak, A., Reimer, D., Walter, D., Hoda, J.C., Heinzle, T., Grabner, M., and Striessnig, J. (2003). Cav1.4alpha1 subunits can form slowly inactivating dihydropyridine-sensitive L-type Ca2+ channels lacking Ca2+-dependent inactivation. J. Neurosci. 23, 6041-6049.

Kraaij, D.A., Spekreijse, H., and Kamermans, M. (2000). The nature of surround-induced depolarizing responses in goldfish cones. J. Gen. Physiol. 115, 3-16.

Kranz, K., Dorgau, B., Pottek, M., Herrling, R., Schultz, K., Bolte, P., Monyer, H., Penuela, S., Laird, D.W., Dedek, K., Weiler, R., and Janssen-Bienhold, U.

(2013). Expression of Pannexin1 in the outer plexiform layer of the mouse retina and physiological impact of its knockout. J. Comp. Neurol. 521, 1119-1135.

Krispel, C.M., Chen, D., Melling, N., Chen, Y.J., Martemyanov, K.A., Quillinan, N., Arshavsky, V.Y., Wensel, T.G., Chen, C.K., and Burns, M.E. (2006). RGS expression rate-limits recovery of rod photoresponses. Neuron 51, 409-416.

Krizaj, D., Bao, J.X., Schmitz, Y., Witkovsky, P., and Copenhagen, D.R. (1999). Caffeine-sensitive calcium stores regulate synaptic transmission from retinal rod photoreceptors. J. Neurosci. 19, 7249-7261.

Krizaj, D., Lai, F.A., and Copenhagen, D.R. (2003). Ryanodine stores and calcium regulation in the inner segments of salamander rods and cones. J. Physiol. 547, 761-774.

KUFFLER, S.W. (1953). Discharge patterns and functional organization of mammalian retina. J. Neurophysiol. 16, 37-68.

Lang T., Bruns D., Wenzel D., Riedel D., Holroyd P., Thiele C., Jahn R. (2001) SNAREs are concentrated in cholesterol-dependent clusters that define docking and fusion sites for exocytosis. EMBO J. 20:2202-2213.

Lasansky, A. (1973). Organization of the outer synaptic layer in the retina of the larval tiger salamander. Philos. Trans. R. Soc. Lond. B. Biol. Sci. 265, 471-489.

Lasansky, A. (1978). Contacts between receptors and electrophysiologically identified neurones in the retina of the larval tiger salamander. J. Physiol. 285, 531-542.

Lee, A., Wang, S., Williams, B., Hagen, J., Scheetz, T.E., and Haeseleer, F. (2015). Characterization of Cav1.4 complexes (alpha11.4, beta2, and alpha2delta4) in HEK293T cells and in the retina. J. Biol. Chem. 290, 1505-1521.

Leskov, I.B., Klenchin, V.A., Handy, J.W., Whitlock, G.G., Govardovskii, V.I., Bownds, M.D., Lamb, T.D., Pugh, E.N.,Jr, and Arshavsky, V.Y. (2000). The gain of rod phototransduction: reconciliation of biochemical and electrophysiological measurements. Neuron 27, 525-537.

Liang, K., Wei, L., and Chen, L. (2017). Exocytosis, Endocytosis, and Their Coupling in Excitable Cells. Front. Mol. Neurosci. 10, 109.

Lipstein, N., Sakaba, T., Cooper, B.H., Lin, K.H., Strenzke, N., Ashery, U., Rhee, J.S., Taschenberger, H., Neher, E., and Brose, N. (2013). Dynamic control of synaptic vesicle replenishment and short-term plasticity by Ca(2+)-calmodulin-Munc13-1 signaling. Neuron 79, 82-96.

Liu, X., Hirano, A.A., Sun, X., Brecha, N.C., and Barnes, S. (2013a). Calcium channels in rat horizontal cells regulate feedback inhibition of photoreceptors through an unconventional GABA- and pH-sensitive mechanism. J. Physiol. 591, 3309-3324.

Liu, X., Kerov, V., Haeseleer, F., Majumder, A., Artemyev, N., Baker, S.A., and Lee, A. (2013b). Dysregulation of Ca(v)1.4 channels disrupts the maturation of photoreceptor synaptic ribbons in congenital stationary night blindness type 2. Channels (Austin) 7, 514-523.

LoGiudice, L., and Matthews, G. (2009). The role of ribbons at sensory synapses. Neuroscientist 15, 380-391.

Logiudice, L., Sterling, P., and Matthews, G. (2009). Vesicle recycling at ribbon synapses in the finely branched axon terminals of mouse retinal bipolar neurons. Neuroscience 164, 1546-1556.

Lollike, K., Borregaard, N., and Lindau, M. (1995). The exocytotic fusion pore of small granules has a conductance similar to an ion channel. J. Cell Biol. 129, 99-104.

Lollike, K., Borregaard, N., and Lindau, M. (1998). Capacitance flickers and pseudoflickers of small granules, measured in the cell-attached configuration. Biophys. J. 75, 53-59.

Lukasiewicz, P.D. (2005). Synaptic mechanisms that shape visual signaling at the inner retina. Prog. Brain Res. 147, 205-218.

MacLeish, P.R., and Nurse, C.A. (2007). Ion channel compartments in photoreceptors: evidence from salamander rods with intact and ablated terminals. J. Neurophysiol. 98, 86-95.

Magupalli, V.G., Schwarz, K., Alpadi, K., Natarajan, S., Seigel, G.M., and Schmitz, F. (2008). Multiple RIBEYE-RIBEYE interactions create a dynamic scaffold for the formation of synaptic ribbons. J. Neurosci. 28, 7954-7967.

Mahapatra, S., Fan, F., and Lou, X. (2016). Tissue-specific dynamin-1 deletion at the calyx of Held decreases short-term depression through a mechanism distinct from vesicle resupply. Proc. Natl. Acad. Sci. U. S. A. 113, E3150-8.

Malchow, R.P., Qian, H., and Ripps, H. (1993). Evidence for hemi-gap junctional channels in isolated horizontal cells of the skate retina. J. Neurosci. Res. 35, 237-245.

Mandell, J.W., Townes-Anderson, E., Czernik, A.J., Cameron, R., Greengard, P., and De Camilli, P. (1990). Synapsins in the vertebrate retina: absence from ribbon synapses and heterogeneous distribution among conventional synapses. Neuron 5, 19-33.

Mangel, S.C. (1991). Analysis of the horizontal cell contribution to the receptive field surround of ganglion cells in the rabbit retina. J. Physiol. 442, 211-234.

Mangel, S.C., and Miller, R.F. (1987). Horizontal cells contribute to the receptive field surround of ganglion cells in the rabbit retina. Brain Res. 414, 182-186.

Maranto, A.R. (1982). Neuronal mapping: a photooxidation reaction makes Lucifer yellow useful for electron microscopy. Science 217, 953-955.

Marks, B., Stowell, M.H., Vallis, Y., Mills, I.G., Gibson, A., Hopkins, C.R., and McMahon, H.T. (2001). GTPase activity of dynamin and resulting conformation change are essential for endocytosis. Nature 410, 231-235.

Matthews, G., and Fuchs, P. (2010). The diverse roles of ribbon synapses in sensory neurotransmission. Nat. Rev. Neurosci. 11, 812-822.

Matthews, G., and Sterling, P. (2008). Evidence that vesicles undergo compound fusion on the synaptic ribbon. J. Neurosci. 28, 5403-5411.

Mazelova, J., Ransom, N., Astuto-Gribble, L., Wilson, M.C., and Deretic, D. (2009). Syntaxin 3 and SNAP-25 pairing, regulated by omega-3 docosahexaenoic acid, controls the delivery of rhodopsin for the biogenesis of cilia-derived sensory organelles, the rod outer segments. J. Cell. Sci. 122, 2003-2013.

McCluskey A., Daniel J.A., Hadzic G., Chau N., Clayton E.L., Mariana A., Whiting A., Gorgani N.N., Lloyd J., Quan A., Moshkanbaryans L., Krishnan S., Perera S., Chircop M., von Kleist L., McGeachie A.B., Howes M.T., Parton R.G., Campbell M., Sakoff J.A., Wang X., Sun J.Y., Robertson M.J., Deane F.M., Nguyen T.H., Meunier F.A., Cousin M.A., Robinson P.J. (2013) Building a better dynasore: the

dyngo compounds potently inhibit dynamin and endocytosis. Traffic. 14:1272-1289.

Mehta B., Snellman J., Chen S., Li W., Zenisek D. (2013) Synaptic ribbons influence the size and frequency of miniature-like evoked postsynaptic currents. Neuron. 77:516-527.

Mercer, A.J., Chen M., Thoreson W.B. (2011a) Lateral mobility of presynaptic L-type calcium channels at photoreceptor ribbon synapses. J Neurosci. 31:4397-4406.

Mercer, A.J., Szalewski R.J., Jackman S.L., Van Hook M.J., Thoreson W.B. (2012) Regulation of presynaptic strength by controlling Ca^{2+} channel mobility: effects of cholesterol depletion on release at the cone ribbon synapse. J Neurophysiol. 107:3468-3478

Mercer, A.J., Thoreson W.B. (2013) Tracking quantum dot–tagged calcium channels at vertebrate photoreceptor synapses: retinal slices and dissociated cells. Curr Prot Neurosci, Chap. 2: Unit 2.18.

Mercer, A.J., Rabl, K., Riccardi, G.E., Brecha, N.C., Stella, S.L.,Jr, and Thoreson, W.B. (2011b). Location of release sites and calcium-activated chloride channels relative to calcium channels at the photoreceptor ribbon synapse. J. Neurophysiol. 105, 321-335.

Morgans, C.W. (1999). Calcium channel heterogeneity among cone photoreceptors in the tree shrew retina. Eur. J. Neurosci. 11, 2989-2993.

Morgans, C.W. (2001). Localization of the alpha(1F) calcium channel subunit in the rat retina. Invest. Ophthalmol. Vis. Sci. 42, 2414-2418.

Morgans, C.W., Brandstatter, J.H., Kellerman, J., Betz, H., and Wassle, H. (1996). A SNARE complex containing syntaxin 3 is present in ribbon synapses of the retina. J. Neurosci. 16, 6713-6721.

Morgans, C.W., Gaughwin, P., and Maleszka, R. (2001). Expression of the alpha1F calcium channel subunit by photoreceptors in the rat retina. Mol. Vis. 7, 202-209.

Morgans, C.W., Zhang, J., Jeffrey, B.G., Nelson, S.M., Burke, N.S., Duvoisin, R.M., and Brown, R.L. (2009). TRPM1 is required for the depolarizing light response in retinal ON-bipolar cells. Proc. Natl. Acad. Sci. U. S. A. 106, 19174-19178.

Moser T, Beutner D. (2000) Kinetics of exocytosis and endocytosis at the cochlear inner hair cell afferent synapse of the mouse. Proc Natl Acad Sci U S A. 97:883-888.

Murakami, M., Shimoda, Y., Nakatani, K., Miyachi, E., and Watanabe, S. (1982). GABA-mediated negative feedback from horizontal cells to cones in carp retina. Jpn. J. Physiol. 32, 911-926.

Muresan, V., Lyass, A., and Schnapp, B.J. (1999). The kinesin motor KIF3A is a component of the presynaptic ribbon in vertebrate photoreceptors. J. Neurosci. 19, 1027-1037.

Nachman-Clewner M, St Jules R, Townes-Anderson E. (1999) L-type calcium channels in the photoreceptor ribbon synapse: localization and role in plasticity. J Comp Neurol. 415:1-16.

Neher E. (2017) Some Subtle Lessons from the Calyx of Held Synapse. Biophys J. 112:215-223.

Neher, E. (2010). What is Rate-Limiting during Sustained Synaptic Activity: Vesicle Supply or the Availability of Release Sites. Front. Synaptic Neurosci. 2, 144.

Neher, E., and Sakaba, T. (2008). Multiple roles of calcium ions in the regulation of neurotransmitter release. Neuron 59, 861-872.

Newton, A.J., Kirchhausen, T., and Murthy, V.N. (2006). Inhibition of dynamin completely blocks compensatory synaptic vesicle endocytosis. Proc. Natl. Acad. Sci. U. S. A. 103, 17955-17960.

Packer, O.S., Verweij, J., Li, P.H., Schnapf, J.L., and Dacey, D.M. (2010). Blue-yellow opponency in primate S cone photoreceptors. J. Neurosci. 30, 568-572.

Pang, J.J., Gao, F., Barrow, A., Jacoby, R.A., and Wu, S.M. (2008). How do tonic glutamatergic synapses evade receptor desensitization? J. Physiol. 586, 2889-2902.

Pang, Z.P., and Sudhof, T.C. (2010). Cell biology of Ca2+-triggered exocytosis. Curr. Opin. Cell Biol. 22, 496-505.

Park RJ, Shen H, Liu L, Liu X, Ferguson SM, De Camilli P. (2013) Dynamin triple knockout cells reveal off target effects of commonly used dynamin inhibitors. J Cell Sci. 126:5305-5312.

Parsons TD, Lenzi D, Almers W, Roberts WM. 1994 Calcium-triggered exocytosis and endocytosis in an isolated presynaptic cell: capacitance measurements in saccular hair cells. Neuron. 13:875-883.

Photowala, H., Blackmer, T., Schwartz, E., Hamm, H.E., and Alford, S. (2006). G protein betagamma-subunits activated by serotonin mediate presynaptic inhibition by regulating vesicle fusion properties. Proc. Natl. Acad. Sci. U. S. A. 103, 4281-4286.

Picaud, S., Larsson, H.P., Wellis, D.P., Lecar, H., and Werblin, F. (1995a). Cone photoreceptors respond to their own glutamate release in the tiger salamander. Proc. Natl. Acad. Sci. U. S. A. 92, 9417-9421.

Picaud, S., Pattnaik, B., Hicks, D., Forster, V., Fontaine, V., Sahel, J., and Dreyfus, H. (1998). GABAA and GABAC receptors in adult porcine cones: evidence from a photoreceptor-glia co-culture model. J. Physiol. 513 (Pt 1), 33-42.

Picaud, S.A., Larsson, H.P., Grant, G.B., Lecar, H., and Werblin, F.S. (1995b). Glutamate-gated chloride channel with glutamate-transporter-like properties in cone photoreceptors of the tiger salamander. J. Neurophysiol. 74, 1760-1771.

Piccolino, M. (1995). The feedback synapse from horizontal cells to cone photoreceptors in the vertebrate retina. Issue 1 14, 141-196.

Piccolino, M., and Gerschenfeld, H.M. (1977). Lateral interactions in the outer plexiform layer of turtle retinas after atropine block of horizontal cells. Nature 268, 259-261.

Preta G, Cronin JG, Sheldon IM. (2015) Dynasore - not just a dynamin inhibitor. Cell Commun Signal. 13:24.

Pugh, E.N., Jr. and T.D. Lamb. (2000). Phototransduction in Vertebrate Rods and Cones: Molecular Mechanisms of Amplification, Recovery and Light Adaptation.. In Handbook of Biological Physics, D.G. Stavenga, W.J. de Grip, and E.N. Pugh, Jr. ed., (Amsterdam: Elsevier Science) pp. 183-255.

Pugh, E.N.,Jr, and Lamb, T.D. (1993). Amplification and kinetics of the activation steps in phototransduction. Biochim. Biophys. Acta 1141, 111-149.

Qin N, Yagel S, Momplaisir ML, Codd EE, D'Andrea MR. (2002) Molecular cloning and characterization of the human voltage-gated calcium channel alpha(2)delta-4 subunit. Mol Pharmacol. 62:485-496.

Rabl, K., and Thoreson, W.B. (2002). Calcium-dependent inactivation and depletion of synaptic cleft calcium ions combine to regulate rod calcium currents under physiological conditions. Eur. J. Neurosci. 16, 2070-2077.

Rabl, K., Cadetti, L., and Thoreson, W.B. (2005). Kinetics of exocytosis is faster in cones than in rods. J. Neurosci. 25, 4633-4640.

Rabl, K., Cadetti, L., and Thoreson, W.B. (2006). Paired-pulse depression at photoreceptor synapses. J. Neurosci. 26, 2555-2563.

Rao, T.C., Santana Rodriguez, Z., Bradberry, M.M., Ranski, A.H., Dahl, P.J., Schmidtke, M.W., Jenkins, P.M., Axelrod, D., Chapman, E.R., Giovannucci, D.R., and Anantharam, A. (2017). Synaptotagmin isoforms confer distinct activation kinetics and dynamics to chromaffin cell granules. J. Gen. Physiol. 149, 763-780.

Rao-Mirotznik, R., Harkins, A.B., Buchsbaum, G., and Sterling, P. (1995). Mammalian rod terminal: architecture of a binary synapse. Neuron 14, 561-569.

Rauen, T., and Kanner, B.I. (1994). Localization of the glutamate transporter GLT-1 in rat and macaque monkey retinae. Neurosci. Lett. 169, 137-140.

Rauen, T., Wiessner, M., Sullivan, R., Lee, A., and Pow, D.V. (2004). A new GLT1 splice variant: cloning and immunolocalization of GLT1c in the mammalian retina and brain. Neurochem. Int. 45, 1095-1106.

Rea, R., Li, J., Dharia, A., Levitan, E.S., Sterling, P., and Kramer, R.H. (2004). Streamlined synaptic vesicle cycle in cone photoreceptor terminals. Neuron 41, 755-766.

Regus-Leidig, H., Atorf, J., Feigenspan, A., Kremers, J., Maw, M.A., and Brandstatter, J.H. (2014). Photoreceptor degeneration in two mouse models for congenital stationary night blindness type 2. PLoS One 9, e86769.

Reim, K., Wegmeyer, H., Brandstatter, J.H., Xue, M., Rosenmund, C., Dresbach, T., Hofmann, K., and Brose, N. (2005). Structurally and functionally unique complexins at retinal ribbon synapses. J. Cell Biol. 169, 669-680.

Reye, P., Sullivan, R., Fletcher, E.L., and Pow, D.V. (2002). Distribution of two splice variants of the glutamate transporter GLT1 in the retinas of humans, monkeys, rabbits, rats, cats, and chickens. J. Comp. Neurol. 445, 1-12.

Ribrault C, Reingruber J, Petković M, Galli T, Ziv NE, Holcman D, Triller A. (2011) Syntaxin1A lateral diffusion reveals transient and local SNARE interactions. J Neurosci. 31:17590–17602.

Richards, D.A., Bai, J., and Chapman, E.R. (2005). Two modes of exocytosis at hippocampal synapses revealed by rate of FM1-43 efflux from individual vesicles. J. Cell Biol. 168, 929-939.

Ripps, H., Shakib, M., and MacDonald, E.D. (1976). Peroxidase uptake by photoreceptor terminals of the skate retina. J. Cell Biol. 70, 86-96.

Rizo, J., and Rosenmund, C. (2008). Synaptic vesicle fusion. Nat. Struct. Mol. Biol. 15, 665-674.

Roux, A., Uyhazi, K., Frost, A., and De Camilli, P. (2006). GTP-dependent twisting of dynamin implicates constriction and tension in membrane fission. Nature 441, 528-531.

Rowan, M.J., Ripps, H., and Shen, W. (2010). Fast glutamate uptake via EAAT2 shapes the cone-mediated light offset response in bipolar cells. J. Physiol. 588, 3943-3956.

Saheki, Y., and De Camilli, P. (2012). Synaptic vesicle endocytosis. Cold Spring Harb Perspect. Biol. 4, a005645.

Schacher, S., Holtzman, E., and Hood, D.C. (1976). Synaptic activity of frog retinal photoreceptors. A peroxidase uptake study. J. Cell Biol. 70, 178-192.

Schaeffer, S.F., and Raviola, E. (1978). Membrane recycling in the cone cell endings of the turtle retina. J. Cell Biol. 79, 802-825.

Schmitz F. (2009) The making of synaptic ribbons: how they are built and what they do. Neuroscientist. 15:611-624.

Schmitz, F., Konigstorfer, A., and Sudhof, T.C. (2000). RIBEYE, a component of synaptic ribbons: a protein's journey through evolution provides insight into synaptic ribbon function. Neuron 28, 857-872.

Schmued, L.C., and Snavely, L.F. (1993). Photoconversion and electron microscopic localization of the fluorescent axon tracer fluoro-ruby (rhodamine-dextran-amine). J. Histochem. Cytochem. 41, 777-782.

Schnapf, J.L., Kraft, T.W., Nunn, B.J., and Baylor, D.A. (1988). Spectral sensitivity of primate photoreceptors. Vis. Neurosci. 1, 255-261.

Schnee ME, Santos-Sacchi J, Castellano-Muñoz M, Kong JH, Ricci AJ. (2011). Calcium-dependent synaptic vesicle trafficking underlies indefatigable release at the hair cell afferent fiber synapse. Neuron. 70:326-338.

Schneider, N., Cordeiro, S., Machtens, J.P., Braams, S., Rauen, T., and Fahlke, C. (2014). Functional properties of the retinal glutamate transporters GLT-1c and EAAT5. J. Biol. Chem. 289, 1815-1824.

Seo, Y., Lee, H.K., Park, J., Jeon, D.K., Jo, S., Jo, M., and Namkung, W. (2016). Ani9, A Novel Potent Small-Molecule ANO1 Inhibitor with Negligible Effect on ANO2. PLoS One 11, e0155771.

Shelley, J., Dedek, K., Schubert, T., Feigenspan, A., Schultz, K., Hombach, S., Willecke, K., and Weiler, R. (2006). Horizontal cell receptive fields are reduced in connexin57-deficient mice. Eur. J. Neurosci. 23, 3176-3186.

Sheng, Z., Choi, S.Y., Dharia, A., Li, J., Sterling, P., and Kramer, R.H. (2007). Synaptic Ca2+ in darkness is lower in rods than cones, causing slower tonic release of vesicles. J. Neurosci. 27, 5033-5042.

Sherry, D.M., and Heidelberger, R. (2005). Distribution of proteins associated with synaptic vesicle endocytosis in the mouse and goldfish retina. J. Comp. Neurol. 484, 440-457.

Shimamoto, K., Lebrun, B., Yasuda-Kamatani, Y., Sakaitani, M., Shigeri, Y., Yumoto, N., and Nakajima, T. (1998). DL-threo-beta-benzyloxyaspartate, a potent blocker of excitatory amino acid transporters. Mol. Pharmacol. 53, 195-201.

Shupliakov, O., Low, P., Grabs, D., Gad, H., Chen, H., David, C., Takei, K., De Camilli, P., and Brodin, L. (1997). Synaptic vesicle endocytosis impaired by disruption of dynamin-SH3 domain interactions. Science 276, 259-263.

Sieber JJ, Willig KI, Kutzner C, Gerding-Reimers C, Harke B, Donnert G, Rammner B, Eggeling C, Hell SW, Grubmüller H, Lang T. (2007) Anatomy and dynamics of a supramolecular membrane protein cluster. Science. 317:1072-1076.

Singer, J.H., and Diamond, J.S. (2006). Vesicle depletion and synaptic depression at a mammalian ribbon synapse. J. Neurophysiol. 95, 3191-3198.

Snellman, J., Mehta, B., Babai, N., Bartoletti, T.M., Akmentin, W., Francis, A., Matthews, G., Thoreson, W., and Zenisek, D. (2011). Acute destruction of the synaptic ribbon reveals a role for the ribbon in vesicle priming. Nat. Neurosci. 14, 1135-1141.

Soykan, T., Maritzen, T., and Haucke, V. (2016). Modes and mechanisms of synaptic vesicle recycling. Curr. Opin. Neurobiol. 39, 17-23.

Spruce, A.E., Breckenridge, L.J., Lee, A.K., and Almers, W. (1990). Properties of the fusion pore that forms during exocytosis of a mast cell secretory vesicle. Neuron 4, 643-654.

Sterling, P., and Matthews, G. (2005). Structure and function of ribbon synapses. Trends Neurosci. 28, 20-29.

Stohr, H., Heisig, J.B., Benz, P.M., Schoberl, S., Milenkovic, V.M., Strauss, O., Aartsen, W.M., Wijnholds, J., Weber, B.H., and Schulz, H.L. (2009). TMEM16B, a novel protein with calcium-dependent chloride channel activity, associates with a

presynaptic protein complex in photoreceptor terminals. J. Neurosci. 29, 6809-6818.

Stroh, S., Puller, C., Swirski, S., Holzel, M.B., van der Linde, L.I.S., Segelken, J., Schultz, K., Block, C., Monyer, H., Willecke, K., et al. (2018). Eliminating Glutamatergic Input onto Horizontal Cells Changes the Dynamic Range and Receptive Field Organization of Mouse Retinal Ganglion Cells. J. Neurosci. 38, 2015-2028.

Sudhof, T.C. (2013). Neurotransmitter release: the last millisecond in the life of a synaptic vesicle. Neuron 80, 675-690.

Sun, J., Pang, Z.P., Qin, D., Fahim, A.T., Adachi, R., and Sudhof, T.C. (2007). A dual-Ca2+-sensor model for neurotransmitter release in a central synapse. Nature 450, 676-682.

Suryanarayanan, A., and Slaughter, M.M. (2006). Synaptic transmission mediated by internal calcium stores in rod photoreceptors. J. Neurosci. 26, 1759-1766.

SVAETICHIN, G., and MACNICHOL, E.F.,Jr. (1959). Retinal mechanisms for chromatic and achromatic vision. Ann. N. Y. Acad. Sci. 74, 385-404.

Sweitzer, S.M., and Hinshaw, J.E. (1998). Dynamin undergoes a GTP-dependent conformational change causing vesiculation. Cell 93, 1021-1029.

Szmajda, B.A., and Devries, S.H. (2011). Glutamate spillover between mammalian cone photoreceptors. J. Neurosci. 31, 13431-13441.

Takahashi, N., Kishimoto, T., Nemoto, T., Kadowaki, T., and Kasai, H. (2002). Fusion pore dynamics and insulin granule exocytosis in the pancreatic islet. Science 297, 1349-1352.

Taschenberger H, Leão RM, Rowland KC, Spirou GA, von Gersdorff H. (2002) Optimizing synaptic architecture and efficiency for high-frequency transmission. Neuron. 36:1127-1143.

Taylor, W.R., and Morgans, C. (1998). Localization and properties of voltage-gated calcium channels in cone photoreceptors of Tupaia belangeri. Vis. Neurosci. 15, 541-552.

Teng, H., Lin, M.Y., and Wilkinson, R.S. (2007). Macroendocytosis and endosome processing in snake motor boutons. J. Physiol. 582, 243-262.

Thoreson, W.B. (2007). Kinetics of synaptic transmission at ribbon synapses of rods and cones. Mol. Neurobiol. 36, 205-223.

Thoreson, W.B., and Bryson, E.J. (2004). Chloride equilibrium potential in salamander cones. BMC Neurosci. 5, 53-2202-5-53.

Thoreson, W.B., and Burkhardt, D.A. (1990). Effects of synaptic blocking agents on the depolarizing responses of turtle cones evoked by surround illumination. Vis. Neurosci. 5, 571-583.

Thoreson, W.B., and Burkhardt, D.A. (1991). Ionic influences on the prolonged depolarization of turtle cones in situ. J. Neurophysiol. 65, 96-110.

Thoreson, W.B., and Mangel, S.C. (2012). Lateral interactions in the outer retina. Prog. Retin. Eye Res. 31, 407-441.

Thoreson, W.B., Babai, N., and Bartoletti, T.M. (2008). Feedback from horizontal cells to rod photoreceptors in vertebrate retina. J. Neurosci. 28, 5691-5695.

Thoreson, W.B., Bryson, E.J., and Rabl, K. (2003). Reciprocal interactions between calcium and chloride in rod photoreceptors. J. Neurophysiol. 90, 1747-1753.

Thoreson, W.B., Nitzan, R., and Miller, R.F. (1997). Reducing extracellular Cl- suppresses dihydropyridine-sensitive Ca2+ currents and synaptic transmission in amphibian photoreceptors. J. Neurophysiol. 77, 2175-2190.

Thoreson, W.B., Rabl, K., Townes-Anderson, E., and Heidelberger, R. (2004). A highly Ca2+-sensitive pool of vesicles contributes to linearity at the rod photoreceptor ribbon synapse. Neuron 42, 595-605.

Thoreson, W.B., Van Hook, M.J., Parmelee, C., and Curto, C. (2016). Modeling and measurement of vesicle pools at the cone ribbon synapse: Changes in release probability are solely responsible for voltage-dependent changes in release. Synapse 70, 1-14.

Townes-Anderson, E., Dacheux, R.F., and Raviola, E. (1988). Rod photoreceptors dissociated from the adult rabbit retina. J. Neurosci. 8, 320-331.

Townes-Anderson, E., MacLeish, P.R., and Raviola, E. (1985). Rod cells dissociated from mature salamander retina: ultrastructure and uptake of horseradish peroxidase. J. Cell Biol. 100, 175-188.

Ullrich A, Böhme MA, Schöneberg J, Depner H, Sigrist SJ, Noé F. (2015) Dynamical organization of syntaxin-1A at the presynaptic active zone. PLoS Comput Biol. 11:e1004407.

Ullrich, B., and Sudhof, T.C. (1994). Distribution of synaptic markers in the retina: implications for synaptic vesicle traffic in ribbon synapses. J. Physiol. Paris 88, 249-257.

Usukura, J., and Yamada, E. (1987). Ultrastructure of the synaptic ribbons in photoreceptor cells of Rana catesbeiana revealed by freeze-etching and freeze-substitution. Cell Tissue Res. 247, 483-488.

Vaithianathan T, Matthews G. (2014) Visualizing synaptic vesicle turnover and pool refilling driven by calcium nanodomains at presynaptic active zones of ribbon synapses.Proc Natl Acad Sci U S A. 111:8655-8660.

Vaithianathan, T., Akmentin, W., Henry, D., and Matthews, G. (2013). The ribbon-associated protein C-terminal-binding protein 1 is not essential for the structure and function of retinal ribbon synapses. Mol. Vis. 19, 917-926.

van den Bogaart G, Meyenberg K, Risselada HJ, Amin H, Willig KI, Hubrich BE, Dier M, Hell SW, Grubmüller H, Diederichsen U, Jahn R. (2011) Membrane protein sequestering by ionic protein-lipid interactions.Nature. 479:552-555.

Van Hook MJ, Thoreson WB. (2014) Endogenous calcium buffering at photoreceptor synaptic terminals in salamander retina. Synapse. 68:518-528.

Van Hook, M.J., and Thoreson, W.B. (2012). Rapid synaptic vesicle endocytosis in cone photoreceptors of salamander retina. J. Neurosci. 32, 18112-18123.

Van Hook, M.J., and Thoreson, W.B. (2013). Simultaneous whole-cell recordings from photoreceptors and second-order neurons in an amphibian retinal slice preparation. J. Vis. Exp. (76). doi, 10.3791/50007.

Van Hook, M.J., and Thoreson, W.B. (2015). Weak endogenous Ca2+ buffering supports sustained synaptic transmission by distinct mechanisms in rod and cone photoreceptors in salamander retina. Physiol. Rep. 3, 10.14814/phy2.12567.

Van Hook, M.J., Parmelee, C.M., Chen, M., Cork, K.M., Curto, C., and Thoreson, W.B. (2014). Calmodulin enhances ribbon replenishment and shapes filtering of synaptic transmission by cone photoreceptors. J. Gen. Physiol. 144, 357-378.

Vandenbranden, C.A., Verweij, J., Kamermans, M., Muller, L.J., Ruijter, J.M., Vrensen, G.F., and Spekreijse, H. (1996). Clearance of neurotransmitter from the cone synaptic cleft in goldfish retina. Vision Res. 36, 3859-3874.

Vardjan, N., Stenovec, M., Jorgacevski, J., Kreft, M., and Zorec, R. (2007). Subnanometer fusion pores in spontaneous exocytosis of peptidergic vesicles. J. Neurosci. 27, 4737-4746.

Verhage M, Sørensen JB. (2008) Vesicle docking in regulated exocytosis. Traffic. 9:1414-1424.

Verweij, J., Hornstein, E.P., and Schnapf, J.L. (2003). Surround antagonism in macaque cone photoreceptors. J. Neurosci. 23, 10249-10257.

Verweij, J., Kamermans, M., and Spekreijse, H. (1996). Horizontal cells feed back to cones by shifting the cone calcium-current activation range. Vision Res. 36, 3943-3953.

Vessey, J.P., Stratis, A.K., Daniels, B.A., Da Silva, N., Jonz, M.G., Lalonde, M.R., Baldridge, W.H., and Barnes, S. (2005). Proton-mediated feedback inhibition of presynaptic calcium channels at the cone photoreceptor synapse. J. Neurosci. 25, 4108-4117.

von Bekesy, G. (1967). Mach band type lateral inhibition in different sense organs. J. Gen. Physiol. 50, 519-532.

von Gersdorff H, Matthews G. (1994a) Inhibition of endocytosis by elevated internal calcium in a synaptic terminal. Nature. 370:652-655.

von Gersdorff, H., and Matthews, G. (1994b). Dynamics of synaptic vesicle fusion and membrane retrieval in synaptic terminals. Nature 367, 735-739.

Von Kriegstein, K., Schmitz, F., Link, E., and Sudhof, T.C. (1999). Distribution of synaptic vesicle proteins in the mammalian retina identifies obligatory and facultative components of ribbon synapses. Eur. J. Neurosci. 11, 1335-1348.

Vroman, R., and Kamermans, M. (2015). Feedback-induced glutamate spillover enhances negative feedback from horizontal cells to cones. J. Physiol. 593, 2927-2940.

Vroman, R., Klaassen, L.J., Howlett, M.H., Cenedese, V., Klooster, J., Sjoerdsma, T., and Kamermans, M. (2014). Extracellular ATP hydrolysis inhibits synaptic transmission by increasing ph buffering in the synaptic cleft. PLoS Biol. 12, e1001864.

Vuong, T.M., Chabre, M., and Stryer, L. (1984). Millisecond activation of transducin in the cyclic nucleotide cascade of vision. Nature 311, 659-661.

Wadiche, J.I., and Kavanaugh, M.P. (1998). Macroscopic and microscopic properties of a cloned glutamate transporter/chloride channel. J. Neurosci. 18, 7650-7661.

Wahl S, Katiyar R, Schmitz F. (2013) A local, periactive zone endocytic machinery at photoreceptor synapses in close vicinity to synaptic ribbons. J Neurosci. 33:10278-10300.

Waldner, D.M., Giraldo Sierra, N.C., Bonfield, S., Nguyen, L., Dimopoulos, I.S., Sauve, Y., Stell, W.K., and Bech-Hansen, N.T. (2018). Cone dystrophy and ectopic

synaptogenesis in a Cacna1f loss of function model of congenital stationary night blindness (CSNB2A). Channels (Austin) 12, 17-33.

Walter, A.M., Groffen, A.J., Sorensen, J.B., and Verhage, M. (2011). Multiple Ca2+ sensors in secretion: teammates, competitors or autocrats? Trends Neurosci. 34, 487-497.

Wang, C.T., Lu, J.C., Bai, J., Chang, P.Y., Martin, T.F., Chapman, E.R., and Jackson, M.B. (2003). Different domains of synaptotagmin control the choice between kiss-and-run and full fusion. Nature 424, 943-947.

Wang, T.M., Holzhausen, L.C., and Kramer, R.H. (2014). Imaging an optogenetic pH sensor reveals that protons mediate lateral inhibition in the retina. Nat. Neurosci. 17, 262-268.

Warren, T.J., Van Hook, M.J., Supuran, C.T., and Thoreson, W.B. (2016a). Sources of protons and a role for bicarbonate in inhibitory feedback from horizontal cells to cones in Ambystoma tigrinum retina. J. Physiol. 594, 6661-6677.

Warren, T.J., Van Hook, M.J., Tranchina, D., and Thoreson, W.B. (2016b). Kinetics of Inhibitory Feedback from Horizontal Cells to Photoreceptors: Implications for an Ephaptic Mechanism. J. Neurosci. 36, 10075-10088.

Watanabe, S., and Boucrot, E. (2017). Fast and ultrafast endocytosis. Curr. Opin. Cell Biol. 47, 64-71.

Watanabe, S., Rost, B.R., Camacho-Perez, M., Davis, M.W., Sohl-Kielczynski, B., Rosenmund, C., and Jorgensen, E.M. (2013). Ultrafast endocytosis at mouse hippocampal synapses. Nature 504, 242-247.

Watanabe, S., Trimbuch, T., Camacho-Perez, M., Rost, B.R., Brokowski, B., Sohl-Kielczynski, B., Felies, A., Davis, M.W., Rosenmund, C., and Jorgensen, E.M. (2014). Clathrin regenerates synaptic vesicles from endosomes. Nature 515, 228-233.

Wen X, Saltzgaber GW, Thoreson WB (2017) Kiss-and-run is a significant contributor to synaptic exocytosis and endocytosis in photoreceptors. Front. Cell. Neurosci. 11:286.

Wenzel, E.M., Morton, A., Ebert, K., Welzel, O., Kornhuber, J., Cousin, M.A., and Groemer, T.W. (2012). Key physiological parameters dictate triggering of activity-dependent bulk endocytosis in hippocampal synapses. PLoS One 7, e38188.

Wiesel, T.N., and Hubel, D.H. (1966). Spatial and chromatic interactions in the lateral geniculate body of the rhesus monkey. J. Neurophysiol. 29, 1115-1156.

Wu, L.G., Hamid, E., Shin, W., and Chiang, H.C. (2014). Exocytosis and endocytosis: modes, functions, and coupling mechanisms. Annu. Rev. Physiol. 76, 301-331.

Wu, S.M. (1991). Input-output relations of the feedback synapse between horizontal cells and cones in the tiger salamander retina. J. Neurophysiol. 65, 1197-1206.

Wu, W., and Wu, L.G. (2007). Rapid bulk endocytosis and its kinetics of fission pore closure at a central synapse. Proc. Natl. Acad. Sci. U. S. A. 104, 10234-10239.

Xiao, H., Chen, X., and Steele, E.C.,Jr. (2007). Abundant L-type calcium channel Ca(v)1.3 (alpha1D) subunit mRNA is detected in rod photoreceptors of the mouse retina via in situ hybridization. Mol. Vis. 13, 764-771.

Xu, J., McNeil, B., Wu, W., Nees, D., Bai, L., and Wu, L.G. (2008). GTP-independent rapid and slow endocytosis at a central synapse. Nat. Neurosci. 11, 45-53.

Xu, J.W., and Slaughter, M.M. (2005). Large-conductance calcium-activated potassium channels facilitate transmitter release in salamander rod synapse. J. Neurosci. 25, 7660-7668.

Zabouri, N., and Haverkamp, S. (2013). Calcium channel-dependent molecular maturation of photoreceptor synapses. PLoS One 8, e63853.

Zampighi, G.A., Schietroma, C., Zampighi, L.M., Woodruff, M., Wright, E.M., and Brecha, N.C. (2011). Conical tomography of a ribbon synapse: structural evidence for vesicle fusion. PLoS One 6, e16944.

Zenisek D, Horst NK, Merrifield C, Sterling P, Matthews G. 2004 Visualizing synaptic ribbons in the living cell. J Neurosci. 24:9752-9759.

Zenisek, D., Steyer, J.A., and Almers, W. (2000). Transport, capture and exocytosis of single synaptic vesicles at active zones. Nature 406, 849-854.

Zenisek, D., Steyer, J.A., Feldman, M.E., and Almers, W. (2002). A membrane marker leaves synaptic vesicles in milliseconds after exocytosis in retinal bipolar cells. Neuron 35, 1085-1097.

Zhang, A.J., and Wu, S.M. (2009). Receptive fields of retinal bipolar cells are mediated by heterogeneous synaptic circuitry. J. Neurosci. 29, 789-797.

Zhang, Q., Li, Y., and Tsien, R.W. (2009). The dynamic control of kiss-and-run and vesicular reuse probed with single nanoparticles. Science 323, 1448-1453.

Zhang, Z., Wu, Y., Wang, Z., Dunning, F.M., Rehfuss, J., Ramanan, D., Chapman, E.R., and Jackson, M.B. (2011). Release mode of large and small dense-core vesicles specified by different synaptotagmin isoforms in PC12 cells. Mol. Biol. Cell 22, 2324-2336.

Zhao, W.D., Hamid, E., Shin, W., Wen, P.J., Krystofiak, E.S., Villarreal, S.A., Chiang, H.C., Kachar, B., and Wu, L.G. (2016). Hemi-fused structure mediates and controls fusion and fission in live cells. Nature 534, 548-552.

Zhou, W., and Jones, S.W. (1996). The effects of external pH on calcium channel currents in bullfrog sympathetic neurons. Biophys. J. 70, 1326-1334.

III. Appendix C: Peer-reviewed publications

Wen X, Van Hook MJ, Grassmeyer JJ, Wiesman A, Rich G, Cork K, and Thoreson WB. Endocytosis sustains release at photoreceptor ribbon synapses by restoring fusion competence. The Journal of General Physiology Apr 2018, 150 (4) 591-611 (**Featured article**)

Wen X, Saltzgaber GW, and Thoreson WB (2017) Kiss-and- Run Is a Significant Contributor to Synaptic Exocytosis and Endocytosis in Photoreceptors. Front. Cell. Neurosci. 11:286. doi: 10.3389/fncel.2017.00286